uOttawa

L'Université canadienne
Canada's university

FACULTÉ DES ÉTUDES SUPÉRIEURES ET POSTOCTORALES

u Ottawa

L'Université canadienne
Canada's university

FACULTY OF GRADUATE AND POSDOCTORAL STUDIES

Matthew Noestheden
AUTEUR DE LA THÈSE / AUTHOR OF THESIS

M.Sc. (Chemistry)
GRADE / DEGREE

Department of Chemistry
FACULTÉ, ÉCOLE, DÉPARTEMENT / FACULTY, SCHOOL, DEPARTMENT

Towards Cellular Imaging with Chemical and Molecular Specificity: Raman and Coherent Anti-strokes Raman (CARS) Microscopy

TITRE DE LA THÈSE / TITLE OF THESIS

Dr. J. Pezacki
DIRECTEUR (DIRECTRICE) DE LA THÈSE / THESIS SUPERVISOR

CO-DIRECTEUR (CO-DIRECTRICE) DE LA THÈSE / THESIS CO-SUPERVISOR

EXAMINATEURS (EXAMINATRICES) DE LA THÈSE / THESIS EXAMINERS

Dr. R. Ben

Dr. D. Richeson

Gary W. Slater
Le Doyen de la Faculté des études supérieures et postdoctorales / Dean of the Faculty of Graduate and Postdoctoral Studies

Towards Cellular Imaging with Chemical and Molecular Specificity:
Raman and Coherent Anti-Stokes Raman (CARS) Microscopy

Matthew Noestheden, B.Sc. Honours

Thesis submitted to the
Faculty of Graduate and Postdoctoral Studies
In partial fulfillment of the requirements for the

MSc degree in Chemistry

Department of Chemistry
Ottawa-Carelton Chemistry Institute
Faculty of Science
University of Ottawa

Your file Votre référence
ISBN: 978-0-494-25812-5
Our file Notre référence
ISBN: 978-0-494-25812-5

Acknowledgements

To begin, I would like to thank my supervisor Dr. John P. Pezacki. His patience and understanding during difficult times were an important part of my journey through graduate school. The mentorship and guidance he provided over the last two years helped me approach research in a more thoughtful and analytical way. These are skills I will continue to use to facilitate my growth as an individual and as a scientist.

Scientifically I would like to extend thanks to Mauro Tomietto for his help with AFM, Farried Bensebba for the use of his DLS spectrometer and Malgosia Daroszewska who was instrumental in trouble-shooting HPLC and LC-MS technical issues. Also, I would like to thank the entire Pezacki lab for their help, especially Jane, Angela, Sylvie and Yanouchka.

A special thank you goes to Dr. Li-Lin Tay. I appreciate the time that she was able to devote to our collaboration, as well as the many scientific discussions we have had in my time at the NRC. Also, thank you to my committee members, Dr. Rob Ben and Dr. Darrin Richeson. I know it was a little long, but I hope you enjoyed reading it.

For their friendship and willingness to help with whatever I could throw at them, I would like to give my sincerest thanks to Trevor Mischki, Selena Sagan and Bojana Rakic. You're all awesome!

My family has been immensely supportive throughout my undergraduate years – thank you Mom, Dad, Lisa, Jan, Kiley and Kate for everything.

Lastly, I am lucky enough to have somebody in my life that has been in the trenches with me over these last two years. Her support through good and bad has been unfaltering and I look forward to a lifetime of ups and downs with her. Thank you for all that you do A.

Abstract

The lack of photobleaching, minimal sample heating, and high acquisition rates associated with coherent anti-Stokes Raman scattering (CARS) microscopy make it an attractive approach for the chemically specific *in vivo* imaging of dynamical processes. However, imaging capabilities are currently confined to classes of macromolecules as opposed to specific molecular targets. The use of cyano and deuterium functional group labels, which possess Raman modes in a spectral region devoid of endogenous cellular resonances, has the potential to surmount this limitation, enabling imaging with chemical *and* molecular specificity using CARS microscopy. Herein, cyano and deuterium vibrational modes have been incorporated into Raman and CARS contrast agents capable of mediating biomolecular modification. Application of this approach will be demonstrated using hepatitis C virus (HCV) RNA and two model protein systems with the end goal of investigating dynamical aspects of HCV molecular virology in real-time *in vivo* using CARS microscopy. The addition of exogenous CARS labels to a biomolecule can have serious structural and functional consequences that may lead to the expression of a phenotype dictated by the effects of the modification rather than the system under investigation. Therefore, the structural and functional consequences of introducing CARS labels needed to be investigated before applying cyano and deuterium modified HCV RNA and proteins to *in vivo* analysis using CARS microscopy.

Table of Contents

List of Abbreviations

163mer	163 nt Transcript
273mer	270 nt Transcript
3-CN-NHS	3-Cyanobenzyl-N-Hydroxysuccinimide
4-CN-M	4-Cyanobenzyl Maleimide
4-CN-NHS	4-Cyanobenzyl-N-Hydroxysuccinimide
5'-CN	5'-4-Cyanobenzyl HCV RNA
5'-F	5'-Fluorescein HCV RNA
A	Adenosine
aaU-163mer	163mer Containing aaU
aaU	5-Aminoallyl Uridine
aaU-CN	3-Cyanobenzyl Modified aaU
aaUTP	5-Aminoallyl Uridine-5'-Triphosphate
aaU-RNA	HCV RNA containing 5-aminoallyl uridine
AFM	Atomic Force Microscopy
BSA	Bovine Serum Albumin
BSA-CN	4-CN-NHS Modified BSA
Bz-NHS	Benzyl-NHS
C	Cytidine
CARS	Coherent Anti-Stokes Raman Scattering
C-D	Carbon-Deuterium mode
CIP	Calf Intestinal Phosphatase
CN	Cyano
CN-aaU-RNA	3-Cyanobenzyl Modified HCV RNA
DLS	Dynamic Light Scattering
DMEM	Dulbecco's Modified Eagle Medium
DNA	Deoxyribonucleic Acid
D-RNA	Deuterated HCV RNA
EMCV	*Encenphalomyocarditis* Virus
ESI-MS	Electrospray Ionization Mass Spectrometry

FBS	Fetal Bovine Serum
FISH	Fluorescence *In Situ* Hybridization
G	Guanosine
GFP	Green Fluorescent Protein
HCV	Hepatitis C Virus
HCV RNA	HCV Subgenomic Replicon RNA
Huh-7	Human Hepatoma Cell Line
$hv_{anti\text{-}Stokes}$	Anti-Stokes Photon
HVHP428	sdAb Directed Against Bacterial Protein A
HVHP428-CN	4-CN-NHS Modified HVHP428
IRES	Internal Ribosomal Entry Site
IVT	*In Vitro* Transcription
K_d	Dissociation Constant
k_{pump}	Pump Beam
k_{Stokes}	Stokes Beam
LC-MS	Liquid Chromatography – Mass Spectrometry
M	Maleimide
MALDI	Matrix-Assisted Laser Desorption Ionization
MS	Mass Spectrometry
NEaa	Non-Essential Amino Acids
NHS	N-hydroxysuccinimide
nt	Nucleotide
ORF	Open Reading Frame
PBS	Phosphate Buffered Saline
RNA	Ribonucleic Acid
rNTP	Ribonucleotide Triphosphate
RU	Resonance Unit
S1	S1 Nuclease
sdAb	Single-Domain Antibody
SPR	Surface Plasmon Resonance
T7	T7 RNA Polymerase

U	Uridine
UTP	Uridine-5'-Triphosphate
UTR	Untranslated Region
vs_1	Virtual State 1
vs_2	Vitrual State 2

List of and Figures

List of Schemes

Chapter 1 – Introduction

This thesis proposes to extend the utility of a new form of microscopy, known as coherent anti-Stokes Raman scattering (CARS) microscopy, to enable the real-time localization of specific molecular targets in live-cells. CARS microscopy is ideally suited to this application because CARS image contrast originates from vibrational transitions, which do not produce the phototoxic effects associated with fluorescence microscopy.

Fundamental contrast limitations due to the lack of unique vibrational signatures amongst the major biopolymers necessitated the development of CARS contrast agents that could introduce bioorthogonal vibrational modes. Designing these contrast agents and establishing a means of chemically conjugating them to biomolecules would facilitate the generation of CARS image contrast with molecular specificity. However, chemical modification can introduce structural and/or functional perturbations that alter the wild-type function of the biomolecule. This fact underscored the importance of quantifying the structural and functional effects of conjugating CARS contrast agents to biomolecules so that the contribution of the chemical modification to observed *in vivo* phenotypic changes can be determined.

Chemical coupling of CARS contrast agents and subsequent structural and functional validations will be applied to the study of hepatitis C virus (HCV), for which live-cell dynamical information is currently lacking. In particular, chemically modified HCV subgenomic RNA will be characterized using chromatographic and spectroscopic analyses, as well as an *in vitro* translation/replication competency assay and several biophysical techniques. Additionally, two model protein systems will be characterized to determine the extent and functional effects of chemical modification, with the end goal of modifying recombinant HCV proteins for *in vivo* tracking using CARS microscopy.

To begin, the structural and functional components of the HCV genome and HCV proteins will be discussed, which will serve two functions: 1) it will underscore the importance of using new techniques like CARS microscopy to study HCV; and 2) it will show that the complexity of the HCV genome make functional and structural validation of chemically modified RNA a paramount concern. These discussions will be followed by a comparison of electronic and vibronic approaches to imaging, which segues to an explanation of the theory, current applications, advantages and limitations of CARS microscopy. A discussion of biomolecular modification is followed by an outline of the important features and design of ideal CARS contrast agents. Finally, an outline of the remaining chapters in this thesis will be presented.

Hepatitis C Virus

First identified in 1989, HCV is a blood-borne pathogen that has developed into a global health problem (Figure 1.1). The World Health Organization estimates that approximately 3% of the world's population is infected with HCV, which means there are more than 170 million chronic carriers of the virus[1-3]. Presently, there is no HCV vaccine and current treatments are only 50% effective when properly administered, with cost and significant side effects also limiting efficacy due to patient non-compliance[4]. Owing to these limitations, there has been a concerted effort within the academic community to establish a comprehensive understanding of HCV molecular virology (>21000 Pubmed citations pertaining to HCV from 1989 – 2006). This effort has generally focused on elucidating structural and functional components of the HCV genome and the proteins for which it codes, as well as identifying host-virus interactions that serve as molecular keystones in the HCV life-cycle.

Region	Population (Millions)	Infected (Millions)	Percentage (%)
Africa	602	31.9	5.3
Americas	785	13.1	1.7
Eastern Mediterranean	466	21.3	4.6
Europe	858	8.9	1.03
South-East Asia	1500	32.3	2.15
Western Pacific	1600	62.2	3.9
Totals	**5811**	**169.7**	**3.1**

Figure 1.1: Global distribution of HCV infection. While infection rates are higher in Africa and Asia, HCV is clearly not confined to third-world nations (adapted from 1999 World Health Organization statistics)[2].

While extensive, current knowledge of HCV is not comprehensive. The development and application of new tools to probe processes related to the HCV life-cycle are needed to expand our understanding of HCV. The following is a concise summary of current knowledge on the organization and structure of the HCV genome and viral protein function that will highlight areas of HCV molecular virology where CARS microscopy may provide novel insights that conventional techniques are not able to resolve.

HCV Genomic Structure and Organization

HCV is a single-stranded RNA virus with a 9.6 kb genome that codes for a single open-reading frame (ORF) of approximately 3000 amino acids (Figure 1.2). The large size of the HCV genome is prohibitive to using standard computational and experimental methods of elucidating RNA structural elements. As a result, researchers have been generally limited to studying higher-order structures within the 5' and 3' terminal untranslated regions (UTR) of the HCV genome. The 5'-UTR, which is highly conserved amongst all HCV genotypes, contains an internal ribosomal entry site (IRES) that is essential for cap-independent translation of the RNA genome and plays a role in viral replication[5-8]. As well, the 5'-UTR contains a stem-loop element 5' of the IRES that is important for viral replication and translation[9, 10]. The 3'-UTR contains three distinct domains: a poly(U/UC) tract, a highly conserved 3'-terminal 98-nt sequence and a variable region. It has been shown that the 3' terminal 125-nt sequence is essential for viral replication, with the remaining 3'-UTR serving to increase replicative activity[11-14]. Finally, researchers have demonstrated that the NS5B coding region contains a *cis*-acting RNA (stem-loop) element that is essential for viral replication, likely via forming a kissing-loop interaction with the 3'-

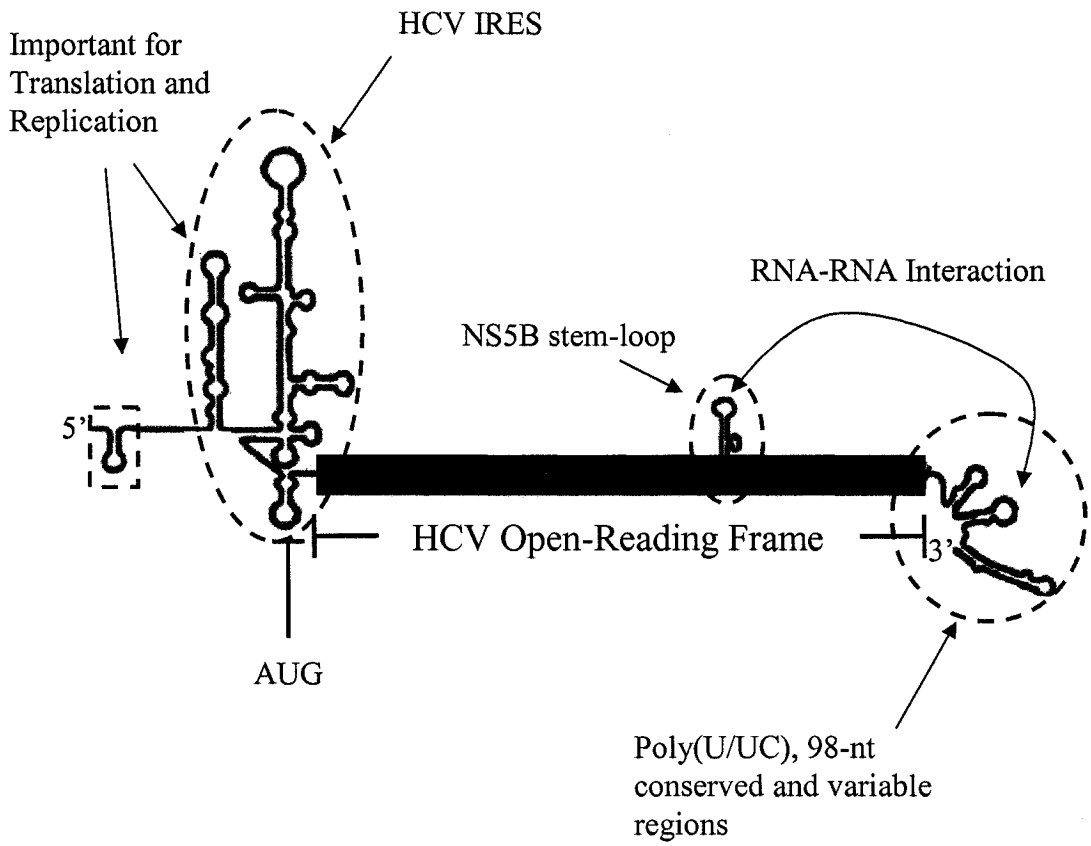

Figure 1.2: HCV genomic structure and organization. The HCV genome encodes a single open-reading frame (orange and blue bars). The 5'-UTR contains the HCV IRES (large green oval), which interacts with the 40S ribosomal subunit and eukaryotic initiation factor 3 to initiate translation and plays a role in viral replication. As well, there is a stem-loop element upstream of the IRES that is important in viral replication and translation (green rectangle). The 3'-UTR contains three distinct domains: a poly(U/UC) tract, a highly conserved 3'-terminal 98-nt sequence and a variable region that are integral to viral replication. The NS5B *cis*-acting RNA element (small green oval) interacts with the 3'-UTR to modulate viral replication. UTRs are not drawn to scale.

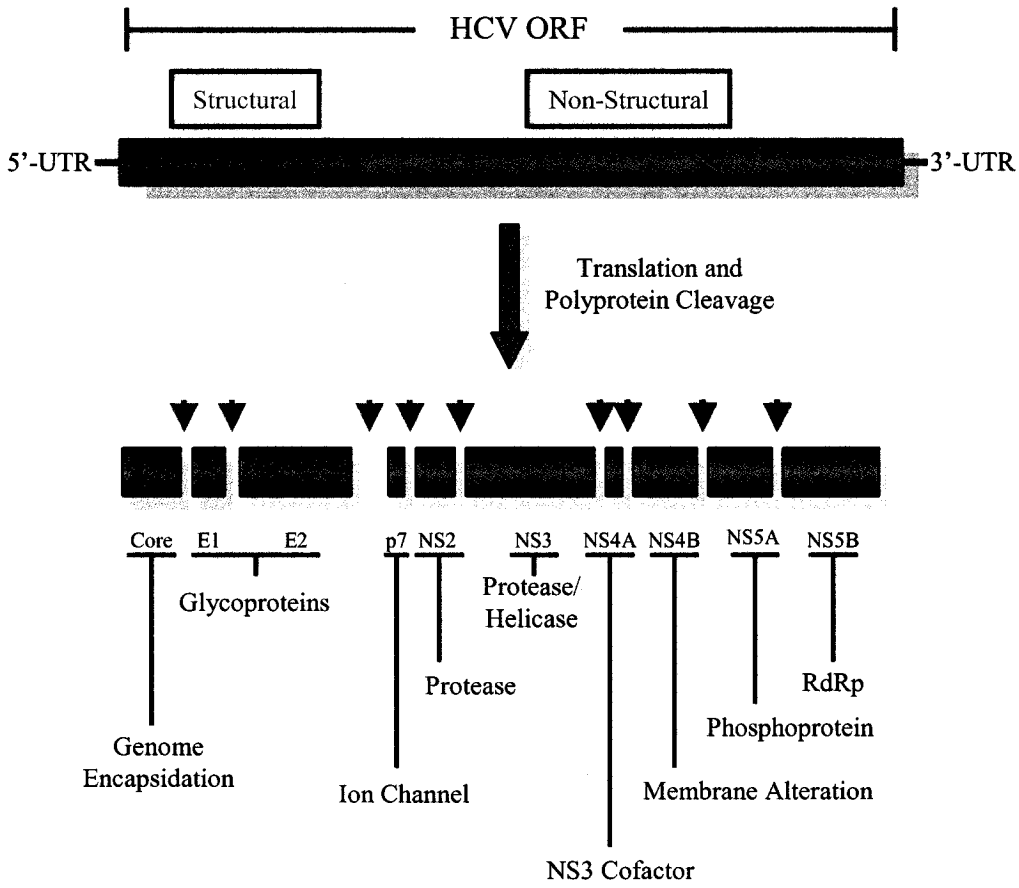

Figure 1.3: The HCV polyprotein. Following translation of the single ORF the polyprotein is cleaved via host (structural) and viral (non-structural) proteases into 10 unique viral proteins. Red arrows indicate host-cell signal peptidase cleavage sites, the blue arrow is the NS2/NS3 cysteine protease cleavage site and the black arrows indicate NS3/NS4A serine protease cleavage sites. The primary functions of the mature proteins are indicated below each cleavage product. The relative size of the proteins are approximated by the size of the bar representing the cleaved protein. RdRp = RNA-dependant RNA polymerase.

UTR[15, 16]. This is the only RNA structural element within the HCV ORF that has been experimentally validated.

The presence of secondary, tertiary and quaternary structural elements are integral features of proteins and RNA that can impose molecular architecture and mediate cellular function[17-20]. For HCV, these functions include translation and replication, as well as viral packing and assembly of mature virion particles. Energetically, the intramolecular interactions involved in forming these higher-order structures range from the weaker, more abundant Van der Waals, hydrogen- bonding and coulombic interactions to the much stronger and less frequent disulfide bonds, which are covalent interactions. However, since the majority of these interactions are inherently weak, moderate systemic perturbations (i.e.: incorporating modified nucleotides, labeling specific residues, altering pH or ionic strength, etc.) can produce serious structural and/or functional perturbations.

Given these considerations, it is of fundamental importance to identify structural and functional perturbations resulting from the chemical modification of the HCV genome, as functionally important structural domains may be altered in the presence of unnatural and/or modified nucleobases. This thesis will examine the functional and structural changes resulting from the chemical modification of HCV subgenomic RNA. Doing so will enable the development of an optimal system (i.e.: one with minimal perturbations) for investigating dynamical processes using CARS microscopy.

HCV Viral Proteins

The polyprotein produced from the HCV ORF is co- and post-translationally cleaved by host (structural proteins) and viral (non-structural proteins) proteases into 10 viral proteins (Figure 1.3)[21]. These 10 proteins are subdivided into two broad categories: the structural

proteins – Core, E1, E2 and p7 – whose primary functions are believed to be packing of infectious viral particles, as well as entry and export from the host-cell following maturation of the intact virion[22, 23]; and the non-structural proteins – NS2, NS3, NS4A, NS4B, NS5A and NS5B – whose varied functions will be discussed in more detail below.

NS2 is an integral membrane protein that has been implicated in host-cell gene regulation, as an inhibitor of apoptosis and a possible cofactor in NS5a phosphorylation[24]. However, the primary function of NS2 is the autocatalytic cleavage of the nascent polypeptide at the NS2-NS3 junction. This protease activity is zinc-dependant and requires the 189 N-terminal amino acids of NS3[21]. NS3 also contains a serine protease domain that, with NS4A as a stabilizer and activator, catalyzes the cleavage of the HCV polyprotein at the NS4A-NS4B, NS4B-NS5A and NS5A-NS5B junctions[25]. Additionally, NS3 contains a helicase domain in the 442 C-terminal amino acids and has been shown to be essential for viral replication via unwinding of double-stranded RNA[26, 27]. NS4B is an integral membrane protein that has recently been shown to facilitate the augmentation of the endoplasmic reticulum to form membranous webs, which are known sites of HCV replication[28, 29]. The primary function of NS5A, a membrane-associated phosphoprotein, is currently unknown. The present consensus, however, is that NS5A is involved, either directly or indirectly, in viral replication, although the mechanism of involvement is yet to be determined[30]. Lastly, NS5B is an RNA-dependent RNA polymerase that fills two fundamental roles during viral replication: 1) synthesis of the negative-sense RNA from the positive-sense genomic RNA; and 2) subsequent synthesis of the subsequent positive-strand progeny RNA[31].

The HCV core, NS3 (helicase) and NS5B proteins, as well as the 40S ribosomal subunit and eukaryotic initiation factor 3 are known to directly interact with structural

domains in the HCV genome to mediate translation, replication and viral assembly[21, 31, 32]. The fundamental role of these protein-RNA interactions to the viral life-cycle underscores the importance of properly characterizing not only chemically modified HCV proteins, but also chemically modified HCV RNA, as the modifications may perturb structural domains that mediate integral components of the HCV life-cycle.

Models of HCV Replication and Infection

In order to study the function of normal and chemically modified HCV RNA and HCV proteins, cell culture models of HCV molecular virology were required. Historically, the primary means of studying the virus *in vivo* was through infection of cell cultures and primary cell lines with HCV-infected sera, or culturing primary cells isolated from persistently infected patients[33]. Later attempts to develop chimpanzee and small animal models of HCV infection met with modest success, but widespread use was limited due to ethical and financial considerations[33-35]. In tandem with *in vitro* biochemical analysis these methods were successful at delineating many aspects of HCV molecular virology. But the lack of viral persistence and low infectivity of these systems necessitated the development of a more efficient methodology for studying HCV.

The legacy of developing an efficient cell culture model of HCV infection began with the discovery that HCV genomic RNA transcribed from a cDNA clone initiated infection and viral hepatitis in chimpanzees[36]. Following from this, Lohmann and co-workers established a human hepatoma cell line (Huh-7) that stably replicated a non-infectious subgenomic HCV replicon (from herein this replicon will be referred to as HCV RNA; Figure 1.4)[37]. The subgenomic replicon contains the NS3 – NS5B segment of the HCV ORF, which is under the control of the *Encenphalomyocarditis* virus (EMCV) IRES, and the 5'- and 3'-UTRs of the

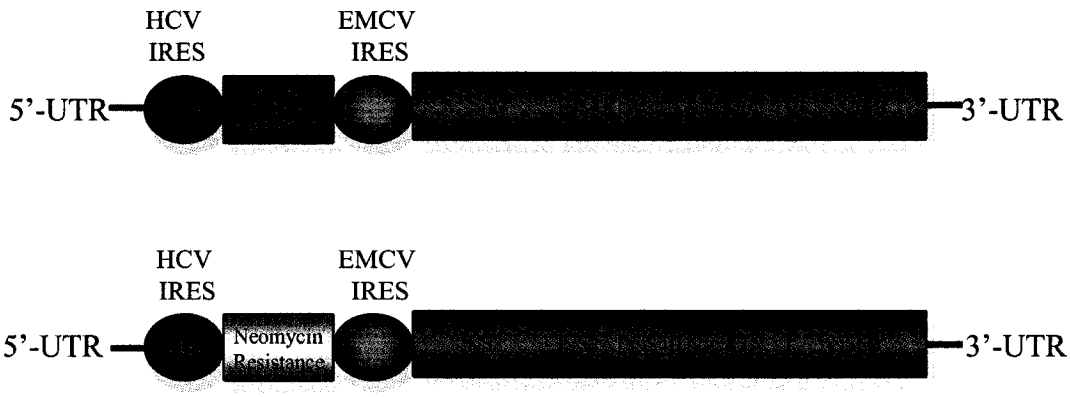

Figure 1.4: Schematic organization of the HCV subgenomic replicon. The 5'- and 3'UTRs and the NS3 – NS5B regions are requisite for viral replication in cell culture. Expression of the HCV coding region is driven by the EMCV promoter. Two variants contain either the firefly luciferase reporter gene (top) or the neomycin resistance selection gene (bottom), both of which are controlled by the HCV IRES.

HCV genome. These are the structural and functional components of the HCV genome that are requisite for efficient viral replication in cell culture[38]. In addition, upstream of the EMCV IRES, the HCV IRES controls the translation of either a neomycin resistance gene or a firefly luciferase reporter gene[38, 39]. Subsequent studies of the clone used to establish the stably replicating Huh-7 cell line revealed that the efficiency of viral replication was due to a series of cell culture-adaptive mutations[39].

Recent work has lead to the development of two cell-based models of HCV infectivity, including the first fully replicating infectious cell culture models of HCV[23, 40-42]. Also, a clone that efficiently replicates in cultured Huh-7 cells in the absence of cell culture-adaptive mutations has been identified[43]. However, working with infectious models of HCV requires Biosafety Level 3 containment procedures, which limits the accessibility of this system. Therefore, despite these recent advances, the Huh-7 subgenomic replicon system is still the work-horse technique for studying HCV molecular virology in cell culture.

The *in vitro* transcription (IVT) of HCV subgenomic replicon RNA to accommodate transient transfection and expression of viral RNA and proteins is well established[39]. This thesis will exploit the IVT of HCV RNA to introduce co- and post-translational chemical modifications that will enable the visualization of modified RNA via CARS microscopy.

Cellular Imaging of HCV

In combination with the subgenomic replicon system, researchers have used a plethora of techniques to characterize the HCV life-cycle. However, studies incorporating imaging of HCV specific effects and viral biomolecules *in vivo* are limited to electron and confocal fluorescence microscopy. Electron microscopy (and derivatives thereof) has found use as a tool for identifying and investigating the membranous web where HCV is known to

replicate[28, 44]. Also, it has been used to characterize the intact virion (*in vivo* and *ex vivo*) and HCV core particles[45-47]. Perhaps the most widely used imaging technique to study HCV has been confocal fluorescence microscopy, which is used in indirect immunofluorescence analysis (for representative examples see [37, 39, 44, 48]).

Noteworthy, is that there have been a limited number of attempts to *directly* localize HCV RNA *in vivo*[44, 49]. Several groups have used 5-bromouridine-5'-triphosphate metabolic labeling to indirectly localize positive-sense RNA by showing that negative-sense RNA co-localizes with components of the viral replication complex[29, 50]. Additionally, the location of the HCV RNA can be deduced by assuming co-localization with proteins of the replication complex. While undoubtedly accurate, these last two examples are still localizations by inference, rather than direct visualization of HCV RNA.

Finally, there is an absence of research examining dynamical aspects of viral protein/RNA localization and HCV-induced phenotypes. The fundamental reason for this is inherent in the primary method used to study HCV in cell culture - indirect immunofluorescence, which requires that cells be chemically fixed to a substrate prior to staining[51]. Owing to this necessity, indirect immunofluorescence can only provide static images of HCV processes.

The lack of suitable tools to study dynamical processes in real-time creates an important information gap between viral entry and RNA processing, motility and localization, as well as viral protein production and localization. Facilitating a synoptical view of HCV molecular virology necessitates filling this gap by performing dynamic analyses of HCV RNA and proteins *in vivo*. This thesis will attempt to expand the utility of an existing imaging modality (CARS microscopy) to enable imaging with molecular specificity. In particular, the chemical modification of HCV RNA and HCV proteins will be

pursued to obtain dynamical information about HCV related processes. A comparison of microscopies grounded in different methods of generating image contrast will be provided to introduce CARS microscopy, as well as underscore its advantages and provide justification for chemically modifying biomolecules to enable its use.

Vibronic Microscopy

The use of electronic (fluorescence) microscopy is ubiquitous in multiple areas of *in vivo* imaging[52-56]. This prevalence has been driven in part by the application of confocal imaging techniques to fluorescence microscopy, as well as by the speed of image acquisition (milliseconds to seconds) and the plethora of small-molecule and protein-derived chromophores that have been developed[57, 58]. A significant drawback of this technique, however, is the time-intensive sample preparation (generating and optimizing expression of fluorescent fusion proteins, staining cells, etc.). Seeing this as an unnecessary hurdle to *in vivo* imaging, many recent studies have used vibronic (Raman and to a lesser extent IR) microscopy as the primary means of microscopic characterization[59-62]. The fundamental reasons behind this resurgence are explained below.

Vibronic versus Electronic Microscopy

When juxtaposing the utility of vibronic and electronic microscopy for *in vivo* analysis, there are three intrinsic differences that must be addressed. Firstly, the energy required to excite a system from the $\nu_0 \rightarrow \nu_1$ vibrational level is approximately 5% of that required for a typical electronic transition [63]. Owing to this, the effects of laser-induced, localized sample heating in Raman and IR are minimized when compared to fluorescence. It follows, that heat-sensitive biological samples will maintain their integrity during

longitudinal vibronic analysis better than in analogous fluorescence-based studies. Thus, the use of vibronic over electronic imaging would be advantageous for an *in vivo* time-course analysis of dynamic cellular processes.

The second difference between vibronic and electronic microscopy pertains to the propensity of fluorescent probes to photobleach upon prolonged or repeated excitation. Such photobleaching often generates reactive species (free radicals) that have repeatedly been shown to have a myriad of deleterious effects when present at elevated cellular levels[64-66]. The build-up of cellular damage from these reactive species has two fundamentally important consequences pertaining to the study of HCV: 1) it can activate apoptotic pathways resulting in cell death; or 2) it may facilitate the expression of an abnormal phenotype that is not characteristic of HCV infection (which includes, but is not exclusive to, an apoptotic phenotype). Since Raman and IR promote vibrational transitions, which do not cause photobleaching, the effects of reactive-species-mediated cellular damage is effectively removed as a confounding variable.

Finally, vibronic microscopy can provide chemically specific information by examining the location and band shape of distinct functional group resonances (i.e.: amide, phosphate, aliphatic, etc.). This approach has been successfully applied to investigate aspects of cancer biology in unstained cells[67-71]. In contrast, electronic microscopy is limited to obtaining spectral information about specific chromophores, which do not carry the same information content found in vibrational resonances. Thus, the diversity of chemical and biochemical information that can be obtained via vibronic microscopy increases the amount of information garnered per experiment.

It should be noted that multiphoton fluorescence microscopy can minimize photobleaching because excitation is confined to a tightly focused, sub-micron sized

volume[72]. Furthermore, since excitation is dependant on multiple low-energy photons rather than one high-energy photon, the effects of localized sample heating can be reduced[72]. However, these effects are still present and could build over longitudinal analyses to produce the deleterious effects outlined above and the information content is still less than that attainable using vibronic microscopy.

Raman versus IR – Scattering or Stretching?

Given the above advantages of using vibronic over electronic approaches to *in vivo* imaging, what then determines the efficacy of Raman versus IR microscopy for studying HCV? While often used to obtain complementary molecular information, there are several elementary differences between Raman scattering and IR absorbance. First, the visible excitation wavelengths used for Raman offer better lateral resolution than the longer excitation wavelengths used in IR microscopy[73]. Second, the selection rules between Raman and IR are different. This is potentially relevant to the intense water absorption flanking the aliphatic region of the Raman spectrum, which can be problematic when imaging certain cellular constituents (i.e.: lipids) by IR[74]. Finally, it is important to consider the requisite time necessary to acquire images by Raman. Raman scattering is an inherently weak technique, with one Raman photon being produced for every 10^{10} incident photons[75]. Also, considering that Raman microscopy is a raster-scanning technique, it can take 10 – 20 hours to collect a single high-resolution (~500 nm lateral resolution) Raman image of a 10 μm cell. Clearly, Raman is an ineffective technique if utilized for the dynamical imaging of live-cells. While the acquisition times for IR microscopy (1 – 2 hours) are markedly better than Raman, they are still long enough to preclude using IR for dynamical real-time analysis *in vivo*.

With the outlined limitations of confocal fluorescence, as well as the above limitations of Raman and IR microscopy it would seem that neither electronic nor vibronic microscopy is ideally suited to studying *in vivo* processes in real-time. However, in 1999 researchers at Pacific Northwestern Laboratories revived a technique known as CARS microscopy, which combines aspects of Raman and fluorescence microscopy that are advantageous to studying such processes into one vibration-based imaging technique[76].

Coherent Anti-Stokes Raman Scattering Microscopy

Theory and Advantages over Raman and IR Microscopy

CARS microscopy is effectively a non-linear optical version of conventional Raman scattering that relies upon two spatially overlapped lasers to generate a coherent anti-Stokes Raman signal (Figure 1.5)[77]. The four-wave-mixing process commences when a pump photon (k_{pump}) brings a system from the ground-state vibrational configuration (v_0) to a virtual excited state (vs_1), which is followed by relaxation to the v_1 vibrational level upon interaction with the Stokes beam (k_{Stokes}). Following the absorbance of a second pump photon the system spontaneously relaxes to the ground-state (via a second virtual state, vs_2). This relaxation is accompanied by the emission of an anti-Stokes photon, henceforth referred to as the CARS signal. When the frequency difference between the pump and Stokes beams is adjusted to correlate with a predetermined $v_0 \rightarrow v_1$ transition, the CARS signal is resonantly enhanced [77]. This gives CARS microscopy the capacity to generate image contrast specific to intrinsic Raman modes (i.e.: amide I band, CH_2 lipid stretch, etc.), making it a label-free approach to *in vivo* imaging. CARS microscopy also possesses all the advantages that vibronic microscopy has when compared with electronic microscopy (as outlined above).

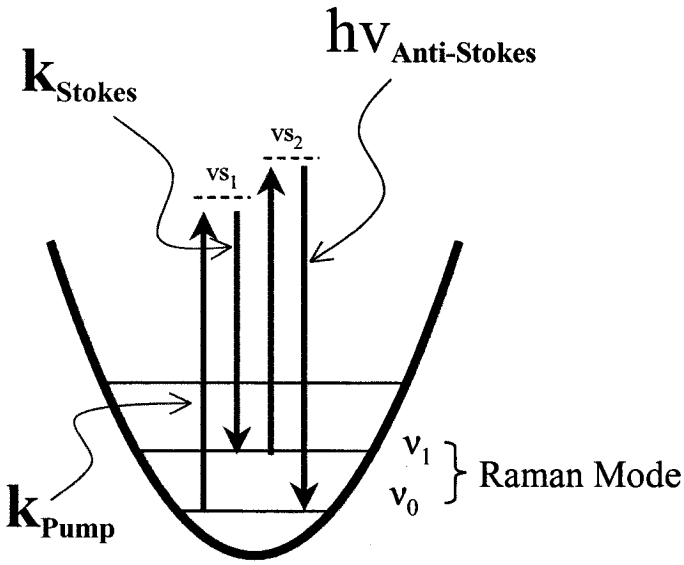

Figure 1.5: Coherent anti-Stokes Raman scattering (CARS). Following excitation from ν_0 to a virtual vibrational state (vs_1) by a pump photon (k_{pump}), a collinearly and temporally aligned Stokes photon (k_{Stokes}) relaxes the system to the ν_1 vibrational level. After this, a second pump photon interacts with the system, with the net result being the spontaneous relaxation of the system (via vs_2) to the ground state and corresponding anti-Stokes photon ($h\nu_{anti\text{-}Stokes}$) emission. The frequency difference between pump and Stokes beams is tuned to correlate to a $\nu_0 \rightarrow \nu_1$ transition that is characteristic of a specific Raman mode (i.e.: amide I band, CH2 lipid stretch, etc.).

However, when contrasted against IR and Raman microscopy (i.e.: other vibronic techniques) the advantages of using CARS become apparent. Firstly, because the anti-Stokes photon is blue-shifted relative to the incident beam, red-shifted phenomena are removed as contaminating light sources. This is significant in that it eliminates one-photon fluorescence, which is a common problem when working with other forms of vibrational microscopy, especially Raman[78]. Secondly, CARS is a coherent process, which means that molecular vibrations within the focal volume interfere constructively and with directionality. This results in the CARS signal being proportional to the squared modulus of the number of vibrational modes within the focal volume, as opposed to being a linear function of concentration as are Raman and IR microscopy[76]. Finally, following from the last point, the coherent and directional CARS signal translates into very fast acquisition times, which have recently been optimized to rates approaching 30 frames per second[79]. This frame rate enables the construction of videos illustrating cellular processes with chemical specificity. Given these advantages and those outlined previously for vibronic microscopy in general, it is clear that CARS microscopy incorporates the sensitivity of fluorescence with the non-invasiveness and chemical selectivity of Raman. Thus, CARS is a promising technique for studying cellular processes in real-time *in vivo*.

Current Applications

The most ubiquitous application of CARS microscopy to date pertains to imaging changes in the lipid profile of live-cells by tuning the CARS microscope to the CH_2 lipid stretch. Specifically, researchers have demonstrated that CARS microscopy can be used to monitor apoptotic changes in lipogenesis, follow organelle transport and can be an important tool in elucidating differentiation kinetics as they relate to lipogenesis[80-82]. More recently,

potential applications to real-time non-invasive optical histology have been demonstrated in mice[79]. On top of these cellular studies, researchers have also examined model lipid bilayers using CARS microscopy to determine lipid distribution profiles across the bilayer, to understand the ordering of water molecules at the bilayer-water interface, as well as to study the orientation and composition of myelin figures (*in vitro* models of myelin sheaths) [83-85].

Following these innovative successes, work from our group (in collaboration with the Xie group from Harvard University) has exploited CARS microscopy to investigate changes in the lipid droplet profile of HCV infected Huh-7 cells following treatment with a small-molecule that perturbs the HCV life-cycle[48]. As well, a novel study that combines CARS with two-photon fluorescence to simultaneously examine the localization of HCV RNA and the changes in lipid homeostasis associated with viral replication and translation was conducted[49].

Limitations of CARS Microscopy

There is a conspicuous absence of research that focuses on Raman modes other than the CH_2 lipid resonance. In fact, to date there have only been five papers reporting on *in vivo* imaging of biomolecules other than lipids[77, 81, 84, 86, 87]. Of these five papers, only one deals with visualizing a dynamic cellular process – namely, transient intracellular hydrodynamics within the microorganism *D. discoideum*. However, it should be pointed out that this study followed the migration of D_2O, as opposed to a biomolecule other than lipids. Three of the remaining four are proof-of-principle papers that use the amide I, O-P-O nucleotide backbone and C-O DNA vibrational modes to demonstrate the application of different CARS experiments to cellular imaging. The final paper examines lipid distribution in model membranes through the use of deuterated and normal lipids (tuning the CARS microscope to

the C-D resonance instead of the C-H resonance generates contrast that is specific to the deuterated lipids).

There are two fundamental limitations to CARS microscopy that are responsible for the lack of research using vibrational modes other than the CH_2 lipid resonance. First, the CARS signal is proportional to the squared modulus of the number of vibrational modes within the focal volume. This is an advantageous feature when studying a molecule that presents a very high mode density within the focal volume; lipids are ideally suited to this, as they possess a very high spatial density of CH_2 vibrational modes. However, when studying proteins, nucleic acids, or other cellular constituents the relative focal volume density of, for example, the amide I or O-P-O nucleotide backbone vibrational resonances are considerably less than the CH_2 lipid resonance. Owing to the quadratic concentration dependence of the CARS signal, this results in an exponential decrease in the CARS signal of these modes. Therefore, the utility of CARS microscopy in the study of biomolecules other than lipids is severely limited.

When the major cellular constituents – proteins, lipids, nucleic acids and carbohydrates – and the different vibrational modes they contain are considered, the second limitation of CARS becomes apparent. As an illustrative example, consider what biomolecule-specific vibrational modes proteins contain in high abundance (low abundance modes will likely not be visible by CARS because of the quadratic concentration dependence outlined above). The only answer that satisfies both of these requirements is the amide I vibrational resonance. What then happens if you want to look at one specific protein? Because there are no vibrational modes unique to any one protein present in sufficient abundance, CARS microscopy cannot generate contrast for a specific protein. Rather, CARS will afford an image of the entire cellular protein complement. Analysis of the other major

cellular constituents yields similar results – CARS is limited to imaging classes of macromolecules as opposed to specific molecular targets.

CARS Contrast Agents

In order to track specific biomolecules in real-time *in vivo* using CARS microscopy there must be a mechanism of generating image contrast that is unique to those particular biomolecules. Having stated that there are no endogenous modes that facilitate this, it becomes apparent that an exogenous Raman mode must be introduced to meet this requirement. There are several desirable properties that such an exogenous Raman mode should possess: 1) it should present a Raman signature that is orthogonal to all endogenous Raman modes; 2) covalent attachment of the probe should be easy and reproducible; 3) it should be chemically inert in a biological context; and 4) the structure of the Raman mode should enable the lowest possible detection limit with current CARS instrumentation (i.e.: it should have a high Raman scattering cross-section).

The necessity of adding additional chemical contrast to image biomolecules with CARS microscopy meant that the ability to generate label-free image contrast was compromised. But CARS still possesses all of the advantages of being a form of vibronic microscopy, as well as those pertaining to advances in instrumentation (specifically, the capacity for video-rate acquisition)[79, 88-91]. The loss of one advantage, therefore, does not diminish the benefits of CARS microscopy for studying biological processes in real-time *in vivo*. Rather, the acquired ability to generate image contrast with both chemical *and* molecular specificity will significantly expand the utility of CARS microscopy, making it more accessible for analyzing cellular processes outside of lipid homeostasis.

With the goal of expanding the utility of CARS microscopy to enable the real-time study of HCV *in vivo*, this thesis will examine the attributes of an ideal CARS contrast agent and identify the Raman modes amenable to *in vivo* analysis following chemical conjugation to a biomolecule.

Designing Optimal CARS Contrast Agents

Ideal Chemical Modification Agents

Tracking specific molecular targets using CARS microscopy required the chemical manipulation of biomolecules to incorporate a bio-orthogonal Raman mode (i.e.: a CARS contrast agent) that facilitates the generation of image contrast specific to the modified biomolecule. There are several important features that a CARS contrast agent should possess: 1) covalent attachment of the probe should be water-compatible, easy and reproducible; 2) a Raman signature that is orthogonal to all endogenous Raman modes; 3) be chemically inert in a biological context; and 4) a structure that maximizes the Raman scattering cross-section of the orthogonal mode. Each of these attributes will now be addressed in more detail.

Biocompatible Chemistry

A survey of the literature revealed a variety of strategies that satisfy the first requirement. The site-specific incorporation of unnatural amino acids via amber suppressor and chemical ligation methodologies were attractive options for incorporating CARS contrast agents, but are limited to protein modifications[92-96]. Taking advantage of water-compatible organic transformations, Staudinger (and traceless Staudinger) ligations and click reactions (Hüisgen [3+2] cycloadditions) have recently been used for the biomolecular modification of

carbohydrates, DNA, protein and lipids[96-98]. Mechanistically, the Staudinger ligation proceeds through an azaphosphine ylide to yield an amide and the corresponding phosphine oxide. Click reactions require a Cu^{2+} catalyst to conjugate an alkyne and an azide in a concerted [3+2] cycloaddition reaction. The synthetic steps necessary to form suitable phosphines in the Staudinger ligation and the fundamental necessity of an alkyne-azide pair for click reactions would limit the ability to rapidly apply these bioconjugation reactions to a variety of systems involving different classes of biomolecules. Therefore, they were not pursued as reactions amenable to chemically coupling CARS contrast agents to biomolecules.

Two methods that generate reproducible biomolecular modification with a minimum of synthetic manipulations utilize N-hydroxysuccinimidyl- (NHS) and maleimide- (M) functionalized compounds[99-101]. NHS-functionalized acids preferentially react with primary amines in aqueous solution, forming a thermodynamically stable amide while consuming the higher-energy ester. Mechanistically, the reaction proceeds via nucleophilic attack by the amine onto the NHS-activated ester, which is followed by collapse of the tetrahedral intermediate to form the thermodynamically favored amide with the release of N-hydroxysuccinimide (Scheme 1.1A). M-functionalized probes target reactive thiols for chemical conjugation; this reaction occurs via 1,4-addition of the thiol to the Michael acceptor contained in the M group (Scheme 1.1B). The subsequent collapse of the enolate intermediate yields the reduced M conjugated to the reactive thiol. By combining these two strategies, it is possible to maximize the number of systems that can be studied with first generation CARS contrast agents. In particular, the modification of HCV RNA and HCV proteins would both be accessible using NHS- and M-activated CARS contrast agents.

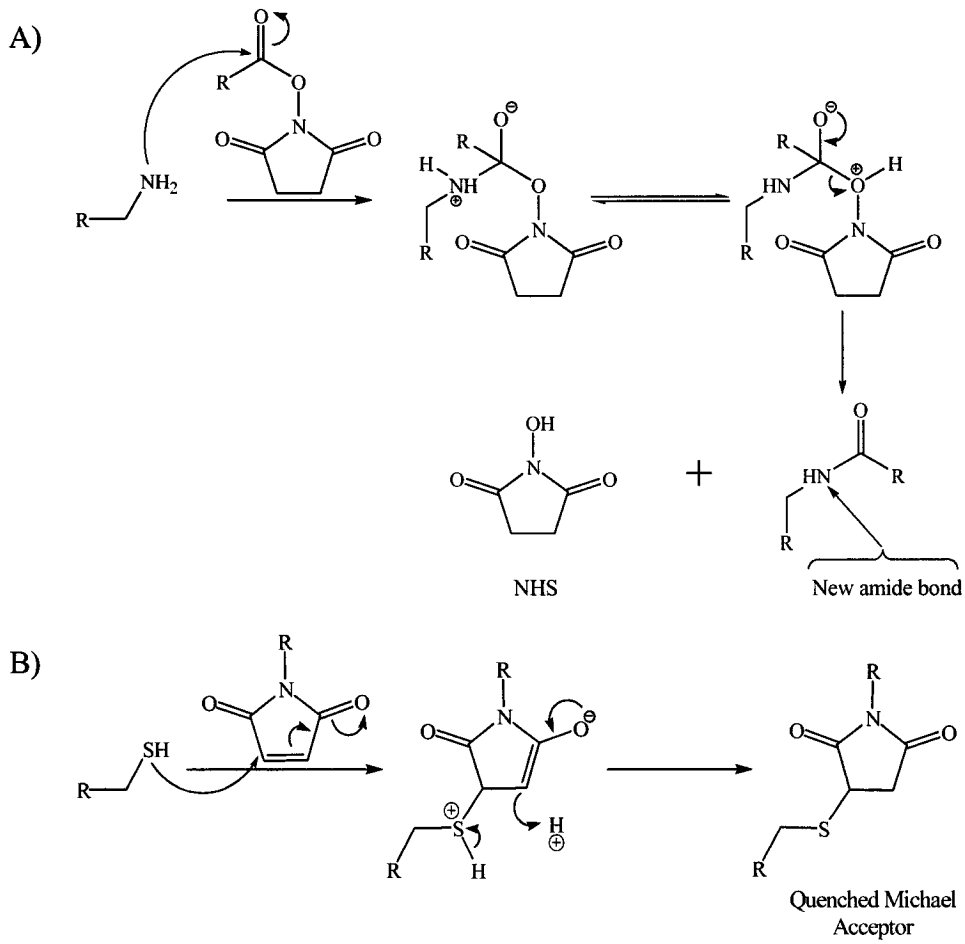

Scheme 1.1: Strategies for biomolecular modification using NHS- and M-activated probes. A) Nucleophilic attack of the primary amine results in a tetrahedral intermediate that collapses to yield the thermodynamically favoured amide bond, with concomitant consumption of the higher energy NHS-ester. B) 1,4-addition of a reactive thiol proceeds via quenching of the Michael acceptor on the M group. R = any biomolecule with primary amines (A) or reactive thiols (B).

Features of Bio-Orthogonal Raman Modes

In order to meet the second requirement, the vibrational modes present in typical eukaryotic cells were assessed by homogenizing and lyophilizing Huh-7 cells and analyzing the resulting lysates by Raman spectroscopy (Figure 1.6). The spectrum displayed all of the expected Raman modes that correlate to the primary cellular constituents: an aliphatic region, primarily displaying lipid CH_2 and CH modes (2700 – 3100 cm^{-1}); a carbon-heteroatom region that contains the amide I band and many other nucleobase, carbohydrate and lipid modes (1000 – 1750 cm^{-1}); and a fingerprint region that does not contain any diagnostically useful resonances (400 – 1000 cm^{-1}). The most striking feature of this spectrum is the Raman transparent region from 1800 to 2700 cm^{-1}. Raman resonances in this region are generally cumulene systems (CO_2, ketene, etc.) or contain triple bonds (acetylenes, molecular nitrogen, azides and cyano). It is also important to note the presence of a carbon-deuterium (C-D) vibrational mode around 2200 cm^{-1}. By synthesizing CARS contrast agents containing a Raman resonance that falls in the transparent region, modified biomolecules can be visualized to the exclusion of all others.

While their Raman signatures are desirable, conjugation to an NHS- or M-activated carrier scaffold is not possible for CO_2 or N_2 because they are inert gases. When surveying the remaining candidates the third requirement must be considered – the CARS contrast agent scaffold should be chemically inert in a cellular context. This prohibited the use of cumulenes, as they hydrolyze in aqueous media[102]. Additionally, the well known toxicity of alkyl-azides precluded their use[103]. The known Raman spectra of unsymmetrical alkyl and aryl acetylene derivatives display weak scattering cross-sections because of the limited polarizability of the alkyne group. This limited the capacity of acetylene derivatives to meet the forth requirement – that the structure of the contrast agent should maximize the Raman

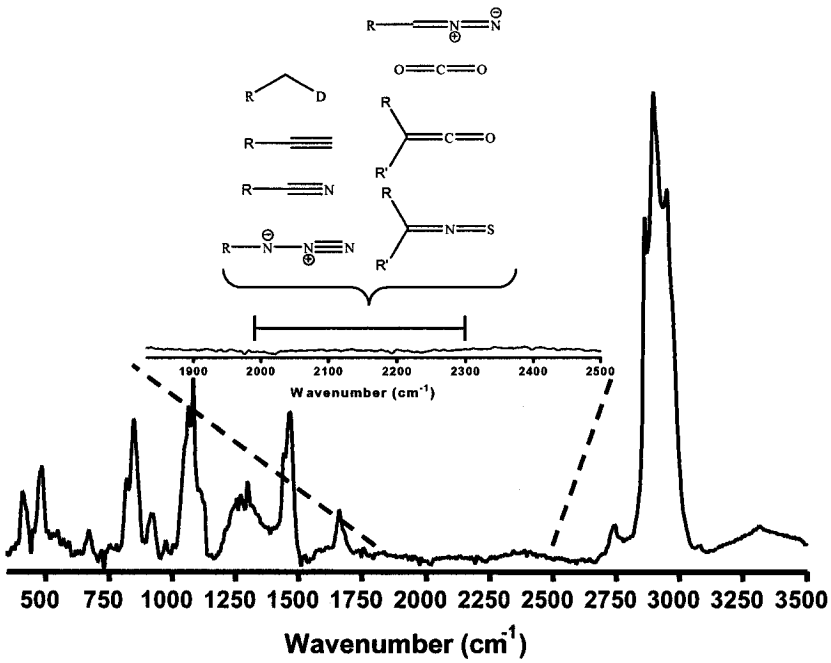

Figure 1.6: Designing CARS contrast agents. The Raman transparent region from 1800 to 2700 cm-1 contains a variety of Raman modes that could be used to develop CARS contrast agents. When weighed against all other considerations, the C-D and CN modes were chosen to be the best suited to creating CARS contrast agents. Spectrum was integrated over 30 sec. R = R' = contrast agent scaffold.

scattering cross-section of the orthogonal mode. Therefore, acetylenic Raman modes were not pursued as CARS contrast agent candidates. With the elimination of all other modes present in the transparent region of the cell, the cyano (CN) and C-D groups were determined to be the optimal candidates for generating vibrational image contrast to localize specific biomolecules in real-time *in vivo* using CARS microscopy.

Initial investigations into the CN mode focused on acetonitrile as a model compound. Following normalization to 10 mM (which is a conservative estimate of eventual *in vivo* localized probe concentration), the Raman scattering cross-section of acetonitrile was determined to be below current CARS detection limits (Figure 1.7). Therefore, if CN was to be used as a CARS contrast agent, the scattering cross-section needed to be increased. This was achieved by increasing the polarizability of the CN via conjugation with an aromatic system. Comparing the acetonitrile data to a system in which the CN mode was conjugated with a benzene ring proved the validity of this concept (Figure 1.7). Therefore, a CN group conjugated to an aromatic system that is further activated with either an NHS ester or M group should serve as an ideal scaffold on which to build a series of CARS contrast agents (Figure 1.8A). Based on these findings, 3- and 4-cyanobenzyl-NHS (3-/4-CN-NHS) and 3- and 4-cyanobenzyl-M (3-/4-CN-M) CARS contrast agents were generated with the goal of chemically modifying biomolecules to pursue *in vivo* detection using CARS microscopy.

Based upon previous successes, the C-D mode was determined to be an excellent candidate for generating CARS contrast agents[84, 86]. However, the intrinsically low scattering cross-section of the C-D mode problematizes the visualization of deuterated molecular targets *in vivo*. Rather than increase the Raman scattering cross-section, it was believed that incorporating a multitude of C-D modes per biomolecule would overcome this issue (Figure 1.8B). The C-D mode is ideally suited to such an approach, as a hydrogen-

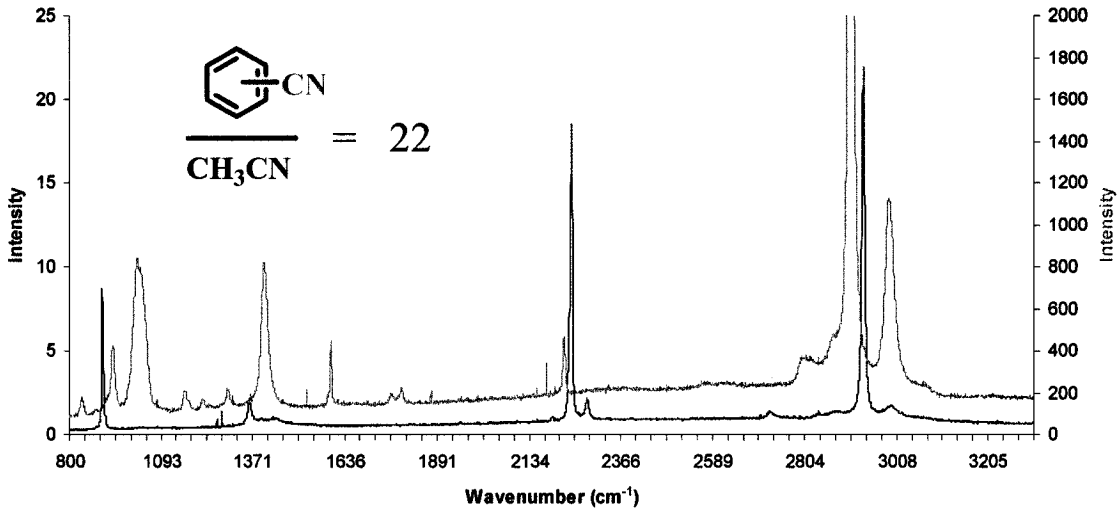

Figure 1.7: Aliphatic versus aromatic CN Raman cross-sections. When the cyano peak of an aromatic CN benzene derivative (2224 cm^{-1}, orange) was contrasted to that of acetonitrile (2244 cm^{-1}, blue), the Raman scattering cross-section of the aromatic CN was found to be 22-fold greater. Both spectra were integrated over 30 sec.

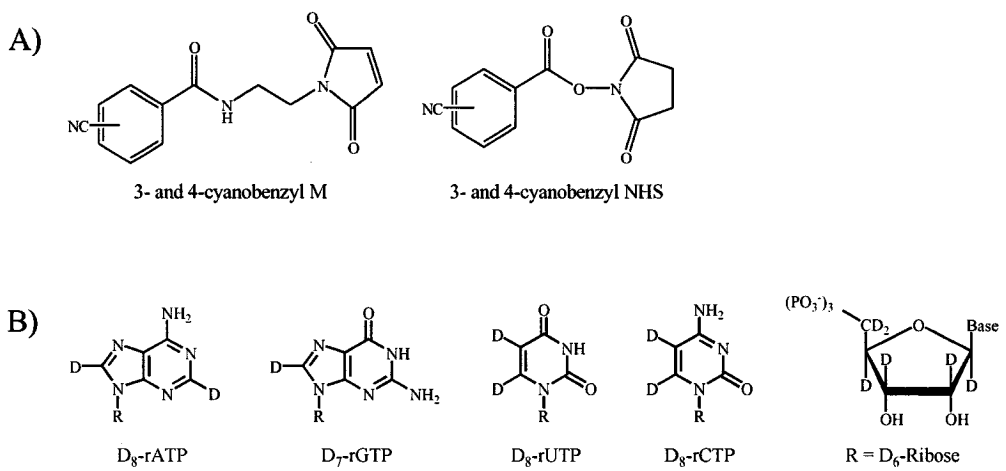

Figure 1.8: Structures of CARS contrast agents. A) Structures of the cyanobenzyl CARS contrast agents. The M series will be used to label reactive thiols and the NHS series will be used to label reactive amines. B) Deuterium substitutions in the nucleobase and ribose sugars that will be used as CARS contrast agents. R = nucleotide backbone.

deuterium substitution is not likely to have a significant structural or functional effect on the modified biomolecule.

This thesis will exploit the location of the CN and C-D vibrational resonances to extend the capabilities of CARS microscopy to include the *in vivo* imaging of specific molecular targets – in this case, those biomolecules modified with CN and C-D modes. The use of NHS- and M-functionalized CARS contrast agents will enable the same CN contrast agents to be used for studying proteins and RNA.

Outline

While largely focused on structural and functional changes to biomolecules following small-molecule modification, the underlying goal of this thesis is to develop a solid framework from which CARS microscopy can expand and fundamental aspects of HCV molecular virology can be investigated. Chapter one begins with a general discussion of the rational design of CARS contrast agents, with emphasis on fulfilling the principles outlined. Following this, the application of CARS contrast agents to studying HCV will be explored through the labeling of HCV subgenomic replicon RNA. Chapter one will conclude with a thorough analysis of labeled HCV RNA to: 1) confirm the success of the labeling reaction and the extent of contrast agent incorporation; and 2) examine the functional and structural effects of modifying HCV RNA with CARS contrast agents.

Chapter two departs from characterizing samples destined for *in vivo* analysis and focuses on the modification of proteins with CARS contrast agents. Method development and validation will be conducted on two model protein systems; bovine serum albumin (BSA) and a single-domain antibody (sdAb) directed against bacterial protein A. However, the end-goal of this research is to apply the methodologies established on the model systems

to the chemical modification of HCV proteins to investigate dynamical processes *in vivo* using CARS microscopy. This thesis will conclude with a summary of key findings and discuss potential avenues for future research.

References

1. Choo, Q., Kuo, G., Weiner, A., Overby, L., Bradley, D., and Houghton, M., Isolation of a cDNA clone derived from a blood-borne non-A, non-B viral hepatitis genome. *Science*, 1989. **244**(4902): p. 359-362.
2. Organization, W.H., Hepatitis C Virus Fact Sheet No. 164. *http://www.who.int /mediacentre/factsheets/fs164/en/index.html*, Revised 1999.
3. Simmonds, P., Genetic diversity and evolution of hepatitis C virus - 15 years on. *J Gen Virol*, 2004. **85**(11): p. 3173-3188.
4. McHutchison, J.G., Bartenschlager, R., Patel, K., and Pawlotsky, J.-M., The face of future hepatitis C antiviral drug development: Recent biological and virologic advances and their translation to drug development and clinical practice. *Journal of Hepatology*, 2006. **44**(2): p. 411-421.
5. Bukh, J., Purcell, R., and Miller, R., Sequence Analysis of the 5' Noncoding Region of Hepatitis C Virus. *PNAS*, 1992. **89**(11): p. 4942-4946.
6. Odreman-Macchioli, F., Baralle, F.E., and Buratti, E., Mutational Analysis of the Different Bulge Regions of Hepatitis C Virus Domain II and Their Influence on Internal Ribosome Entry Site Translational Ability. *J. Biol. Chem.*, 2001. **276**(45): p. 41648-41655.
7. Honda, M., Ping, L.-H., Rijnbrand, R.C.A., Amphlett, E., Clarke, B., Rowlands, D., and Lemon, S.M., Structural Requirements for Initiation of Translation by Internal Ribosome Entry within Genome-Length Hepatitis C Virus RNA. *Virology*, 1996. **222**(1): p. 31-42.
8. Honda, M., Brown, E.A., and Lemon, S.M., Stability of a stem-loop involving the initiator AUG controls the efficiency of internal initiation of translation on hepatitis C virus RNA. *RNA*, 1996. **2**(10): p. 955-968.
9. Friebe, P., Lohmann, V., Krieger, N., and Bartenschlager, R., Sequences in the 5' Nontranslated Region of Hepatitis C Virus Required for RNA Replication. *J. Virol.*, 2001. **75**(24): p. 12047-12057.
10. Beguiristain, N., Robertson, H.D., and Gomez, J., RNase III cleavage demonstrates a long range RNA: RNA duplex element flanking the hepatitis C virus internal ribosome entry site. *Nucl. Acids Res.*, 2005. **33**(16): p. 5250-5261.
11. Friebe, P. and Bartenschlager, R., Genetic Analysis of Sequences in the 3' Nontranslated Region of Hepatitis C Virus That Are Important for RNA Replication. *J. Virol.*, 2002. **76**(11): p. 5326-5338.
12. Ito, T. and Lai, M., Determination of the secondary structure of and cellular protein binding to the 3'-untranslated region of the hepatitis C virus RNA genome. *J. Virol.*, 1997. **71**(11): p. 8698-8706.
13. Yi, M. and Lemon, S.M., 3' Nontranslated RNA Signals Required for Replication of Hepatitis C Virus RNA. *J. Virol.*, 2003. **77**(6): p. 3557-3568.
14. Yi, M. and Lemon, S.M., Structure-function analysis of the 3' stem-loop of hepatitis C virus genomic RNA and its role in viral RNA replication. *RNA*, 2003. **9**(3): p. 331-345.
15. Lee, H., Shin, H., Wimmer, E., and Paul, A.V., cis-Acting RNA Signals in the NS5B C-Terminal Coding Sequence of the Hepatitis C Virus Genome. *J. Virol.*, 2004. **78**(20): p. 10865-10877.

16. Friebe, P., Boudet, J., Simorre, J.-P., and Bartenschlager, R., Kissing-Loop Interaction in the 3' End of the Hepatitis C Virus Genome Essential for RNA Replication. *J. Virol.*, 2005. **79**(1): p. 380-392.
17. Onoa, B. and Tinoco, J., Ignacio, RNA folding and unfolding. *Current Opinion in Structural Biology*, 2004. **14**(3): p. 374-379.
18. Das, S.R., Fong, R., and Piccirilli, J.A., Nucleotide analogues to investigate RNA structure and function. *Current Opinion in Chemical Biology*, 2005. **9**(6): p. 585-593.
19. Helm, M., Post-transcriptional nucleotide modification and alternative folding of RNA. *Nucl. Acids Res.*, 2006. **34**(2): p. 721-733.
20. Thirumalai, D. and Hyeon, C., RNA and Protein Folding: Common Themes and Variations. *Biochemistry*, 2005. **44**(13): p. 4957-4970.
21. François Penin, J.D., Felix A. Rey, Darius Moradpour, Jean-Michel Pawlotsky,, Structural biology of hepatitis C virus. *Hepatology*, 2004. **39**(1): p. 5-19.
22. Ray, R.B. and Ray, R., Hepatitis C virus core protein: intriguing properties and functional relevance. *FEMS Microbiology Letters*, 2001. **202**(2): p. 149-156.
23. Bartosch, B., Dubuisson, J., and Cosset, F.-L., Infectious Hepatitis C Virus Pseudo-particles Containing Functional E1-E2 Envelope Protein Complexes. *J. Exp. Med.*, 2003. **197**(5): p. 633-642.
24. Franck, N., Le Seyec, J., Guguen-Guillouzo, C., and Erdtmann, L., Hepatitis C Virus NS2 Protein Is Phosphorylated by the Protein Kinase CK2 and Targeted for Degradation to the Proteasome. *J. Virol.*, 2005. **79**(5): p. 2700-2708.
25. Hahm, B., Han, D., Back, S., Song, O., Cho, M., Kim, C., Shimotohno, K., and Jang, S., NS3-4A of hepatitis C virus is a chymotrypsin-like protease. *J. Virol.*, 1995. **69**(4): p. 2534-2539.
26. Kim D. W., Gwack Y., Han J. H., and Choe J., C-Terminal Domain of the Hepatitis C Virus NS3 Protein Contains an RNA Helicase Activity. *Biochemical and Biophysical Research Communications*, 1995. **215**(1): p. 160-166.
27. Gwack, Y., Kim, D.W., Han, J.H., and Choe, J., Characterization of RNA Binding Activity and RNA Helicase Activity of the Hepatitis C Virus NS3 Protein. *Biochemical and Biophysical Research Communications*, 1996. **225**(2): p. 654-659.
28. Egger, D., Wolk, B., Gosert, R., Bianchi, L., Blum, H.E., Moradpour, D., and Bienz, K., Expression of Hepatitis C Virus Proteins Induces Distinct Membrane Alterations Including a Candidate Viral Replication Complex. *J. Virol.*, 2002. **76**(12): p. 5974-5984.
29. Gosert, R., Egger, D., Lohmann, V., Bartenschlager, R., Blum, H.E., Bienz, K., and Moradpour, D., Identification of the Hepatitis C Virus RNA Replication Complex in Huh-7 Cells Harboring Subgenomic Replicons. *J. Virol.*, 2003. **77**(9): p. 5487-5492.
30. Blight, K.J., Kolykhalov, A.A., and Rice, C.M., Efficient Initiation of HCV RNA Replication in Cell Culture. *Science*, 2000. **290**(5498): p. 1972-1974.
31. Bartenschlager, R., Frese, M., and Pietschmann, T., *Novel Insights into Hepatitis C Virus Replication and Persistence*, in *Advances in Virus Research*, a.A.J.S. Karl Maramorosch, Editor. 2004, Academic Press. p. 71-180.
32. Ivanyi-Nagy, R., Kanevsky, I., Gabus, C., Lavergne, J.-P., Ficheux, D., Penin, F., Fosse, P., and Darlix, J.-L., Analysis of hepatitis C virus RNA dimerization and core-RNA interactions. *Nucl. Acids Res.*, 2006. **34**(9): p. 2618-2633.
33. Bartenschlager, R. and Lohmann, V., Novel cell culture systems for the hepatitis C virus. *Antiviral Research*, 2001. **52**(1): p. 1-17.

34. Mercer, D.F., Schiller, D.E., Elliott, J.F., Douglas, D.N., Hao, C., Rinfret, A., Addison, W.R., Fischer, K.P., Churchill, T.A., Lakey, J.R.T., Tyrrell, D.L.J., and Kneteman, N.M., Hepatitis C virus replication in mice with chimeric human livers. 2001. **7**(8): p. 927-933.
35. Hong, Z., Beaudet-Miller, M., Lanford, R.E., Guerra, B., Wright-Minogue, J., Skelton, A., Baroudy, B.M., Reyes, G.R., and Lau, J.Y.N., Generation of Transmissible Hepatitis C Virions from a Molecular Clone in Chimpanzees. *Virology*, 1999. **256**(1): p. 36-44.
36. Kolykhalov, A.A., Agapov, E.V., Blight, K.J., Mihalik, K., Feinstone, S.M., and Rice, C.M., Transmission of Hepatitis C by Intrahepatic Inoculation with Transcribed RNA. *Science*, 1997. **277**(5325): p. 570-574.
37. Lohmann, V., Körner, F., Koch, J.-O., Herian, U., Theilmann, L., and Bartenschlager, R., Replication of Subgenomic Hepatitis C Virus RNAs in a Hepatoma Cell Line. *Science*, 1999. **285**(5424): p. 110-113.
38. Appel, N., Schaller, T., Penin, F., and Bartenschlager, R., From Structure to Function: New Insights into Hepatitis C Virus RNA Replication. *J. Biol. Chem.*, 2006. **281**(15): p. 9833-9836.
39. Krieger, N., Lohmann, V., and Bartenschlager, R., Enhancement of Hepatitis C Virus RNA Replication by Cell Culture-Adaptive Mutations. *J. Virol.*, 2001. **75**(10): p. 4614-4624.
40. Hsu, M., Zhang, J., Flint, M., Logvinoff, C., Cheng-Mayer, C., Rice, C.M., and McKeating, J.A., Hepatitis C virus glycoproteins mediate pH-dependent cell entry of pseudotyped retroviral particles. *PNAS*, 2003. **100**(12): p. 7271-7276.
41. Lindenbach, B.D., Evans, M.J., Syder, A.J., Wolk, B., Tellinghuisen, T.L., Liu, C.C., Maruyama, T., Hynes, R.O., Burton, D.R., McKeating, J.A., and Rice, C.M., Complete Replication of Hepatitis C Virus in Cell Culture. *Science*, 2005. **309**(5734): p. 623-626.
42. Wakita, T., Pietschmann, T., Kato, T., Date, T., Miyamoto, M., Zhao, Z., Murthy, K., Habermann, A., Krausslich, H.-G., Mizokami, M., Bartenschlager, R., and Liang, T.J., Production of infectious hepatitis C virus in tissue culture from a cloned viral genome. 2005. **11**(7): p. 791-796.
43. Ikeda, M., Yi, M., Li, K., and Lemon, S.M., Selectable Subgenomic and Genome-Length Dicistronic RNAs Derived from an Infectious Molecular Clone of the HCV-N Strain of Hepatitis C Virus Replicate Efficiently in Cultured Huh7 Cells. *J. Virol.*, 2002. **76**(6): p. 2997-3006.
44. Sagan, S.M., Rouleau, Y., Leggiadro, C., Supekova, L., Schultz, P.G., Su, A.I., and Pezacki, J.P., The influence of cholesterol and lipid metabolism on host cell structure and hepatitis C virus replication. *BIochemistry and Cell Biology*, 2006. **84**(1): p. 67-79.
45. Rouille, Y., Helle, F., Delgrange, D., Roingeard, P., Voisset, C., Blanchard, E., Belouzard, S., McKeating, J., Patel, A.H., Maertens, G., Wakita, T., Wychowski, C., and Dubuisson, J., Subcellular Localization of Hepatitis C Virus Structural Proteins in a Cell Culture System That Efficiently Replicates the Virus. *J. Virol.*, 2006. **80**(6): p. 2832-2841.
46. Y K Shimizu, S.M.F., M Kohara, R H Purcell, H Yoshikura,, Hepatitis C virus: Detection of intracellular virus particles by electron microscop. *Hepatology*, 1996. **23**(2): p. 205-209.

47. Ishida, S., Kaito, M., Kohara, M., Tsukiyama-Kohora, K., Fujita, N., Ikoma, J., Adachi, Y., and Watanabe, S., Hepatitis C virus core particle detected by immunoelectron microscopy and optical rotation technique. *Hepatology Research*, 2001. **20**(3): p. 335-347.
48. Rakic, B., Sagan, S.M., Noestheden, M., Belanger, S., Nan, X., Evans, C.L., Xie, X.S., and Pezacki, J.P., Peroxisome Proliferator-Activated Receptor [alpha] Antagonism Inhibits Hepatitis C Virus Replication. *Chemistry & Biology*, 2006. **13**(1): p. 23-30.
49. Nan, X., Tonary, A., M., Stolow, A., Xie, X.S., and Pezacki, J.P., Intracellular imaging of HCV RNA and lipids: simultaneous fluorescence and coherent anti-stokes Raman scattering microscopy. *ChemBioChem*, 2006.
50. Aizaki, H., Choi, K., Liu, M., Li, Y.-j., and Lai, M., Polypyrimidine-tract-binding Protein is a Component of the HCV RNA Replication Complex and Necessary for RNA Synthesis. *Journal of Biomedical Science*, 2006: p. 1-12.
51. Wheatley, S.P. and Wang, Y.L., Indirect immunofluorescence microscopy in cultured cells. *Methods Cell Biol.*, 1998. **57**: p. 313-32.
52. Hoffman, R.M., Advantages of multi-color fluorescent proteins for whole-body and in vivo cellular imaging. *Journal of Biomedical Optics*, 2005. **10**(4): p. 041202.
53. Hoffman, R.M., In vivo imaging with fluorescent proteins: the new cell biology. *Acta Histochemica*, 2004. **106**(2): p. 77-87.
54. Dirks, R.W., Molenaar, C., and Tanke, H.J., Visualizing RNA molecules inside the nucleus of living cells. *Methods*, 2003. **29**(1): p. 51-57.
55. van Roessel, P. and Brand, A.H., Imaging into the future: visualizing gene expression and protein interactions with fluorescent proteins. 2002. **4**(1): p. E15-E20.
56. Thomas, N., Lighting the Circle of Life. *Cell Cycle*, 2003. **2**(6): p. 545-549.
57. David, A.S. and Nicholas, A.W., Confocal scanning microscopy: three-dimensional biological imaging. *Trends in Biochemical Sciences*, 1989. **14**(11): p. 435-439.
58. Giepmans, B.N.G., Adams, S.R., Ellisman, M.H., and Tsien, R.Y., The Fluorescent Toolbox for Assessing Protein Location and Function. *Science*, 2006. **312**(5771): p. 217-224.
59. Notingher, I. and Hench, L.L., Raman microspectroscopy: a noninvasive tool for studies of individual living cells in vitro. *Expert Review of Medical Devices*, 2006. **3**(2): p. 215-234.
60. Uzunbajakava, N., Lenferink, A., Kraan, Y., Volokhina, E., Vrensen, G., Greve, J., and Otto, C., Nonresonant Confocal Raman Imaging of DNA and Protein Distribution in Apoptotic Cells. *Biophys. J.*, 2003. **84**(6): p. 3968-3981.
61. Chan, J.W., Taylor, D.S., Zwerdling, T., Lane, S.M., Ihara, K., and Huser, T., Micro-Raman Spectroscopy Detects Individual Neoplastic and Normal Hematopoietic Cells. *Biophys. J.*, 2006. **90**(2): p. 648-656.
62. Essendoubi, M., Toubas, D., Bouzaggou, M., Pinon, J.-M., Manfait, M., and Sockalingum, G.D., Rapid identification of Candida species by FT-IR microspectroscopy. *Biochimica et Biophysica Acta*, 2005. **1724**(3): p. 239-247.
63. Sharma, A., *Introduction to fluorescence spectroscopy / Ashutosh Sharma and Stephen G. Schulman.*, ed. S.G.S.G. Schulman, 1940-. c1999., New York :: J. Wiley,.
64. Valko, M., Rhodes, C.J., Moncol, J., Izakovic, M., and Mazur, M., Free radicals, metals and antioxidants in oxidative stress-induced cancer. *Chemico-Biological Interactions*, 2006. **160**(1): p. 1-40.

65. Terman, A. and Brunk, U.T., Oxidative Stress, Accumulation of Biological 'Garbage', and Aging. *Antioxidants & Redox Signaling*, 2006. **8**(1-2): p. 197-204.
66. Cakir, Y. and Ballinger, S.W., Reactive Species-Mediated Regulation of Cell Signaling and the Cell Cycle: The Role of MAPK. *Antioxidants & Redox Signaling*, 2005. **7**(5-6): p. 726-740.
67. van Manen, H.J., Kraan, Y.M., Roos, D., and Otto, C., Single-cell Raman and fluorescence microscopy reveal the association of lipid bodies with phagosomes in leukocytes. *Proceedings of the National Academy of Sciences of the United States of America*, 2005. **102**(29): p. 10159-10164.
68. Schuster, K.C., Reese, I., Urlaub, E., Gapes, J.R., and Lendl, B., Multidimensional Information on the Chemical Composition of Single Bacterial Cells by Confocal Raman Microspectroscopy. *Anal. Chem.*, 2000. **72**(22): p. 5529-5534.
69. Mourant, J.R., Short, K.W., Carpenter, S., Kunapareddy, N., Coburn, L., Powers, T.M., and Freyer, J.P., Biochemical differences in tumorigenic and nontumorigenic cells measured by Raman and infrared spectroscopy. *Journal of Biomedical Optics*, 2005. **10**(3): p. 031106.
70. Huang, Y.-S., Karashima, T., Yamamoto, M., and Hamaguchi, H., Molecular-Level Investigation of the Structure, Transformation, and Bioactivity of Single Living Fission Yeast Cells by Time- and Space-Resolved Raman Spectroscopy. *Biochemistry*, 2005. **44**(30): p. 10009-10019.
71. Huang, W.E., Griffiths, R.I., Thompson, I.P., Bailey, M.J., and Whiteley, A.S., Raman Microscopic Analysis of Single Microbial Cells. *Anal. Chem.*, 2004. **76**(15): p. 4452-4458.
72. Williams, R.M., Zipfel, W.R., and Webb, W.W., Multiphoton microscopy in biological research. *Current Opinion in Chemical Biology*, 2001. **5**(5): p. 603-608.
73. Holtom, G.R., Thrall, B.D., Chin, B.-Y., Wiley, H.S., and Colson, S.D., Achieving Molecular Selectivity in Imaging Using Multiphoton Raman Spectroscopy Techniques. *Traffic*, 2001. **2**(11): p. 781-788.
74. Xiao, C., Moore, D.J., Rerek, M.E., Flach, C.R., and Mendelsohn, R., Feasibility of Tracking Phospholipid Permeation into Skin Using Infrared and Raman Microscopic Imaging. 2005. **124**(3): p. 622-632.
75. Potma, E.O. and Xie, S.X., CARS Microscopy For Biology and Medicine. *Optics & Photonics News*, 2004: p. 40-45.
76. Zumbusch, A., Holtom, G.R., and Xie, X.S., Three-Dimensional Vibrational Imaging by Coherent Anti-Stokes Raman Scattering. *Physical Review Letters*, 1999. **82**(20): p. 4142-4145.
77. Cheng, J.X., Volkmer, A., and Xie, X.S., Theoretical and experimental characterization of coherent anti-Stokes Raman scattering microscopy. *J. Opt. Soc. Am. B*, 2002. **19**(6): p. 1363-1375.
78. Luis G. Rodriguez, S.J.L., Gary R. Holtom,, Coherent anti-stokes Raman scattering microscopy: A biological review. *Cytometry Part A*, 2006. **69**(8): p. 779-791.
79. Evans, C.L., Potma, E.O., Puoris'haag, M., Cote, D., Lin, C.P., and Xie, X.S., Chemical imaging of tissue in vivo with video-rate coherent anti-Stokes Raman scattering microscopy. *PNAS*, 2005. **102**(46): p. 16807-16812.
80. Nan, X., Potma, E.O., and Xie, X.S., Nonperturbative Chemical Imaging of Organelle Transport in Living Cells with Coherent Anti-Stokes Raman Scattering Microscopy. *Biophys. J.*, 2006. **91**(2): p. 728-735.

81. Cheng, J.-X., Jia, Y.K., Zheng, G., and Xie, X.S., Laser-Scanning Coherent Anti-Stokes Raman Scattering Microscopy and Applications to Cell Biology. *Biophys. J.*, 2002. **83**(1): p. 502-509.
82. Nan, X., Cheng, J.-X., and Xie, X.S., Vibrational imaging of lipid droplets in live fibroblast cells with coherent anti-Stokes Raman scattering microscopy. *J. Lipid Res.*, 2003. **44**(11): p. 2202-2208.
83. Cheng, J.-X., Pautot, S., Weitz, D.A., and Xie, X.S., Ordering of water molecules between phospholipid bilayers visualized by coherent anti-Stokes Raman scattering microscopy. *PNAS*, 2003. **100**(17): p. 9826-9830.
84. Li, L., Wang, H., and Cheng, J.-X., Quantitative Coherent Anti-Stokes Raman Scattering Imaging of Lipid Distribution in Coexisting Domains. *Biophys. J.*, 2005. **89**(5): p. 3480-3490.
85. Potma, E.O.X., X. S., Detection of single lipid bilayers with coherent anti-Stokes Raman scattering (CARS) microscopy. *Journal of Raman Spectroscopy*, 2003. **34**(9): p. 642-650.
86. Potma, E.O., de Boeij, W.P., van Haastert, P.J.M., and Wiersma, D.A., Real-time visualization of intracellular hydrodynamics in single living cells. *PNAS*, 2001. **98**(4): p. 1577-1582.
87. Cheng, J.-x., Volkmer, A., Book, L.D., and Xie, X.S., An Epi-Detected Coherent Anti-Stokes Raman Scattering (E-CARS) Microscope with High Spectral Resolution and High Sensitivity. *J. Phys. Chem. B*, 2001. **105**(7): p. 1277-1280.
88. Cheng, J.-x., Volkmer, A., Book, L.D., and Xie, X.S., Multiplex Coherent Anti-Stokes Raman Scattering Microspectroscopy and Study of Lipid Vesicles. *J. Phys. Chem. B*, 2002. **106**(34): p. 8493-8498.
89. Potma, E.O., Evans, C.L., and Xie, S.X., Heterodyne coherent anti-Stokes Raman scattering (CARS) imaging. *Optics Letters*, 2006. **31**: p. 241-243.
90. Cheng, J.-X., Book, L.D., and Xie, S.X., Polarization coherent anti-Stokes Raman scattering microscopy ,. *Optics Letters*, 2001. **26**: p. 1341-1343.
91. Ganikhanov, F., Evans, C.L., Saar, B.G., and Xie, S.X., High-sensitivity vibrational imaging with frequency modulation coherent anti-Stokes Raman scattering (FM CARS) microscopy,. *Optics Letters*, 2006. **31**: p. 1872-1874.
92. Wang, L. and Schultz, P.G., A general approach for the generation of orthogonal tRNAs. *Chemistry & Biology*, 2001. **8**(9): p. 883-890.
93. Ryu, Y. and Schultz, P.G., Efficient incorporation of unnatural amino acids into proteins in Escherichia coli. 2006. **3**(4): p. 263-265.
94. Deiters, A. and Schultz, P.G., In vivo incorporation of an alkyne into proteins in Escherichia coli. *Bioorganic & Medicinal Chemistry Letters*, 2005. **15**(5): p. 1521-1524.
95. Dawson, P.E. and Kent, S.B.H., Synthesis of Native Proteins by Chemical Ligation. *Annual Review of Biochemistry*, 2000. **69**(1): p. 923-960.
96. Dawn S. Y. Yeo, R.S., Grace Y. J. Chen, Shao Q. Yao,, Expanded Utility of the Native Chemical Ligation Reaction. *Chemistry - A European Journal*, 2004. **10**(19): p. 4664-4672.
97. Gierlich, J., Burley, G.A., Gramlich, P.M.E., Hammond, D.M., and Carell, T., Click Chemistry as a Reliable Method for the High-Density Postsynthetic Functionalization of Alkyne-Modified DNA. *Org. Lett.*, 2006. **8**(17): p. 3639-3642.

98. Sawa, M., Hsu, T.-L., Itoh, T., Sugiyama, M., Hanson, S.R., Vogt, P.K., and Wong, C.-H., Glycoproteomic probes for fluorescent imaging of fucosylated glycans in vivo. *PNAS*, 2006. **103**(33): p. 12371-12376.
99. Chen, C., Gorin, M., and Sigman, D., Sequence-Specific Scission of DNA by the Chemical Nuclease Activity of 1, 10-Phenanthroline-Copper (I) Targeted by RNA. *PNAS*, 1993. **90**(9): p. 4206-4210.
100. 't Hoen, P.A.C., de Kort, F., van Ommen, G.J.B., and den Dunnen, J.T., Fluorescent labeling of cRNA for microarray applications. *Nucl. Acids Res.*, 2003. **31**(5): p. e20-.
101. Hilario, E., End labeling procedures: an overview. *Mol. Biotechnol.*, 2004. **28**(1): p. 77-80.
102. Poon, N.L. and Satchell, D.P.N., Kinetics and mechanisms of the reactions of ketenes with water and alcohols in dioxane solutions. *Journal of the Chemical Society, Perkin Transactions 2*, 1986. **1986**(9): p. 1485-1490.
103. Chang, S. and Lamm, S.H., Human Health Effects of Sodium Azide Exposure: A Literature Review and Analysis. *International Journal of Toxicology*, 2003. **22**(3): p. 175-186.

Chapter 2 – Chemical Modification of HCV RNA

Introduction

The fundamental role of the HCV genome in negative-strand synthesis during viral replication, translational regulation and the assembly of mature virions necessitated the elucidation of the genomic structural and functional interactions that mediate these processes (for a review see [1]). Many of the interactions involved in these key events of the HCV life-cycle have been thoroughly investigated. However, a comprehensive understanding of the *in vivo* kinetics of HCV genomic synthesis, processing and transport have yet to be delineated. Thus, there is an important gap in our understanding of HCV molecular virology, which masks potentially novel therapeutic targets.

Filling this information gap would require the dynamical analysis of HCV RNA *in vivo* in real-time. Currently, live-cell RNA kinetics are investigated using a variety of fluorescence based techniques, of which the most widely used are based on fluorescence *in situ* hybridization (FISH). In this approach, fluorescently labelled RNA oligonucleotides probes that are complementary to a specific RNA sequence are introduced to the cell, after which they bind to their target RNA sequence and are subsequently imaged[2-4]. While FISH has been used to localize positive-sense HCV RNA in fixed cells, it has yet to applied to the real-time analysis of HCV RNA kinetics[5]. More recently, the microinjection of fluorescently labelled tRNA for the real-time detection of cytosolic mRNA targets was demonstrated[6]. However, similar to the analysis of HCV replication using 5-bromouridine-5'-triphosphate metabolic labeling, this method (and FISH) is an indirect analysis of HCV localization. Therefore, it is not an ideal system to investigate the intricacies of RNA kinetics because a variety of difficult to control variables could interfere with probe-target interactions. Researchers have also discovered a library of styryl small-molecule dyes that

could be used to profile the RNA content of a cell in real-time[7]. However, this technique is limited to imaging the entire cellular RNA complement, as opposed to RNA derived from a specific origin. Recently, 5'-FITC labelled HCV RNA was visualized in live-cells using two-photon fluorescence microscopy[8]. Unfortunately, the limitations of live-cell fluorescence microscopy preclude the use of this approach to investigate dynamical cellular processes in real-time. Finally, several researchers have used fluorescently tagged RNA binding proteins to image specific RNA targets *in vivo* in real-time[9, 10]. However, the cumbersome nature of constructing recombinant RNA binding proteins for different RNA targets potentially limits the use of this strategy.

The limitations of these techniques and those generally associated with live-cell fluorescence analysis precluded the use of these approaches for the longitudinal analysis of cellular processes surrounding HCV RNA synthesis, processing and transport. Moreover, the lack of a suitable method underscored the importance of developing tools capable of achieving real-time *in vivo* analysis of RNA. The modification of HCV RNA with CARS contrast agents will expand the imaging capabilities of CARS microscopy to include the dynamical analysis of specific molecular targets *in vivo*. This will aid in our understanding of the synthesis, processing and transport of HCV RNA, as well as provide a new tool to investigate general aspects of RNA kinetics unrelated to HCV in real-time *in vivo*.

Results

Synthesis of Modified HCV RNA

Deuterated HCV RNA

Deuterated HCV RNA (D-RNA) was synthesized using the IVT reaction outlined in the materials and methods. Despite the decreased concentration of nucleotides in the IVT

reaction (50 mM D-rNTP versus 75 mM rNTP), yields of D-RNA ranged from 60 – 80 μg per IVT reaction, which was reasonably consistent with the yields of HCV RNA (70 – 90 μg per IVT reaction). Additionally, the electrophoretic migration and homogeneity of the D-RNA was consistent with that of HCV RNA (Figure 2.1).

Aminoallylated HCV RNA

HCV RNA containing 5-aminoallyl uridine (aaU; Figure 2.2A) was synthesized as outlined in the materials and methods. A titration to determine the optimal amount of aaU-5'-triphosphate (aaUTP) for the IVT reaction showed that a 1:1 mole ratio with uridine-5'-triphosphate (UTP) produced an intact, homogeneous transcript population (Figure 2.2B). Analysis of the electropherograms of the other aaUTP:UTP ratios revealed heterogeneous mixtures of transcripts, which suggested an increase in the frequency of early termination products (Figure 2.2C). The electrophoretic migration of HCV RNA containing aaU (aaU-RNA) suggested that either an early termination product was the primary transcript or that the electrophoretic migration of aaU-RNA was altered relative to HCV RNA. A similar trend in migration was observed for smaller 163 nt (163mer) and 270 nt (270mer) RNA transcripts with and without aaU (Figure 2.2D). This demonstrated that the migration shift was a general consequence of using aaUTP and supported the conclusion that the aberrant electrophoretic migration of aaU-RNA was likely due to altered physicochemical properties rather than a predefined early termination site. The typical yield for an aaU IVT reaction was 40 - 60 μg of aaU-RNA, which was lower than yields of standard IVT reactions. However, quantities were still sufficient for further functionalization and characterization.

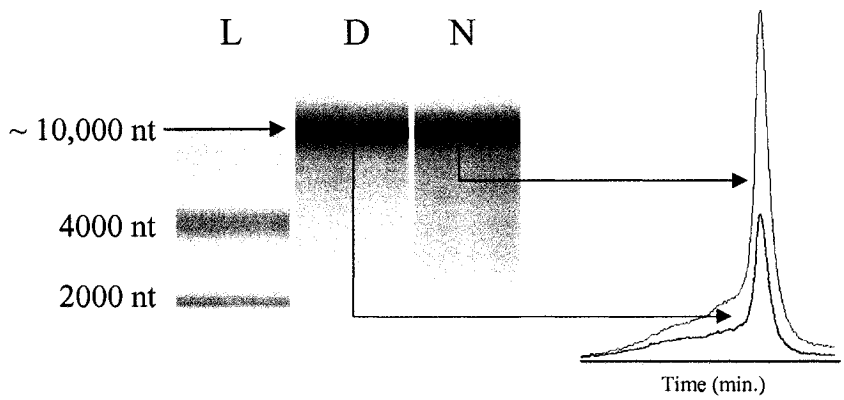

Figure 2.1: Validation of D-RNA synthesis. Electrophoretic migration (left) of HCV RNA (N) and D-RNA (D) were identical, indicating that the D-RNA reaction produced a full-length (~10,000 nt) transcript population. The electropherograms (right) illustrated the lack of early termination products for HCV RNA (blue) and D-RNA (red). L = RNA ladder.

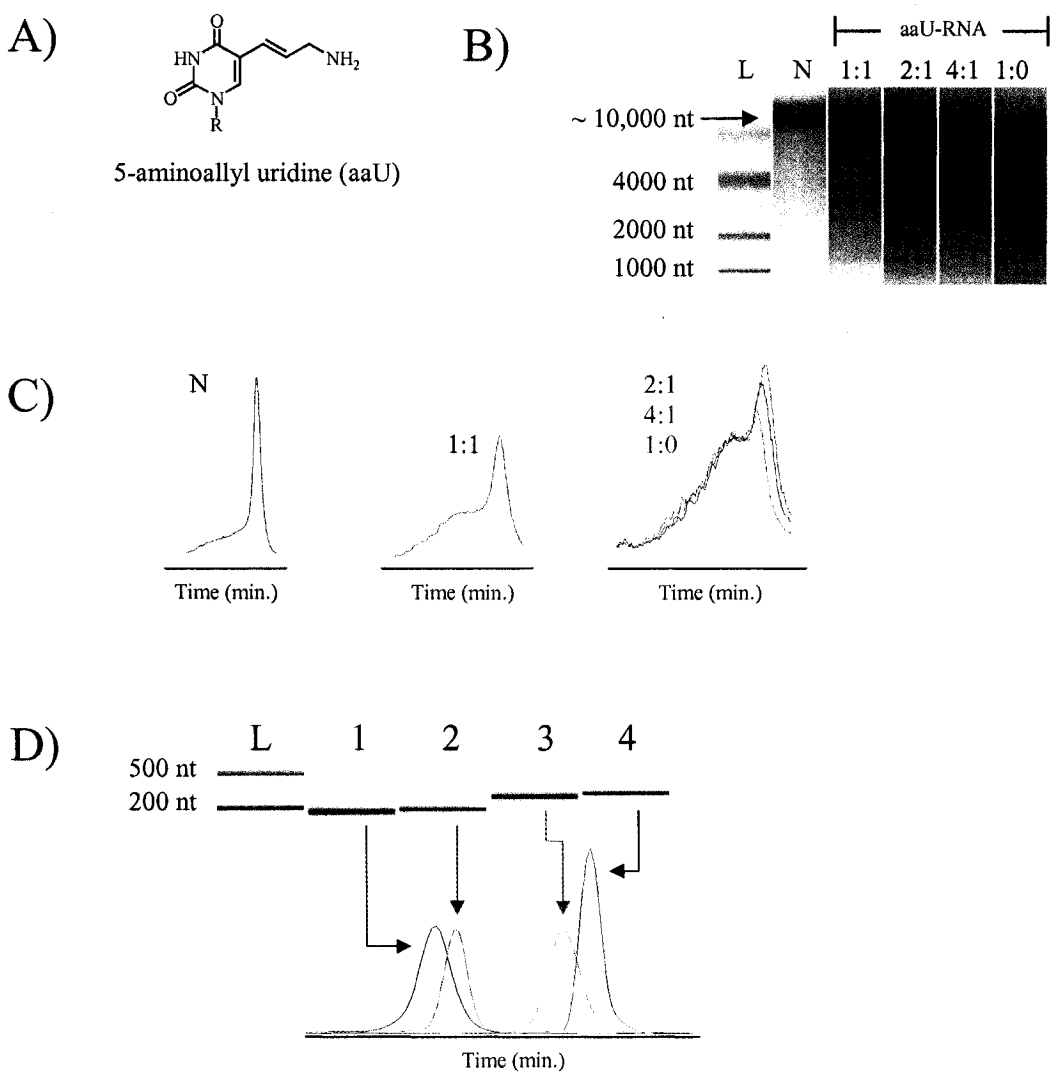

Figure 2.2: Validation of aaU-RNA synthesis. A) Structure of aaU. B) Electrophoresis of HCV RNA (N) and aaU-RNA, which was synthesized with increasing ratios of aaUTP:UTP (indicated above the remaining lanes). C) As the amount of aaUTP in the transcription reaction increased, the electropherograms showed a corresponding increase in the amount of early termination products. Comparing the amounts of early termination products illustrated that the optimal ratio of aaUTP:UTP was 1:1. All electropherograms were on the same time scale. D) A similar trend in migration was observed for smaller transcripts. Lanes 2 and 4 are aaU-163mer/270mer, respectively. Lanes 1 and 3 are unmodified control transcripts. R = ribose ; L = RNA ladder.

5'-End-Labeled HCV RNA

The conjugation of 4-cyanobenzyl-M (4-CN-M) was performed as outlined in the materials and methods to yield 5'-4-CN HCV RNA (5'-CN; Figure 2.3A). The reaction product was analyzed by electrophoretic comparison with HCV RNA and 5'-fluorescein HCV RNA (5'-F; Figure 2.3B). The results implied that the labeling reaction was successful, although the apparent mass-shift did not correlate with the mass of either fluorescein or 4-CN-M. Also, the widths of the 5'-labeled RNA bands indicated the possibility of a heterogeneous population of modified RNAs or that the 5'-labeled RNAs had different chemical properties than HCV RNA, which lead to a change in their electrophoretic migration.

Due to these ambiguous results, atomic force microscopy (AFM; discussed in structural characterization section) was also used to examine these materials. Analysis of the AFM images showed that the 5'-modified and HCV RNA samples had approximately equivalent degrees of heterogeneity (data not shown). Therefore, similar to the conclusion made for aaU-RNA, the abnormal migration data was likely caused by a change in the physicochemical properties of HCV RNA following 5'-modification.

Characterization of Modified HCV RNA

Elution and Ionization Conditions

Initial attempts focused on using the four naturally occurring RNA nucleobases – cytosine (C), guanosine (G), adenosine (A) and uridine (U) – as their respective mononucleotides (phosphorylated) to avoid a dephosphorylation step when analyzing modifications to HCV RNA. Even though the HPLC conditions were optimized, the mononucleotides eluted within 1.5 min. of each other (data not shown). Thus, while each

peak was spatially resolved, the intervening distances limited the capacity to resolve additional eluents (aaU and modified aaU).

Following from these results, the focus shifted to optimizing the elution and ionization of mononucleosides (dephosphorylated). Using the conditions outlined in the materials and methods, the five mononucleosides present in aaU-RNA were successfully resolved by HPLC, with sufficient peak-to-peak separation to accommodate the resolution of aaU and its derivatives (Figure 2.4A). The HPLC elution order was: C, 3.8 min.; U, 5.6 min.; aaU, 10.4 min.; G, 12.5 min., A, 20.6 min. Liquid chromatography – mass spectrometry (LC-MS) analysis confirmed this elution order (Figure 2.4B). However, a 10 mM solution of each nucleoside was needed to obtain a detectable electrospray ionization mass spectrometry (ESI-MS) signal from the LC-MS. This problem was the most pronounced for aaU.

To increase the ionization potential of the nucleosides, the buffer pH was adjusted to 3.2 and 1.4. Unfortunately, as the buffer pH decreased, so did the signal to noise, which off-set any gains in ionizability (data not shown). An alternative was to force molecular ionization by increasing the mass spectrometry (MS) cone voltage. Starting from the original 10 V, the cone voltage was increased to 30 V for all 5 nucleosides (data not shown). For the four natural nucleosides, the increased voltage resulted in the homolytic fragmentation of the nucleobase from the sugar and only yielded modest gains in signal intensity. For aaU, the increased cone voltage clearly resulted in fragmentation but the precise fragments were difficult to identify. The modest gains in signal intensity and difficulties identifying aaU fragments precluded using an increased cone voltage to aid in ionization. Therefore, 0.1 M NH_4OAc, pH 6.5 at a flow-rate of 0.2 mL/min. was determined to be optimal for the HPLC/LC-MS resolution and ionization of the six nucleobases integral to this study.

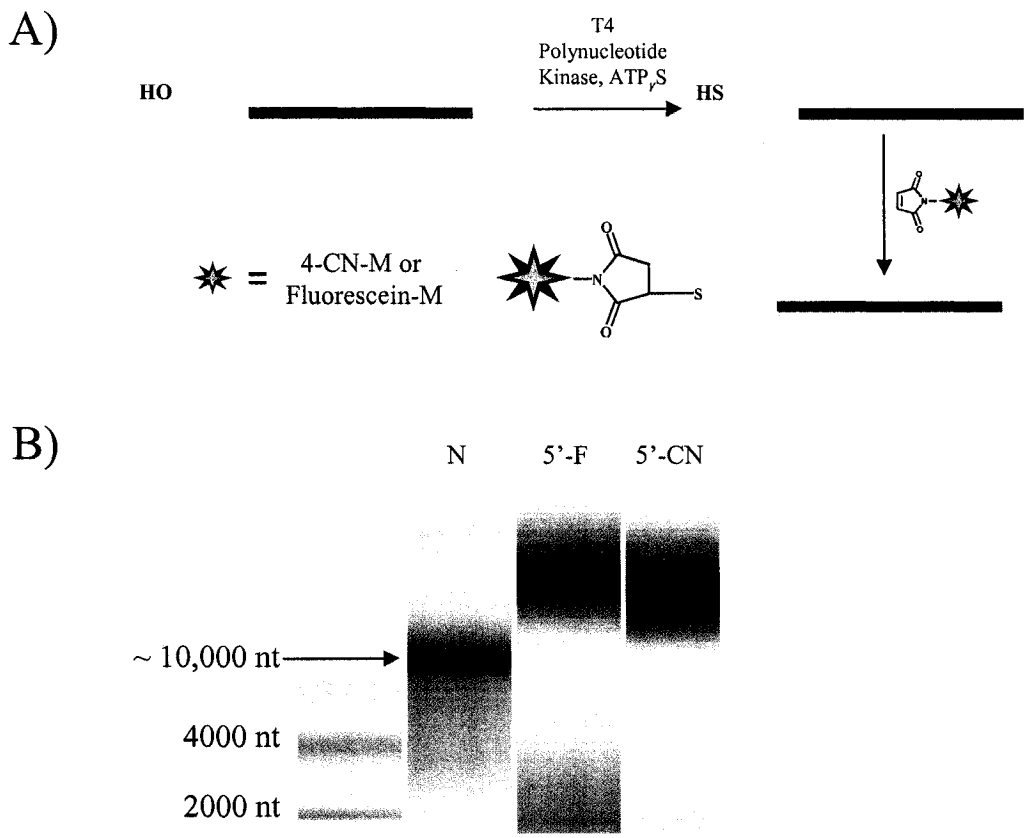

Figure 2.3: Synthesis and analysis of 5'-labeled HCV RNA products. A) The 5'-OH is exchanged for a thiophosphate group through the action of T4 polynucleotide kinase (only the thiol has been shown for simplicity). The 5'-thiol then reacts via 1,4-addition with a M probe to yield 5'-labeled RNA. B) Relative to HCV RNA (N) the electrophoretic migration of 5'-F and 5'-CN RNA displayed a large mass-shift indicating a much higher molecular weight, which did not correlate with the mass of fluorescein or 4-CN-M.

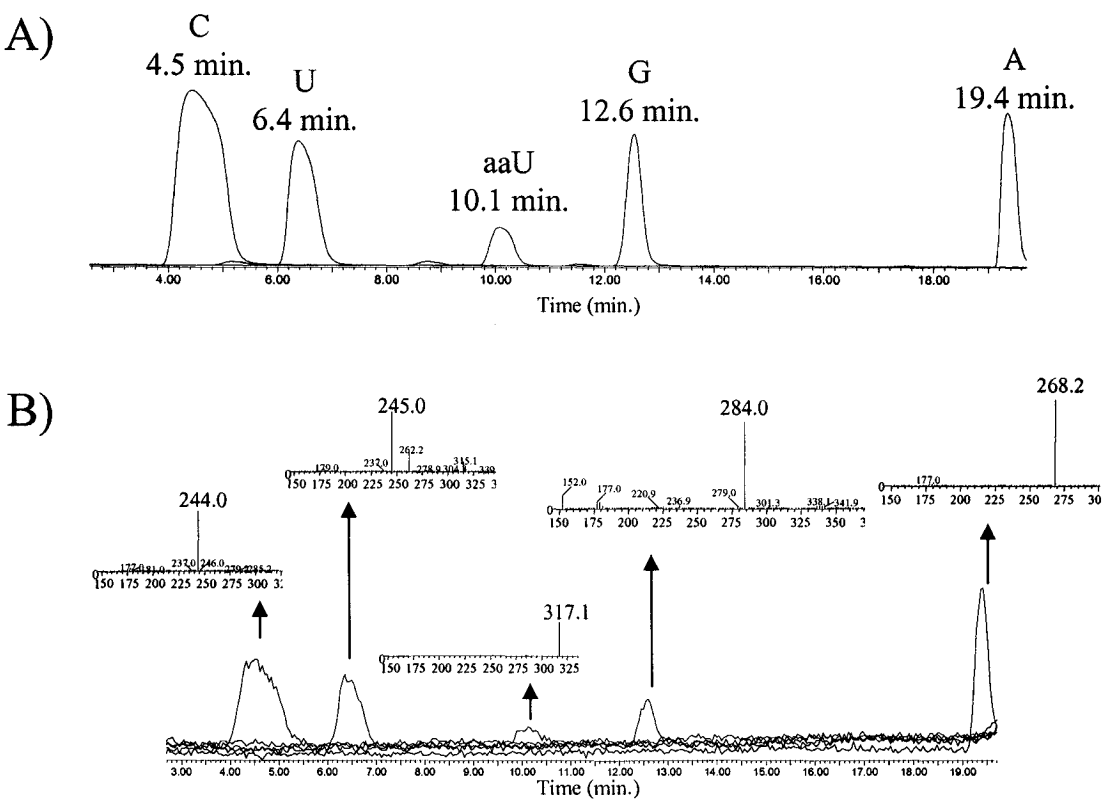

Figure 2.4: Optimizing the elution conditions of 5 mononucleosides. A) C, U, A, G and aaU were all resolved as shown by this overlay of their respective elution profiles. Samples were detected at 254 nm. B) C, U, A and G were identified by LC-MS as molecular ions (M+1) at a concentration of 10 mM. The modified uridine, aaU, was identified from a weekly ionizing ammonium adduct (M+18) at a concentration of 6 mM. Even after accounting for concentration differences the ionization of aaU was low.

HPLC/LC-MS Analysis of Normal and Modified HCV RNA

Before the optimized HPLC/LC-MS conditions were applied to the analysis of modified RNAs, digestion and dephosphorylation of HCV RNA and aaU-RNA were performed to obtain the constituent mononucleosides. HPLC/LC-MS analysis clearly showed that the mononucleoside components of HCV RNA and aaU-RNA were resolved following digestion and dephosphorylation as described in the materials and methods (Figure 2.5).

To determine if the digestion conditions were achieving maximal sample decomposition, the concentration and time dependence of the reaction was examined. The results of the concentration dependence experiment showed that the HCV RNA and aaU-RNA reactions appeared to saturate with 10 – 25U of S1 nuclease (Figure 2.6A). Furthermore, the time dependence experiment showed that the digestion reaction saturated after 1 hour (Figure 2.6B). It should be noted that aaU-RNA appeared to require more S1 nuclease to achieve an equivalent level of digestion to HCV RNA, but the reaction still saturated at 25U. This was likely a result of the aaU nucleobase interfering with S1 nuclease substrate recognition. Taken together, these findings demonstrated that the protocol established for digestion of HCV RNA and aaU-RNA was saturating the amount of RNA (normal and modified) that could be digested.

To determine if the digestion saturation point was a function of substrate concentration, quantification of the digested mononucleosides was performed as described in the materials and methods. Analysis of the results revealed that the current conditions achieved 80 – 90% digestion of HCV RNA and aaU-RNA, which was consistent with the requirements of this assay (developed herein). Owing to these results, the completion of the calf intestinal phosphatase (CIP) dephosphorylation reaction was not investigated.

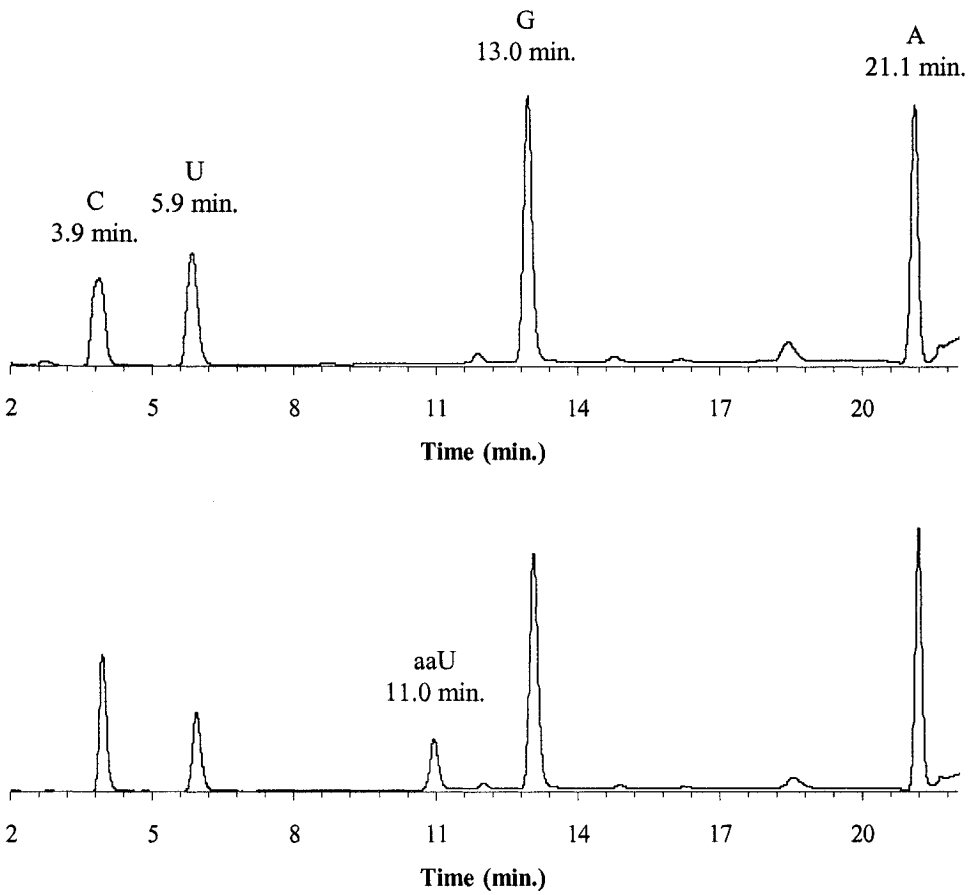

Figure 2.5: HPLC resolution of digested and dephosphorylated RNA. HCV RNA (top) clearly showed the presence of C, U, G and A. Analysis of aaU-RNA (bottom) showed an additional eluent that corresponded to aaU. Slight differences in elution profiles between HPLC and LC-MS were accounted for as negligible systematic errors. Samples were detected at 254 nm.

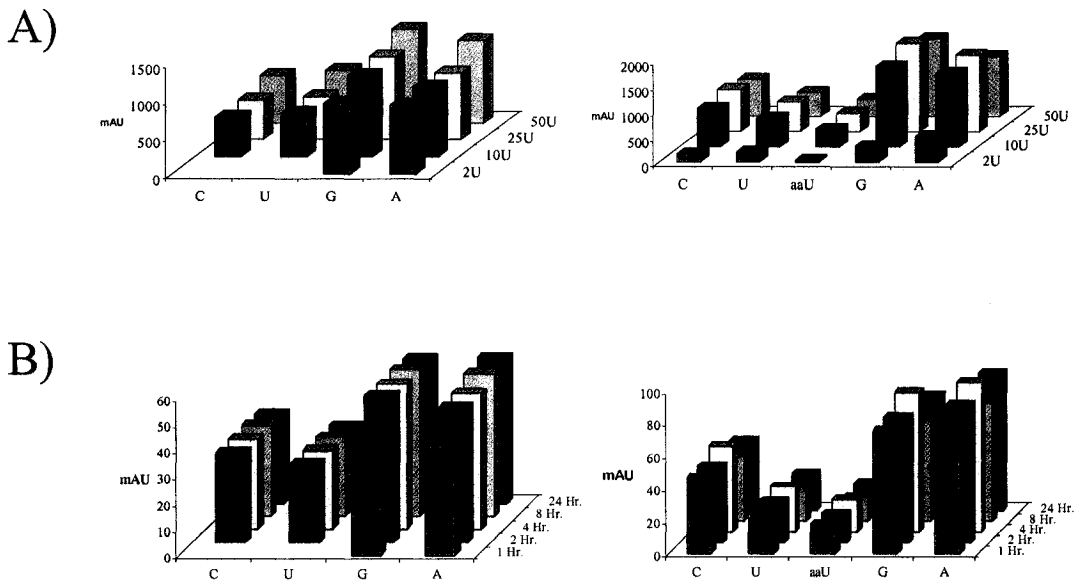

Figure 2.6: Validating the digestion of HCV RNA and aaU-RNA. A) The digestion reaction saturated between 2 – 10U for HCV RNA (left) and 10 – 25U for aaU-RNA (right). B) The digestion of HCV RNA (left) and aaU-RNA (right) saturated after 2 hours. C and U 2U (A) and 1 Hr. (B) data points were not collected.

Evaluating the Extent of aaU Incorporation

Given the structural complexity and size of the HCV genome, the 163mer model RNA system previously used to characterize the electrophoretic migration of aaU-modified transcripts (Figure 2.2D) was used to investigate the ability of T7 RNA polymerase (T7) to incorporate aaU as described in the materials and methods. The results of the 163mer digestion and dephosphorylation indicated that the aaU:U ratio in the transcribed RNA was approximately 1:1. Application of this analysis to aaU-RNA showed an aaU:U ratio of 1.1:1 – 1.3:1, which was consistent with the results of the 163mer. These results demonstrated that T7 incorporated aaUTP with approximately the same frequency as UTP.

Further characterization of aaU-RNA was done to demonstrate that the amount of aaU incorporated could be regulated. By decreasing the amount of aaUTP in the IVT reaction, the apparent size of the primary transcript increased, with a 1:4 aaUTP:UTP ratio producing a transcript population whose electrophoretic migration and sample heterogeneity were closer to HCV RNA (Figure 2.7A). Additionally, HPLC analysis of these samples showed an increase in the U:aaU ratio in favour of U as the concentration of aaUTP in the IVT reaction decreased (Figure 2.7B). This data demonstrated that the extent of aaU incorporation could be evaluated using HPLC and regulated by adjusting the amount of aaUTP in the transcription reaction.

CN Modification of aaU-RNA

Repeated attempts at modifying aaU and aaU-RNA with 4-cyanobenzyl-NHS (4-CN-NHS) were unsuccessful. Believing this to be a stereoelectronic effect, the labelling reaction was attempted using NHS-activated benzoic acid (Bz-NHS) and aaU as outlined in the materials and methods. HPLC analysis of Bz-NHS and buffer alone revealed a peak that was

specific to Bz-NHS at 22.5 min. (Figure 2.8A). Direct identification of the 22.5 min. eluent was not possible by LC-MS due to difficulties in detecting the molecular ion of Bz-NHS. However, ^{1}H-NMR confirmed that the Bz-NHS starting material was authentic and similar difficulties were encountered when attempting to characterize Bz-NHS by ESI-MS. With this information in hand, it was concluded that the 22.5 min. peak must be Bz-NHS. When the reaction was conducted in the presence of a limiting quantity of aaU there was a new eluent peak at 23.6 min., which LC-MS identified as the benzyl-modified aaU (m/z = 404 and 421; Figure 2.8A) and the aaU starting material peak at 10.6 min. disappeared. These results were indicative of a successful coupling reaction between Bz-NHS and aaU.

The Bz-NHS reaction was next applied to an aaU-modified 163mer (aaU-163mer). Examining the electrophoretic migrations indicated a successful reaction since the increased apparent mass of the labelled RNA was consistent with the chemical conjugation of Bz-NHS to the aaU-163mer (Figure 2.9A). In addition, when compared with the elution profile of a control reaction, the clear appearance of a new peak at 23.6 min. was seen for the Bz-NHS labeling reaction (Figure 2.9B). This peak corresponded to the benzyl-modified aaU previously identified from the aaU reaction. Bolstering this conclusion was the disappearance of the aaU peak at 10.6 min, which also indicated that modification had occurred. Taken together, these findings demonstrated that the conjugation of Bz-NHS to aaU-163mer was successful.

These results also supported the assumption that the problem with the 4-CN-NHS labeling reaction was related to stereoelectronic effects. To further corroborate this assumption 3-cyanobenzyl-NHS (3-CN-NHS; Hammett σ_m = 0.62), which was electronically closer to benzoic acid (σ = 0.0) than 4-CN-NHS (σ_p = 0.70), was used to label aaU-163mer. Again, initial analysis of the electrophoretic migration showed an increase in the apparent

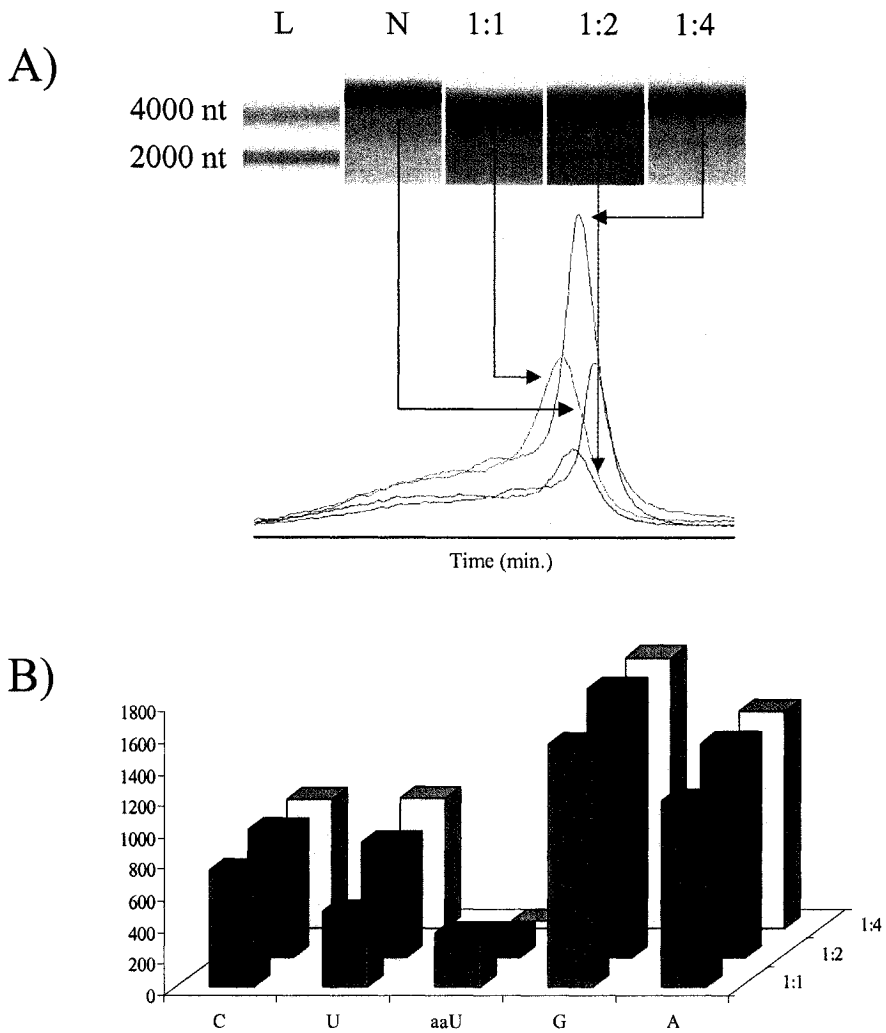

Figure 2.7: Regulating the extent of aaU incorporation. A) Electrophoretic migration of HCV RNA compared to aaU-RNA synthesized with decreasing amounts of aaU. As the amount of aaU is decreased the migration of aaU-RNA begins to approach that of HCV RNA. B) HPLC analysis displayed a reciprocal relationship between aaU and U as the concentration of aaU in the transcription reaction was decreased. X:Y = aaU:UTP in transcription reaction

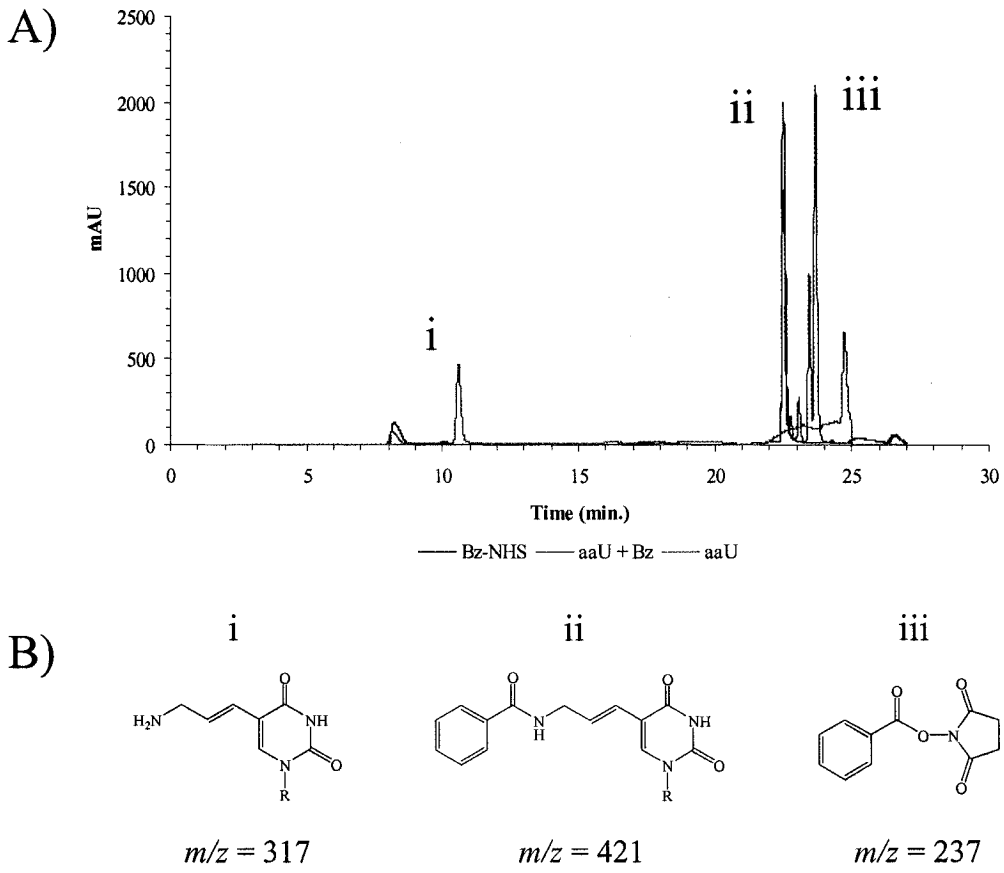

Figure 2.8: Evaluating aaU modification with Bz-NHS. A) Bz-NHS eluted at 22.5 min. (blue). In the presence of aaU a new peak at 23.6 min. (pink) appeared, in addition to the Bz-NHS peak. This coincided with the disappearance of the aaU peak at 10.6 min. (green). B) Structures of aaU (i), aaU-Bz (ii) and Bz-NHS (iii). LC-MS confirmed the identity of the peaks corresponding to these materials. R = dephosphorylated ribose sugar.

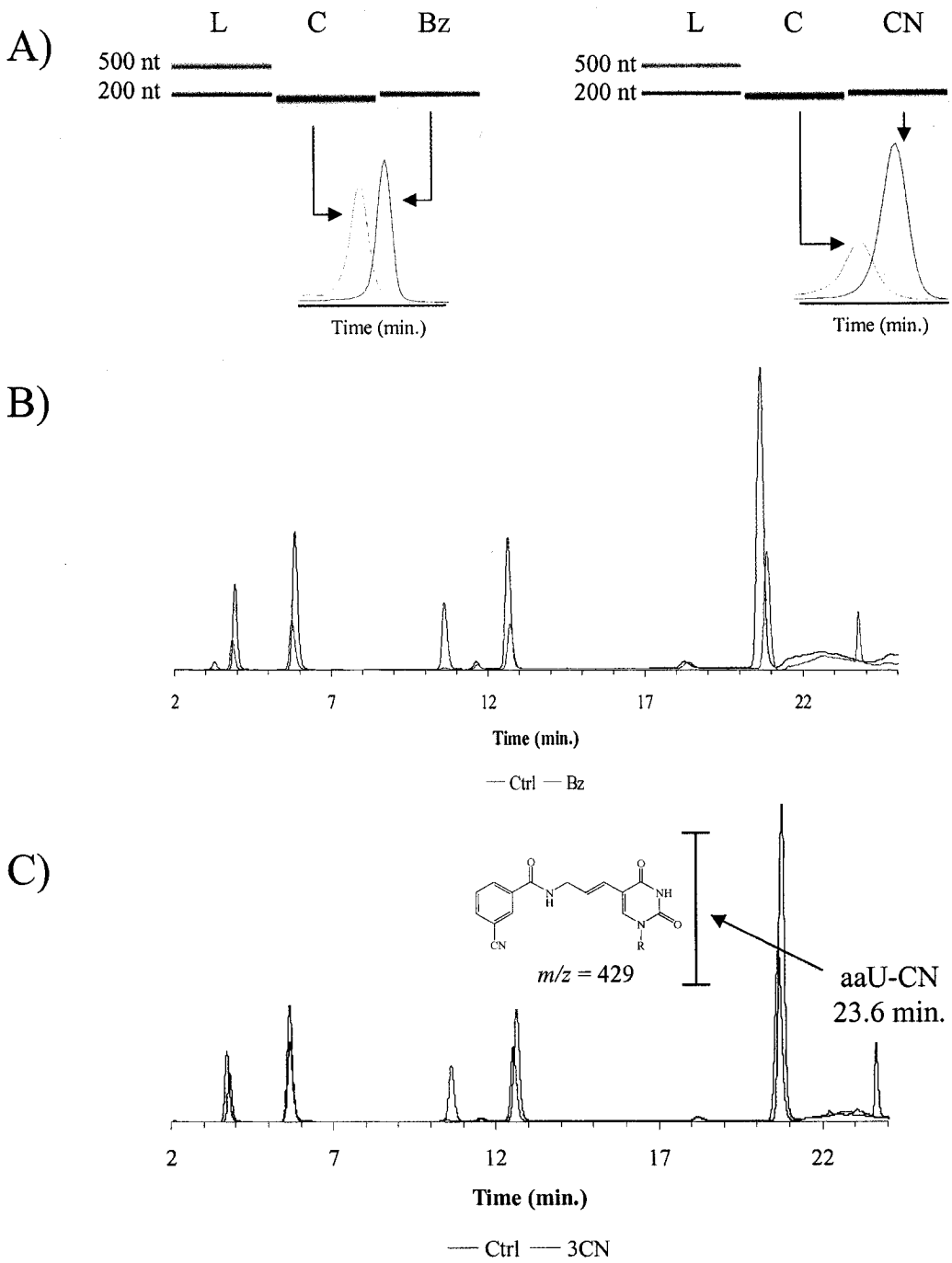

Figure 2.9: Labeling of a model RNA system with Bz-NHS and 3-CN-NHS. A) Electrophoretic migration of 163mer modified with Bz-NHS (left) and 3-CN-NHS (right). Labeled products showed an increase in apparent mass. B) HPLC showing the disappearance of aaU (10.6 min.) and the appearance of Bz-modified aaU (23.6 min.) when control (Ctrl, blue) and Bz-modified (Bz, pink) 163mer reactions were analyzed. C) HPLC comparison of 163mer control (Ctrl, blue) and 3-CN-NHS (3CN, red) labeling reactions showing the appearance of aaU-CN (23.6 min.) and corresponding disappearance of aaU (10.6 min.).

mass of labelled aaU-163mer, which was consistent with a successful reaction (Figure 2.9A). HPLC comparison to control reactions clearly showed the appearance of a new product at 23.6 min., with a corresponding disappearance of the aaU peak at 10.5 min., both of which were indicative of a successful reaction (Figure 2.9C). Based on the concentration of aaU required for LC-MS detection the practicality of synthesizing quantities of the 23.6 min. eluent sufficient for LC-MS precluded the direct identification of this material. However, ESI-MS analysis of the digested nucleoside mixture showed a weak signal for the 3-CN-modified aaU (aaU-CN; $m/z = 429$).

Having indirectly shown that 3-CN-NHS labelled aaU-163mer, the reaction was applied to the modification of aaU-RNA. Electrophoretic analysis of 3-CN-NHS modified aaU-RNA (CN-aaU-RNA) revealed a mass-shift that was consistent with those seen for Bz-NHS and 3-CN-NHS modified aaU-163mer (Figure 2.10A). Furthermore, the presence of the peak believed to be aaU-CN was immediately apparent at 23.6 min (Figure 2.10B). Taken together, these findings offered compelling evidence supporting the conclusion that 3-CN-NHS was successfully modifying aaU-RNA.

Regulating the Extent of 3-CN-NHS Modification

Using aaU-163mer, a titration was performed to demonstrate that the extent of modification could be regulated by altering the concentration of 3-CN-NHS in the labeling reaction (Figure 2.11A; reactions were otherwise performed as outlined in the materials and methods). The results of this experiment showed that as the concentration of 3-CN-NHS decreased, the electrophoretic mobility of the modified 163mer approached that of aaU-163mer. Furthermore, HPLC analysis displayed an increase in aaU and a decrease in aaU-CN as the concentration of 3-CN-NHS decreased. Both of these results were consistent with

a decrease in the extent of modification as the concentration of 3-CN-NHS in the labeling reaction decreased.

A similar methodology was performed with aaU-RNA to demonstrate this approach on a more complex RNA system (Figure 2.11B). HPLC analysis showed an increase in aaU and a decrease in aaU-CN as the concentration of 3-CN-NHS in the labeling reaction decreased. Also noteworthy from these experiments was the finding that using the labelling conditions outlined in the materials and methods lead to >90% labelling efficiency. These results demonstrated that 3-CN-NHS modification of aaU-RNA was highly efficient and that the extent of modification could be regulated by modulating the concentration of 3-CN-NHS in the labelling reaction.

Raman Analysis of Modified RNAs

Standard borosilicate microscope slides, CaF_2 wafers and N-type silicon wafers were evaluated to determine their degrees of Raman transparency (data not shown). The standard microscope slides displayed a broad fluorescence that coincided with the Raman transparent region identified from analysis of Huh-7 lysates. CaF_2 was transparent from 450 – 4000 cm^{-1} – the entire range of interest for cellular analysis. However, at approximately $50 USD per wafer, the cost of CaF_2 made their use unfeasible. Silicon had a substantial 1st order resonance around 500 cm^{-1}, a smaller 2nd order band around 1000 cm^{-1} and a nominal 3rd order band around 1400 cm^{-1}, but was otherwise transparent. Given these considerations, silicon was the substrate of choice for Raman analysis.

The complete Raman spectrum of D-RNA indicated that all aliphatic modes were shifted to the Raman transparent region of the cell, which was expected since all the non-exchangeable aromatic and aliphatic protons were substituted with deuterium (Figure 2.12A).

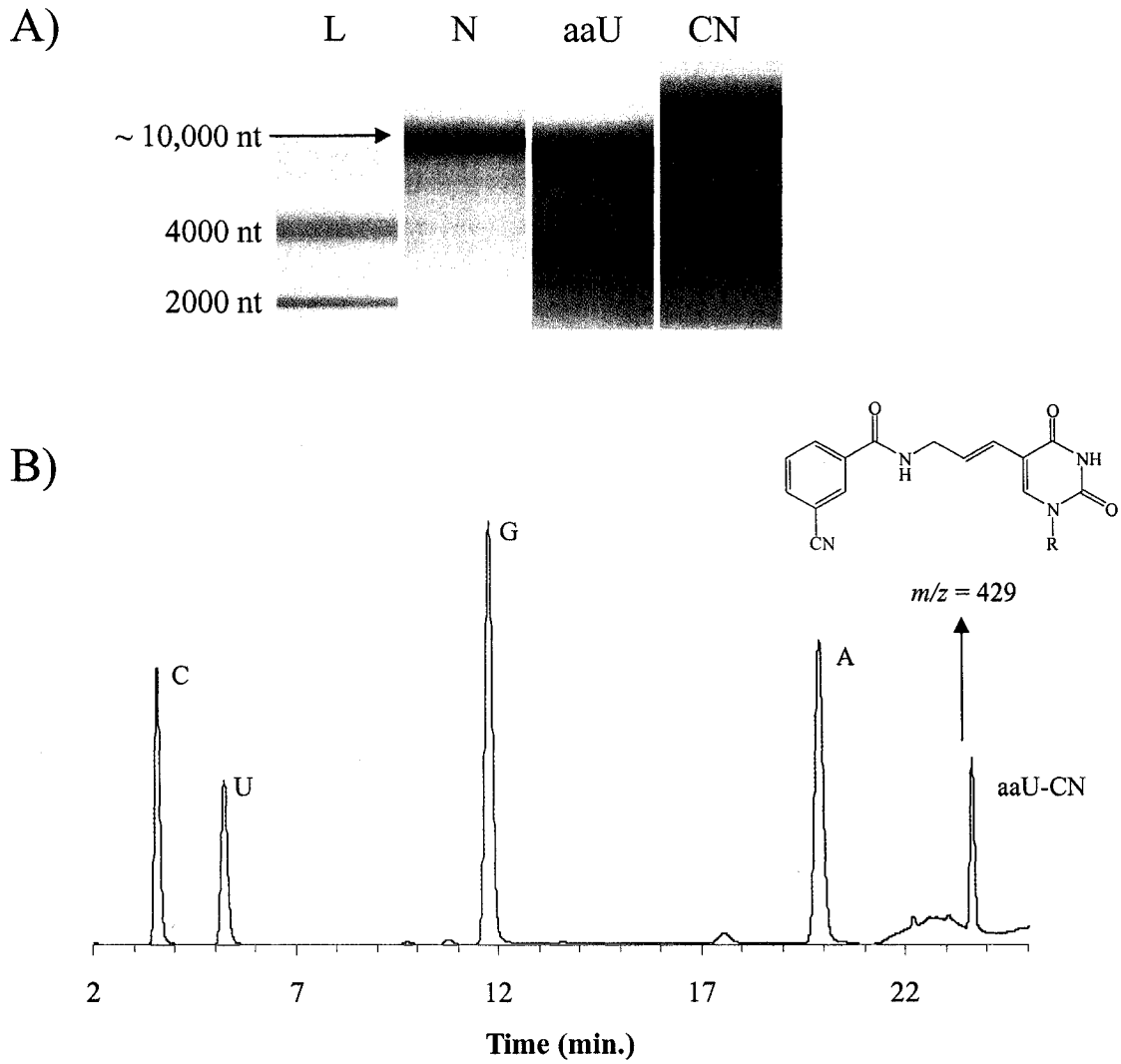

Figure 2.10: Analysis of CN-RNA. A) Electrophoretic analysis showed a mass-shift upon modification of aaU-RNA that indicated a successful reaction. B) The clear disappearance of aaU (10.6 min.) and appearance of aaU-CN (23.6 min.) was also indicative of a successful labeling reaction. L = RNA Ladder; N = HCV RNA; aaU = aaU-RNA; CN = CN-RNA.

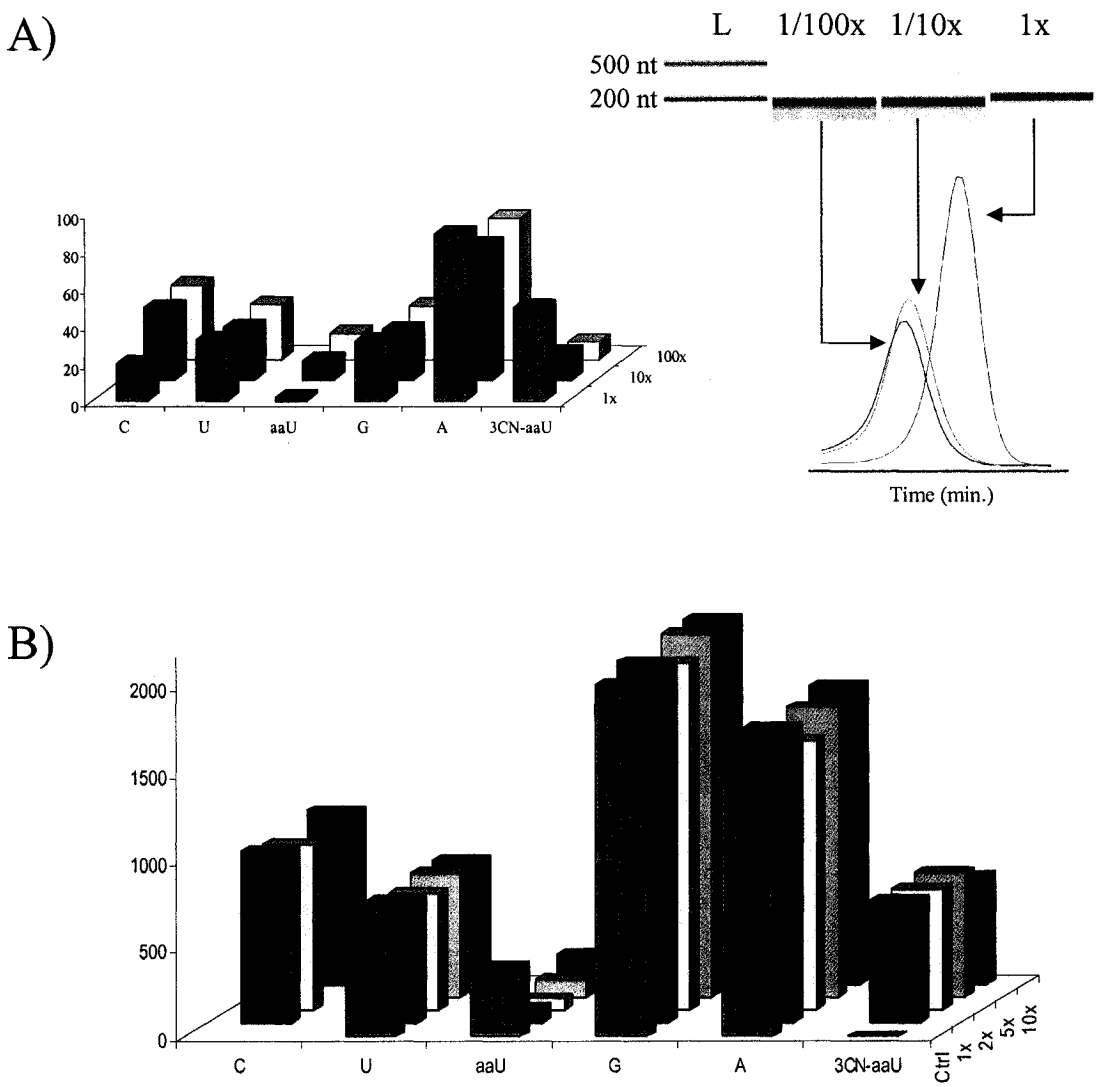

Figure 2.11: Regulating the extent of 3-CN-modification. A) Electrophoretic mobility (right) of aaU-163mer RNA exposed to decreasing amounts of 3-CN-NHS. As the concentration of 3-CN-NHS decreases, the apparent mass-shift also decreases. In addition, HPLC shows an increase in the amount of aaU and corresponding decrease in 3-CN-aaU as the concentration of 3-CN-NHS decreases (left). B) A similar trend is observed when decreasing amounts of 3-CN-NHS are applied to labeling aaU-RNA. The inset shows the reciprocal relationship between aaU and 3-CN-aaU for aaU-RNA. 1x, 2x, 5x, 10x and 100x refer to the dilution factor applied to 3-CN-NHS relative to a 25 mM solution.

Raman imaging, which was performed as described in the materials and methods, showed that contrast specific to the C-D mode could be generated by tuning into the C-D spectral region (2050 – 2300 cm^{-1}; Figure 2.12B).

To obtain definitive evidence that supported the conclusion drawn from HPLC/LC-MS experiments, Raman imaging of CN-aaU-RNA was conducted. Analysis revealed a spectrally well-resolved signal corresponding to the CN mode at 2238 cm^{-1} (Figure 2.13A). Additionally, image contrast specific to CN-aaU-RNA could be generated by integrating the Raman image from 2200 – 2260 cm^{-1} (Figure 2.13B). Thus, when coupled with the HPLC/LC-MS data presented thus far, the Raman data clearly show that the modification of aaU-RNA with 3-CN-NHS was successful.

Functional Validation of Modified RNAs

In the presence of Mg^{2+}, ATP and the beetle luciferin substrate luciferase catalyzes the production of light and the amount of light produced can be correlated to the amount of luciferase protein that was translated *in vivo*[11, 12]. As outlined in the introduction, one of the HCV replicon systems contains the luciferase gene under the control of an HCV IRES. Using this system, changes in luciferase expression could be directly correlated to translation changes and indirectly correlated to replicative changes that resulted from the modifications introduced to enable tracking via CARS microscopy. Therefore, to examine the functional effects of modifying HCV RNA with deuterium and 3-CN-NHS CARS contrast agents a luciferase reporter assay was performed as described in the materials and methods.

The expression of the luciferase reporter gene was investigated following RNA modification at the transcriptional and post-transcriptional level (Figure 2.14). The results showed that the luciferase activity was severely affected for aaU-RNA (5%), CN-aaU-RNA

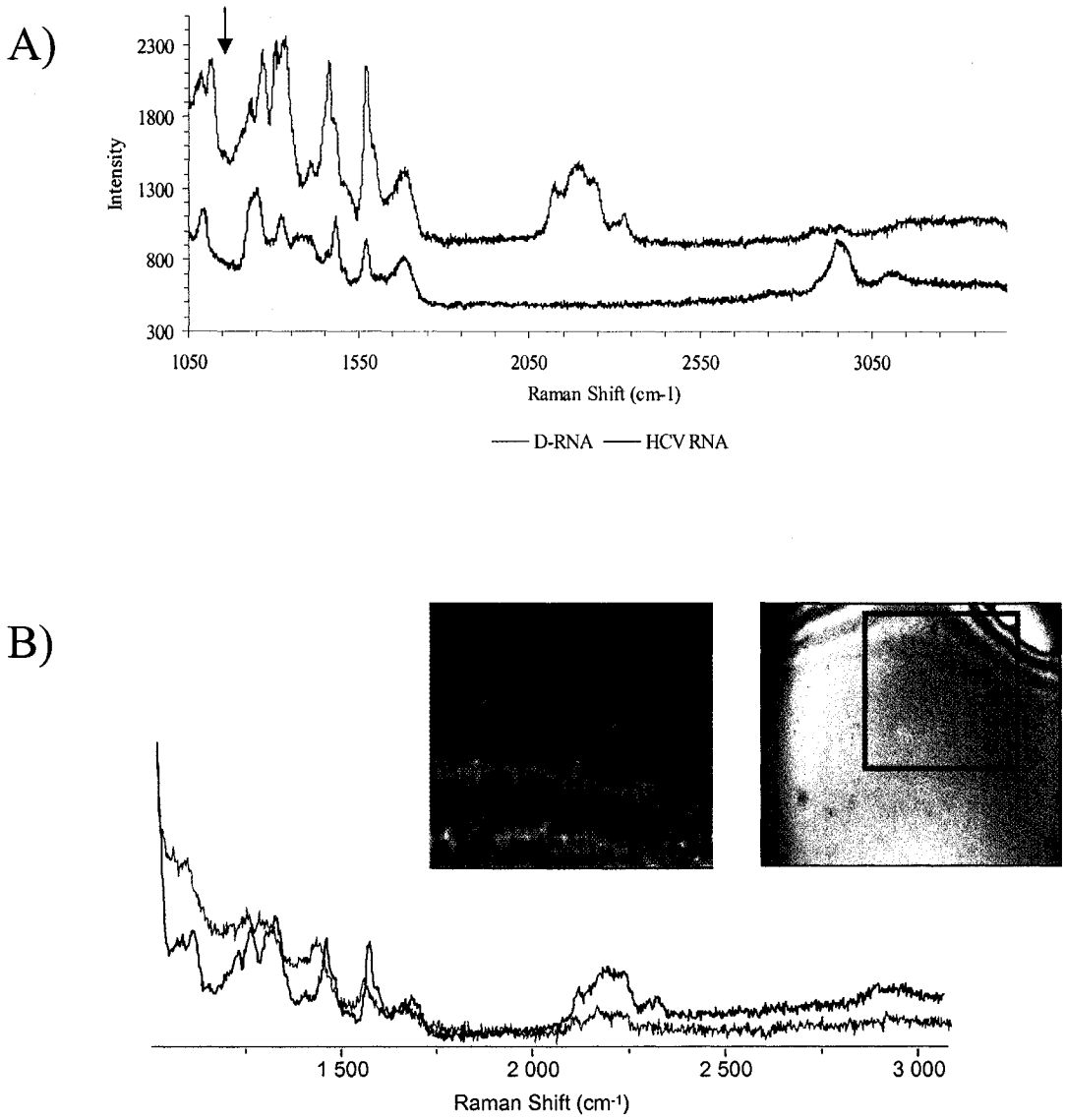

Figure 2.12: Raman microscopy analysis of D-RNA. A) Raman spectra of D-RNA (pink) and HCV RNA (blue) illustrating the shift of the aliphatic resonances to the C-D region of the spectrum. The O-P-O nucleotide backbone stretch (1090 cm^{-1}; black arrow) gave confirmation that it was RNA under examination. Spectra were acquired with 5 sec. integrations from 10 $\mu g/\mu L$ spots that were dried onto a silicon substrate. B) A Raman image of the area outlined in green (inset; 40x40 μm) was obtained using a three second integration time and 0.5 μm steps. The Raman image shown (center) is a summation of all Raman modes from 2050 – 2300 cm^{-1}. The Raman spectra shown are from an area of bright intensity in the Raman image (blue), which is indicative of an abundance of C-D modes, and a low intensity region (orange). This image clearly showed that image contrast specific to the C-D mode of D-RNA could be generated.

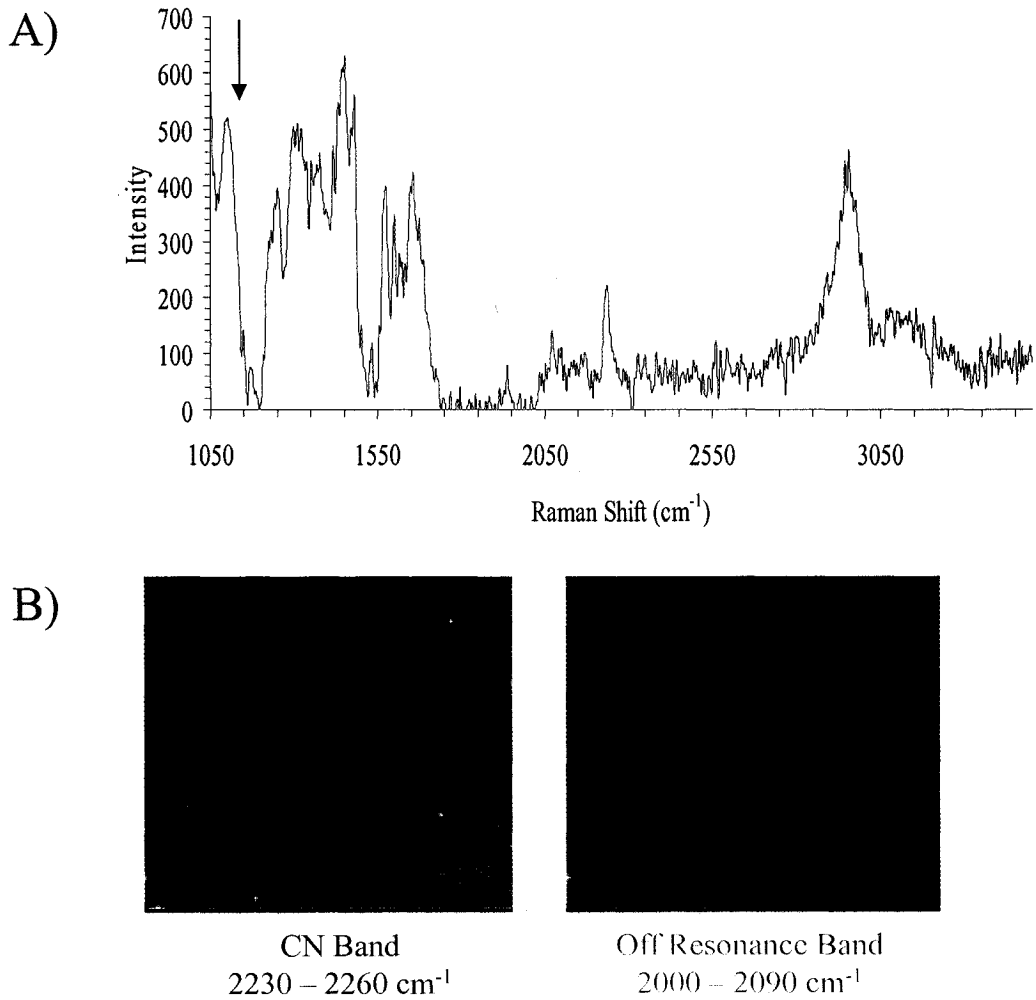

Figure 2.13: Raman microscopy analysis of CN-RNA. A) A clear peak at 2238 cm^{-1} (between red lines) was final evidence that the 3-CN-NHS modification of aaU-RNA was successful. Also evident was the O-P-O nucleotide backbone resonance at 1090 cm^{-1} (black arrow), which gave confirmation that it was RNA under examination. B) Raman image contrast was generated by integrating the CN band from 2230 – 2260 cm^{-1}. While noisy, a clear intensity difference when compared to an image of an off resonance band was observed.

(15%), 5'-CN (20%) and 5'-F (50%) when compared to HCV RNA. In contrast to these samples, D-RNA maintained approximately 60% of wild-type luciferase activity when contrasted against HCV RNA. The fact that these trends continued through the 48 hour time-point was indicative of a replicative and/or translational deficiency introduced by the modification of HCV RNAs.

Interestingly, when the aaUTP:UTP ratio in the IVT reaction was increased from 1:1 to 1:3 the luciferase activity began to rebound, showing a two-fold increase (Figure 2.15A). While still suffering a severe deficiency, this suggested that the functional deficit may be related to perturbations introduced by the modified nucleobase. Similarly, when HCV RNA transcripts containing one of the deuterated nucleosides per IVT reaction were analyzed, the luciferase activity of G/C and A/U substitutions was observed to be markedly different (Figure 2.15B). In fact, when the activities of the G/C and A/U substitutions were averaged, they yielded an activity that was comparable to D-RNA. These results indicated that the decrease in luciferase activity was causally linked to RNA modification and, more specifically, to particular base substitutions.

Structural Validation of Modified RNAs

Structural modifications to HCV RNA were likely to induce changes in the hydrodynamic radius of the folded RNA. To investigate this theory, dynamic light scattering (DLS), which uses scattered light to approximate the hydrodynamic radii of nanoscale particles, was used as a first-line means of characterizing the modified RNAs. While no clear difference in the hydrodynamic radius was observed upon DLS analysis of HCV RNA, D-RNA, aaU-RNA and CN-aaU-RNA, it was interesting to note that the size calculated by

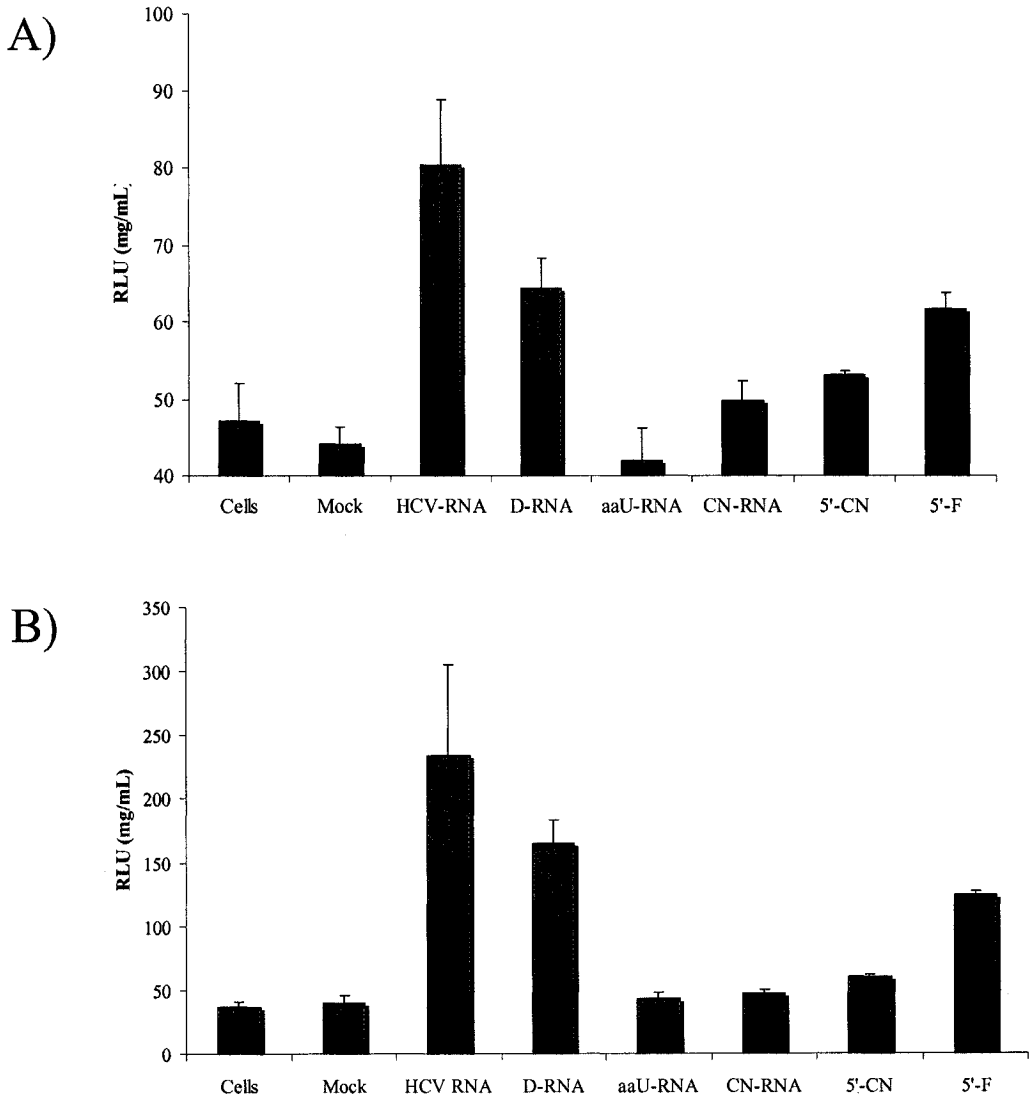

Figure 2.14: Luciferase activity of modified HCV RNAs. 24 (A) and 48 (B) hour endpoints were examined. Data showed that aaU-RNA, CN-RNA and 5'-CN suffered severe functional deficits as a result of modification. However, the luciferase assay only reports on translation of the reporter gene, not on RNA replication and expression of viral proteins. Mock treatment was with transfection reagent only. All measurements were made in triplicate and are reported as mean values ± one standard deviation.

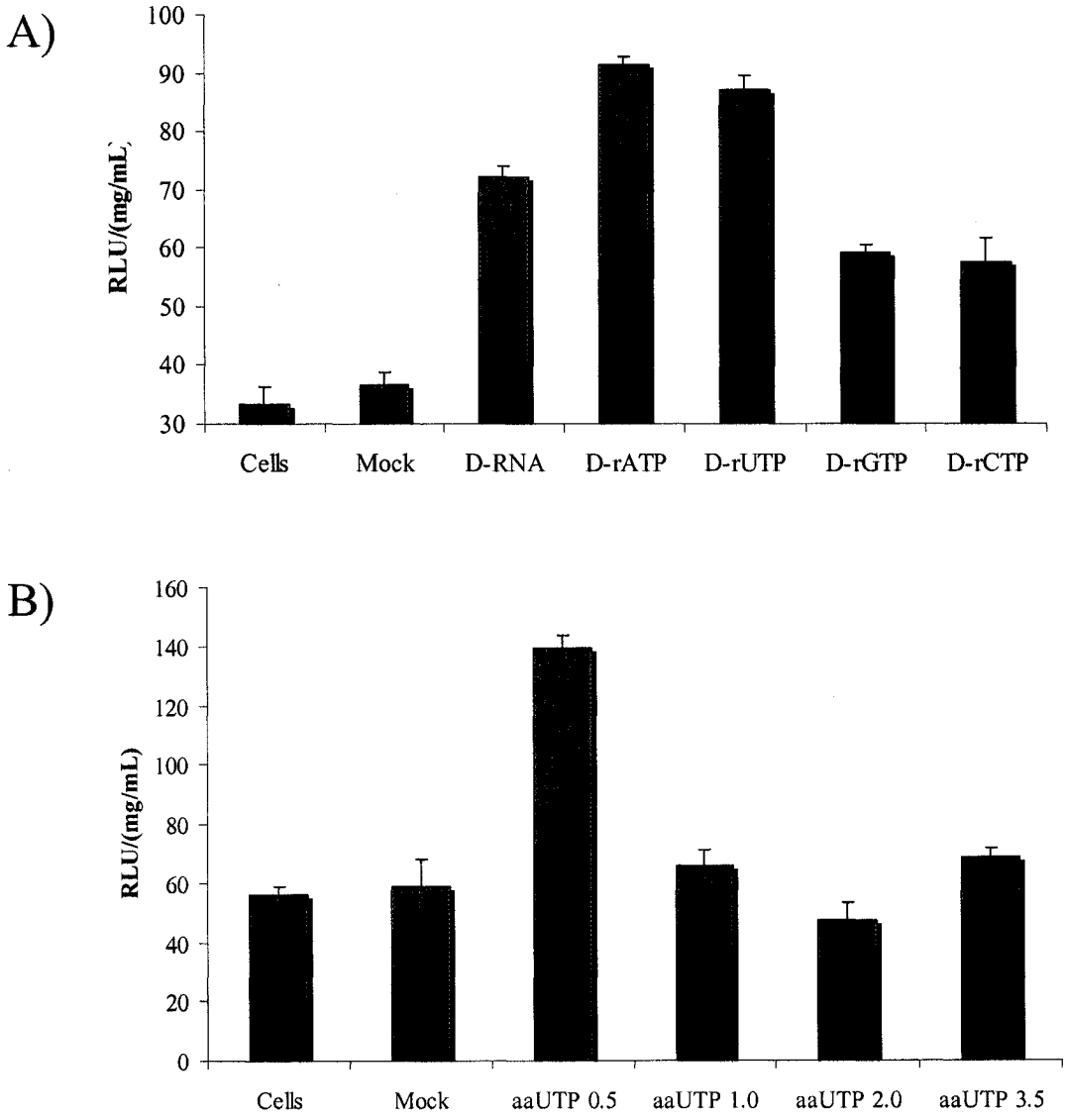

Figure 2.15: Decreases in luciferase activity were causally linked to the incorporation of modified bases into HCV RNA. A) Incorporation of deuterated ATP and UTP affected luciferase activity less than deuterated GTP and CTP. The reasons for this remain unclear. B) A four-fold decrease in aaU during the IVT reaction lead to a 2-fold increase in luciferase activity. All measurements were made in triplicate and are reported as mean values ± one standard deviation.

DLS was consistent with the approximate size necessary to fit inside assembled HCV Core protein microparticles (Figure 2.16)[13].

AFM analysis of HCV RNA, aaU-RNA and CN-aaU-RNA revealed critical information about the stability of higher-order structural elements within the modified HCV RNAs (Figure 2.17). All samples appeared to disperse onto the mica surface, as the effective radius was nearly tripled (90 – 110 nm) when compared to the hydrodynamic radii determined by DLS. This result was expected, as the Mg^{2+}-coated surface provided extensive coordination sites that could interact with the phosphate backbone. However, when the morphology of the modified RNAs on the mica surface was examined, noticeable differences were identified. Most apparent, was the probable dissolution of higher-order structural elements in aaU-RNA and CN-aaU-RNA. This suggested that HCV RNA structural elements were being weakened by the modifications such that it was energetically more stable to coordinate with surface Mg^{2+} than through intramolecular contacts.

Discussion

The non-invasive, chemically specific detection strategy used in CARS microscopy is an attractive method to facilitate real-time *in vivo* analysis. Thus far, limitations in generating CARS images with chemical *and* molecular specificity have hindered its application in this area. The development of CARS contrast agents that confer a unique Raman signature to labelled biomolecules was undertaken to overcome this limitation. In particular, this thesis has identified two modifications at the nucleobase level that may facilitate the tracking of HCV RNA *in vivo* using CARS microscopy. The use of deuterated nucleotides and NHS/M-activated cyanobenzoic acid derivatives will mediate the incorporation of the bioorthogonal Raman modes necessary to generate image contrast *in*

	Diameter (nm)	Spread (nm)
HCV RNA	30.7	17.7
aaU-RNA	28.5	14.7
D-RNA	24.3	10.0
CN-RNA	31.6	17.5

Figure 2.16: DLS analysis of modified HCV RNAs. No clear difference between the normal and modified HCV RNAs could be resolved using DLS. However, the size of the collapsed state approximated that required to fit inside the mature HCV virion (~30 nm). All values are reported as mean of 100 measurements. Diameter = mean hydrodynamic diameter; Spread = size of population distribution.

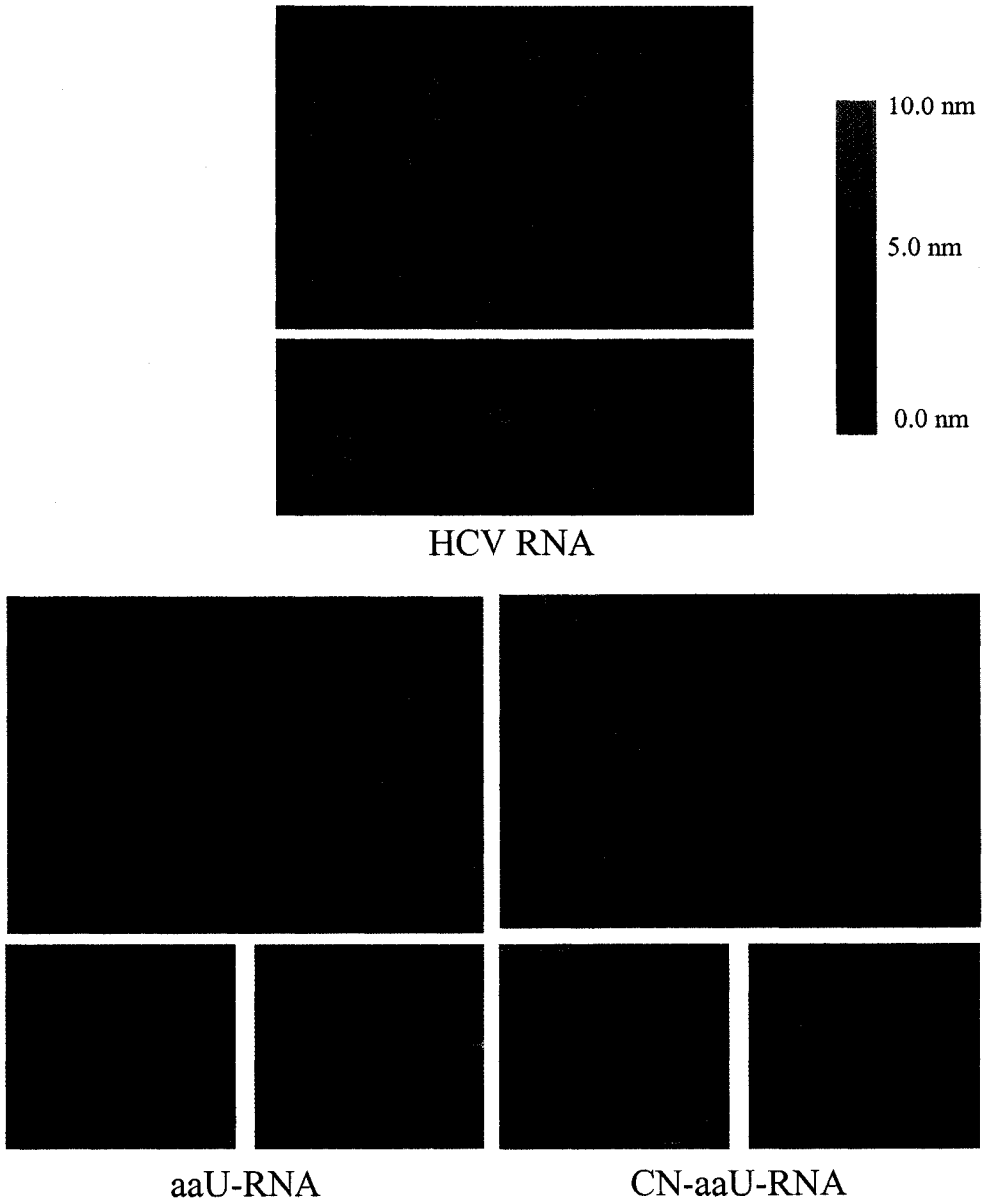

Figure 2.17: AFM analysis of modified HCV RNAs. Unmodified HCV RNA appeared as tight clusters indicating that non-specific tertiary interactions in the collapsed state remained intact. The presence of single-stranded segments and generally more open appearance of aaU-RNA and CN-aaU-RNA implied that the collapsed state tertiary interactions were dissociating in favour of coordinating with surface Mg^{2+}. This was concluded to be a direct result of aaU and aaU-CN destabilizing these interactions such that coordinating with surface Mg^{2+} was energetically favoured. All scale bars are 100 nm.

vivo with molecular specificity. However, before applying the modified RNAs to *in vivo* experiments a thorough structural and functional characterization was carried out to provide a comprehensive understanding of the effects that these modifications have on HCV RNA. This, in turn, will enable the optimization of the modifications so that HCV RNA structure and function can be balanced against the detection limits of CARS microscopy.

Synthesis of Deuterated HCV RNA

Unlike small-molecule labels, which possess intrinsic spatial requirements that can elicit perturbations when incorporated into a biomolecule, deuterium does not have additional steric requirements over that of hydrogen (the added neutron does not appreciably increase the van der Waals radius of deuterium). Therefore, deuterium was an ideal candidate for developing CARS contrast agents because incorporating it into structurally sensitive molecules (i.e.: HCV RNA) was not expected to elicit appreciable functional and structural consequences. Also, the C-D Raman resonance falls within a spectral region that is devoid of endogenous cellular resonances. Therefore, contrast specific to deuterated biomolecules can potentially be generated using CARS microscopy by tuning the microscope to excite the C-D mode. Finally, the substitution of deuterium for hydrogen does not implicitly require the addition of exogenous functional groups to facilitate conjugation of a deuterated probe to the biomolecule. Rather, deuterated building blocks can be fed to an organism or used *in vitro* to enzymatically synthesize deuterium-modified biomolecules[14-16]. These properties make deuterium labeling an elegant and non-perturbative means of incorporating unnatural functionality for the purpose of real-time *in vivo* detection using CARS microscopy.

A potential drawback of using deuterium was the intrinsically weak scattering cross-section of the C-D mode. Moreover, this problem could be exacerbated *in* vivo due to the focal volume mode density required to generate C-D image contrast with CARS microscopy. To overcome this limitation, the number of C-D modes introduced needed to be maximized so that the quadratic concentration dependence of CARS microscopy can be exploited. Deuterium substitution is ideally suited to large scale incorporation because it is expected to elicit nominal structural and functional deficits. This statement is supported by the fact that deuterium does not alter the electronegativity or van der Waals radius at the site of modification. With these considerations in mind, the synthesis of fully deuterated HCV RNA was undertaken, using deuterated nucleotides as substrates for the IVT reaction (Figure 1.8B).

Whether or not the polymerase in question efficiently utilizes the modified substrate is a fundamental consideration when exploiting enzymatic reactions to facilitate biomolecular modifications. The IVT protocol used for synthesizing RNA (see materials and methods) relied on T7, which has been used to incorporate ATP and UTP nucleobase analogues, as well as heavily modified fluorescent 5' cap analogues into RNA through IVT reactions[17, 18]. Given the relative severity of these modifications when contrasted with deuterium substitution, it was expected that T7 would efficiently incorporate the deuterated nucleotide analogues.

The yields of D-RNA were generally 80 – 90% when compared to those of normal HCV RNA transcripts. This was an excellent yield when compared to the yields of other T7 IVT reactions using modified substrates, which ranged from 45 – 100%[17-20]. Thus, T7 appeared to incorporate the deuterated nucleotides with nearly the same efficiency as wild-type substrates, which supported the assumption that deuterium substitutions present nominal

structural perturbations – if they did, then a lower yield due to the substitutions interfering with chain elongation would have been observed. Further evidence in support of this was found in the absence of early termination products, which was indicated by the tight band corresponding to the full-length D-RNA transcript and the absence of lower weight fragments in the D-RNA electropherogram (Figure 2.1). If T7 did not efficiently incorporate the deuterated nucleotides then the frequency of smaller transcripts resulting from early termination would be expected to increase, as in previous studies[17-20]. Since this was not observed, these results clearly indicated that T7 efficiently incorporated the deuterated nucleotides into the D-RNA transcript.

Having shown that the IVT reaction produced a full-length transcript in excellent yield, it remained to be proven that the deuterium substitutions conferred exogenous Raman modes to the D-RNA. Raman spectroscopic analysis of the D-RNA revealed that the entire aliphatic region shifted into the Raman transparent window of the cell, which was conclusive evidence that the deuterated nucleotides were incorporated during the IVT reaction (Figure 2.12A). Furthermore, the spectroscopic data illustrated that the bulk scattering cross-section of the C-D mode can be quite prominent despite the weak cross-section of individual C-D modes. In addition to the C-D modes from 2050 – 2300 cm^{-1}, the presence of the O-P-O nucleotide backbone resonance (1090 cm-1) was also apparent. This was an important control resonance to identify as it gave confirmation that the material being analyzed was D-RNA and not the substrate or other surface contaminants (i.e.: salt, dust, etc.).

Given that the length of HCV RNA is approximately 10,000 nucleotides and there was an average of 7.5 deuterium substitutions per nucleobase, the number of C-D modes present in a single D-RNA molecule was approximated to be 75,000. Previous calculations established a conservative estimate for the detection limit of CARS microscopy to be $1x10^6$

modes within the focal volume[21]. Therefore, it may be possible to detect 10 – 15 D-RNA molecules provided that they are all present in the focal volume. As a proof-of-principle experiment, the D-RNA was analyzed by Raman microscopy to show that contrast specific to the D-RNA could be generated by isolating the C-D modes from 2050 – 2300 cm^{-1}.

It would be ideal to analyze the D-RNA in solution so that absolute cross-sections could be determined based on known solution concentrations of RNA. However, due to secondary scattering of Raman photons the sensitivity of solution Raman was not sufficient to enable the visualization of D-RNA. Therefore, the data presented here was collected from aliquots of D-RNA that were spotted onto a silicon substrate and allowed to dry in ambient conditions. Although this methodology prevented quantitative comparison to determine absolute scattering cross-sections, qualitative analysis was sufficient to demonstrate that contrast specific to the C-D modes of D-RNA could be generated.

The D-RNA imaging experiment showed that contrast specific to the C-D mode was generated (Figure 2.12B). Obviously the concentrations used for this assay (1 and 10 μg/μL) enabled a C-D mode density that was qualitatively higher than would be attainable *in vivo*. However, owing to the coherence and directionality of the CARS signal, the collection efficiency of CARS microscopy is approximately 10,000-fold greater than for conventional Raman scattering when using a lens with the same numerical aperture[21]. Using these values as a guidepost, a semi-quantitative detection limit for D-RNA by CARS microscopy is in the range of 100 – 1000 pg/μL (25 – 250 nM). This is approximately 15 D-RNA molecules in the CARS microscope focal volume of 1 fL, which was in good agreement with the detection limit postulated based on the number of C-D modes per RNA (10 – 15 molecules).

These preliminary results implicitly showed that D-RNA has the potential to function as an important tool in the *in vivo* study of HCV RNA using CARS microscopy.

Elaborations on the functional and structural consequences of deuterium substitution are discussed in subsequent sections.

Synthesis of aaU-Modified HCV RNA

Since Bergstrom and Ruth reported the synthesis of C-5 uridine derivatives using organopalladium intermediates, a variety of uridine analogues have been developed[22-25]. Most notable among these modifications is aaU, which has been used extensively as a reactive handle to which various tags were conjugated for downstream applications[26-28]. Herein, the synthesis of aaU-RNA and utility of the reactive aaU to incorporate cyanobenzyl CARS contrast agents was demonstrated. Accordingly, it was relevant that T7 has been used to incorporate aaU and other 5-modified uridine derivatives into short *in vitro* generated transcripts[19, 20]. Literature yields of transcripts containing aaU were around 80% when compared with unmodified control reactions. The present study reports a yield between 60 – 80% for aaU-RNA and upwards of 90 – 100% for shorter transcripts (163mer and 270mer). These results gave preliminary evidence that aaU was effectively incorporated into the aaU-RNA transcript by T7, which was in agreement with previous studies[19, 20].

A common problem when working with modified nucleobases is premature termination of transcription that results when the modified substrate interferes with the elongation process during the IVT reaction. A significant quantity of early termination products were produced when small (10 – 50 nt) transcripts were synthesized by T7 using modified nucleotides, including aaU[17-20]. Thus, it was expected that such products would also be produced during the synthesis of aaU-RNA and aaU-163mer (and the 270mer with aaU).

Early terminations were characterized by the presence of smaller fragments when the IVT reaction products were analyzed by Agilent electrophoresis. For aaU-163mer (and the

270mer with aaU), no early termination products were detected by electrophoresis (Figure 2.2D). Contrary to this, a small population of early termination products was produced in the aaU-RNA IVT reaction (Figure 2.2C). However, the percentages of total RNA synthesized were nominal, especially when compared to the amount produced from smaller transcripts[17-20].

The most likely reason for this difference arose from the IVT reaction components. The cited IVT reactions all used 100% of the modified substrates in place of wild-type nucleotides. A titration to optimize the amount of aaUTP in the transcription reaction revealed that 100% aaUTP produced a plethora of early termination products (Figure 2.2C). When the amount of aaUTP was decreased from 100% to 1:1 aaUTP:UTP, the IVT reaction yielded a homogenous transcript population. Thus, while advantageous for introducing more reactive amines, the increase in early termination products precluded using 100% aaUTP in the IVT reaction.

It is also important to note the general finding that modified transcripts (including those with aaU) display electrophoretic migrations that were higher than unmodified transcripts[17-20]. This finding follows logically from the fact that most nucleotide analogues are heavier than their wild-type counterparts. Therefore, transcripts containing the heavier nucleotide analogues would migrate slower under an applied current than unmodified controls. Opposing this, was the finding that aaU-RNA and aaU-163mer/270mer displayed retarded migration velocities relative to the parent 163mer and 270mer transcripts (Figure 2.2B and 2.2D). Conversely, further modification of these transcripts resulted in a decreased electrophoretic migration velocity, which was consistent with previous studies (Figure 2.9A and 2.10A)[17-20].

The discrepancy between modified and unmodified aaU transcripts and literature values may stem from the following: 1) the cited literature used transcripts less than 100 nt – electrophoretic effects on a 10,000 nt transcript (like HCV RNA) could be much different; 2) a sequence in the 3' region of the HCV RNA template DNA (such as the poly(U/UC) tract) consistently mediated early termination in the presence of aaU; or 3) an undetermined variable inherent to Agilent electrophoretic analysis influenced the migration of transcripts containing aaU.

Since T7 was used for all the IVT reactions discussed (literature and experimental), the probability of incorporating the modified substrate was presumed to constant. Therefore, if different template sequences had the same percentage of thymidine they would be expected to have the same aaU:U ratio in the resulting transcript. In fact, even if one template contained a higher percentage of thymidine residues, the aaU:U ratio would still be expected to remain constant. However, transcripts containing aaU would be heavier than unmodified controls and thus the electrophoretic migration should decrease. Additionally, at pH 7 the aminoallyl group carries a positive charge that would effectively neutralize a portion of the negative charge of the phosphate backbone. Since negative charge facilitates cathode-directed migration, a decrease in the magnitude of that charge would retard the migration velocity. The migration of aaU-RNA and the smaller transcripts containing aaU deviated from these theoretically predicated results, which indicated that increased molecular weight and charge neutralization effects did not contribute to the increased migration velocity of aaU transcripts.

The frequency of abortive transcripts often increases when using modified substrates with template sequences known to be difficult for T7 to transcribe[19]. Given this, it was postulated that the poly(U/UC) tract in the 3'-UTR of HCV RNA could account for the

reproducible migration difference between aaU-RNA and HCV RNA. However, similar migration results were obtained for aaU-163mer/270mer, which were produced from a different template than HCV RNA (see materials and methods). Since the effect was not specific to the HCV RNA template, the decreased migration velocity of transcripts containing aaU was likely not sequence dependent.

Eliminating these explanations lead to the conclusion that the increase in migration velocity for transcripts containing aaU was caused by an undetermined variable associated with Agilent electrophoretic analysis. Since literature migrations were determined using conventional denaturing RNA gel analysis, the migratory behaviour of modified RNAs could be quite different when compared to their migration using Agilent electrophoresis.

The results presented here gave excellent preliminary evidence that aaU was incorporated into HCV RNA via an IVT reaction that utilized the promiscuity of T7 for modified substrates. The electrophoretic migration of aaU-RNA left some ambiguity as to the length of this transcript, but careful examination of the results indicated that full-length aaU-RNA was likely produced. Chemical modification of aaU-RNA to enable visualization using CARS microscopy and examinations of the functional and structural modifications introduced to HCV RNA will be presented in subsequent sections. However, before this could be done a means of quantifying the extent of aaU modification needed to be developed.

HPLC and LC-MS Analysis of Modified RNAs

Establishing CARS detection limits for the C-D and CN modes required quantifying the number of these exogenous vibrational modes present within the focal volume. Furthermore, determining the labelling efficiency of the 3-CN-NHS reaction required knowledge of the number of aaU residues incorporated during the IVT reaction. For D-RNA

this was not an issue because the number of deuterium atoms and the length of HCV RNA were known. From this known data, the number of C-D modes per RNA was calculated (~75,000) and the CARS microscopy detection limit for the C-D mode could be determined. The precise number of aaU residues was unknown because a 1:1 ratio of aaUTP:UTP was used in the IVT reaction. Therefore, the number of aaU residues was dependant upon the ability of T7 to incorporate wild-type versus modified substrates.

The necessity of performing Raman analysis on dry samples meant that Raman spectroscopy could provide binary data on the presence or absence of CN modes, but could not be used for quantitative analysis. Also, aaU does not possess Raman modes that differentiate it from other RNA modes. Therefore, Raman spectroscopy could not be used to characterize aaU-RNA and CN-aaU-RNA. IR spectroscopy could provide quantitative analysis on the number of CN modes present. However, attempts to analyze samples by IR were hindered due to the absorption of IR radiation by water, which severely decreased the signal-to-noise ratio (data not shown). Furthermore, IR spectroscopy would also be unable to resolve resonances that were unique to aaU. Matrix-assisted laser desorption ionization (MALDI) MS was another option that is frequently used to identify modified ribonucleobases[29, 30]. However, there is a size restriction for MALDI-MS analysis of RNA of around 1200 nt and it is difficult to obtain quantitative data[31-33]. Since HCV RNA is 10,000 nt transcript and required quantitative results, MALDI-MS was also unsuitable for characterizing aaU-RNA and CN-aaU-RNA.

Another technique used to characterize modified ribonucleobases is HPLC, which is capable of providing diagnostic and quantitative data[34-36]. LC-MS can also be used as an auxiliary means of confirming the identity of particular eluents. However, before transcripts

as large as aaU-RNA and CN-aaU-RNA could be analyzed they needed to be enzymatically degraded to their constituent monomers.

To streamline the analysis of modified RNA by HPLC and LC-MS, resolution was first attempted using mononucleotides, which would eliminate the necessity of dephosphorylating the digested RNA before analysis. While effective resolution of the four naturally occurring nucleotides was achieved, the intervening distance between eluents was minimal. This was a direct result of using a C18 column instead of an ion-exchange column, which are frequently used to examine complex mixtures of mono- and oligonucleotides[37, 38]. Due to the hydrophobicity of the C18 column, the formal charge on the phosphate group was the primary determinant of retention time. Decreasing the mobile phase pH to 1 neutralized the formal charges on the phosphate oxygen atoms ($pK_a \approx 2$), and increased the peak-to-peak retention times. However, when attempting to identify eluents by LC-MS at low pH, the signal-to-noise of concentrated (10 mM) standard solutions was significantly decreased. This indicated that it would be difficult to identify peaks from digested RNA reactions, as they would be present in much lower concentrations and therefore, would likely be unremarkable amongst the increased noise. Therefore, a dephosphorylation step was included so that the primary determinant of chromatographic resolution would be nucleoside structure and not the presence of phosphate formal charges.

Once the focus was shifted to mononucleosides, HPLC conditions were optimized to maximize the peak-to-peak retention times and LC-MS analysis confirmed the identity of each eluent (Figure 2.4A and 2.4B). While C, U, G and A were identified as their respective molecular ions, aaU was detected by MS as a weakly ionizing ammonium adduct. Given that the concentration of the aaU standard solution was 6 mM, it was concluded that detecting aaU by MS following digestion and dephosphorylation was unlikely. However,

since the elution profile of aaU had already been established, this proved not to be a issue.

The problematic ionization observed for aaU was also observed for the ESI-MS analysis of 3-CN-NHS. As these are the starting materials for forming aaU-CN, it was not surprising that detection of aaU-CN was also hindered by poor ionization (discussed below). The reason for the problematic ionization of these materials is still undetermined.

A paramount consideration when designing a protocol for the digestion and dephosphorylation of modified RNAs was the specificity of the nuclease and phosphatase for unnatural substrates. While several studies have used snake venom phosphodiesterase to mediate RNA digestion for HPLC analysis, it was postulated that this enzyme cannot fully degrade RNA containing uridine analogues, including aaU[20, 34-36]. As a result S1 nuclease (S1) was chosen to develop this methodology, as it has been shown to efficiently digest alkylated, depurinated and UV-irradiated substrates[39]. S1 is also known to catalyze the digestion of double-stranded and single-stranded RNA segments, which was important due to the highly complex secondary and tertiary structural elements present in HCV RNA[39].

In order to prove that HCV RNA was being digested to completion a series of control experiments were conducted. First, it was necessary to show that 50U of S1 was a saturating concentration of enzyme. This was done by comparing the absorbance of the constituent nucleosides following digestion with varying concentration of S1. Results showed that the digestion reaction saturated for HCV RNA and aaU-RNA with 10U of S1 (Figure 2.6A). However, given the lag in aaU-RNA digestion from 2U to 10U when compared to HCV RNA, it was decided that the reaction should still be done with 50U of S1 to ensure maximal digestion. Next, the time dependence was tested as a second means of confirming that digestion was maximized. The digestion reaction saturated after 2 hours and thus, an

overnight digestion was determined sufficient to saturate the digestion of normal and modified HCV RNA (Figure 2.6B).

The fact that the digestion reaction was saturating did not necessarily have any correlation to the percentage of RNA that was converted to mononucleosides. This was an important aspect of validating the HPLC/LC-MS analysis protocol and, therefore, warranted investigation. Comparison of experimentally determined nucleoside concentrations with those calculated from the mass of RNA digested indicated that the reaction was 80 – 90% complete. The CIP reaction was not investigated because the absence of early eluents indicating phosrphorylated nucleotides demonstrated that it was completely dephosphorylating all substrates present. When taken as a whole, these findings showed that HCV RNA and aaU-RNA where being digested to near completion, which was an integral point of validation if HPLC was to be used to quantitatively to investigate modifications to HCV RNA.

Once the validity of the HPLC/LC-MS analysis was proven, it was possible to investigate the extent of aaU incorporation with the surety that the results obtained were representative of the entire modified transcript. Of note to this goal was a 2004 study that specifically investigated the efficacy with which T7 incorporated various 5-modified uridine analogues, two of which bear similarities to aaU[19]. The authors found that uridine derivatives bearing a positively charged group (primary amine or histidine) at the 5-position produced full-length transcripts from a sequence designed to be difficult for T7 to transcribe as well or better than reactions using wild-type substrates. This implied that uridine analogues bearing a positive charge were potentially incorporated preferentially over wild-type uridine. This finding fit very well with the experimentally determined aaU:U ratio in aaU-RNA transcripts of 1:1.1 – 1:1.3, which implied that aaUTP was incorporated more

efficiently than UTP. There are 2166 uridines in HCV RNA, which meant that there were 1100 – 1200 aaU residues incorporated into aaU-RNA. This also meant that there are 1100 – 1200 reactive primary amines amenable to modification with cyanobenzyl groups.

Being able to effectively characterize modifications to HCV RNA was a necessity if the detection limit of CARS microscopy for CN modes is to be established. The results presented here demonstrated that a combination of enzymatic reactions, HPLC and LC-MS were able to characterize the extent of aaU incorporation. These techniques were also key elements in determining the labelling efficiency following reaction of aaU with 3-CN-NHS (discussed below).

Post-Transcriptional Modification of HCV RNA

Modification of HCV RNA was achieved using M linking chemistry, which is a well established method for modifying oligonucleotides (Figure 2.3A). This approach to labeling RNA with cyanobenzyl groups has the advantage of only incorporating one label per RNA, which is a minimal perturbation that was expected to cause limited structural and functional consequences. In the present study, 4-CN-M and fluorescein-M were used as modifying agents. Electrophoretic analysis of the modified HCV RNAs showed that there was an apparent mass increase that was not proportional to the mass of either 4-CN-M or fluorescein-M (Figure 2.3B). Subsequent characterization by AFM showed that the heterogeneity of 5'-modified and normal HCV RNA did not appreciably differ (data not shown). Also, the absence of small fragments in the AFM images suggested that the modified RNAs were intact. These findings gave preliminary evidence that the 5'-modification of HCV RNA with 4-CN-M was successful. Further characterization of 5'-CN

was not carried out, as the detection of one CN mode per HCV RNA was not possible with Raman spectroscopy or HPLC due to inadequate detection limits.

In addition to 5'-labeling of HCV RNA, post-translation modification of aaU-RNA with NHS-activated cyanobenzoic acid derivatives was investigated with the hope of developing a CN-labelled HCV RNA that would facilitate *in vivo* detection using CARS microscopy. The problematic ionization of aaU and 3- and 4-cyanobenzyl-NHS dictated that CN-aaU would also likely be difficult to detect by LC-MS analysis of digested and dephosphorylated CN-aaU-RNA. Therefore, to obtain quantities sufficient for identification by ESI-MS and/or LC-MS the characterization needed to be done on the CN-aaU mononucleoside.

Initial attempts at conjugating aaU with 4CN-NHS met with repeated failure. This was odd because the aaU peak disappeared by HPLC and the labeling of lysine residues with 4-CN-NHS was successful (see Chapter 2). Structural comparison of lysine with the aminoallyl group of aaU revealed that electronic differences between the reactive portion of these two molecules was not the source of differential reactivity. Rather, it was postulated that having the cyano in the *para* position made the NHS-ester so reactive that other nucleophiles present on aaU (-OH, secondary amine) were being modified to yield of mixture of differentially modified aaU derivatives.

To test this hypothesis Bz-NHS was used as the labeling reagent. It was believed that the tempered reactivity of Bz-NHS ($\sigma = 0.0$ versus $\sigma = 0.70$ for 4-CN-NHS) would result in selective labeling of the most reactive nucleophile, which in this case meant the primary amine of the aminoallyl group. The ionization problem encountered with cyanobenzyl-NHS compounds was not carried over to Bz-NHS, as it was clearly identified by LC-MS as an ammonium adduct ($m/z = 237$) that eluted at 22.5 min (Figure 2.8A). Upon reaction with

aaU a new eluent was observed at 23.6 min and the peak for aaU at 10.6 min. disappeared (Figure 2.8A). LC-MS identified the 23.6 min. eluent as an ammonium adduct of Bz-aaU (m/z = 421), which confirmed that the conjugation of Bz-NHS and aaU was successful. To show that the reaction would work with oligonucleotides the Bz-NHS reaction was next applied to labeling aaU-163mer. The short transcript was chosen because it represented a simplified system that labeling reactions could be optimized on before applying them to the much more complex HCV RNA.

Following the labeling reaction, aaU-163mer showed a decrease in electrophoretic migration velocity that was consistent with a successful labeling reaction (Figure 2.9A). These findings also supported previous conclusions regarding the aberrant migration of aaU-being linked to variables intrinsic to the Agilent electrophoretic analysis of aaU-modified RNAs. HPLC analysis of the Bz-labelled aaU-163mer showed a clear disappearance of the aaU peak at 10.6 min. that corresponded to the appearance of the Bz-aaU product peak at 23.6 min (Figure 2.9B). Comparison of aaU peak intensities before and after the conjugation reaction gave a labeling efficiency >90%. The fact that there was no peak for Bz-NHS (22.5 min.) indicated that the removal of unreacted Bz-NHS was achieved. This was an important point because the presence of unconjugated cyanobenzyl labels would produce false positives when analyzing CN-aaU-RNA by Raman and CARS microscopy.

Having shown that the reaction proceeded with the less reactive Bz-NHS, conjugation of aaU with 3-CN-NHS (σ = 0.62) was attempted. Since 3-CN-NHS was less reactive than 4-CN-NHS (as indicated by the lower Hammett σ parameter), it was believed that 3-CN-NHS would react in a manner analogous to Bz-NHS. Electrophoretic analysis of the conjugation reaction again showed a decreased migration velocity for the labelled aaU-163mer, which was indicative of a successful labeling reaction (Figure 2.9A). Further

evidence was provided by HPLC analysis that showed the disappearance of aaU (10.6 min.) corresponded to the appearance of CN-aaU at 23.6 min (Figure 2.9C). Subsequent analysis by LC-MS was unable to confirm the identity of this new product that eluted at the same time as Bz-aaU. However, ESI-MS revealed a weak signal at $m/z = 429$, which was the molecular ion peak of aaU-CN. Again, a labeling efficiency >90% was obtained.

In the penultimate step of characterizing CN-modified HCV RNA, the reaction of 3-CN-NHS with aaU-RNA was investigated. Electrophoretic and HPLC analysis were identical to the results of CN-labelling the 163mer, which indicated that labeling of aaU-RNA with 3CN-NHS was successful (Figure 2.10A and 2.10B). Not only was the reaction a success, but the labeling efficiency was still >90%. This was an impressive result when working with a system as structurally complex as the replicon RNA. Calculating from the number of aaU residues determined by HPLC, the number of CN modes per HCV RNA was around 1000. While significantly less than the approximately 75,000 C-D modes in D-RNA, the scattering cross-section of the CN mode should effectively compensate for this difference.

As the final step in characterizing CN-aaU-RNA, Raman spectroscopy and microscopy were conducted to gain definitive proof that conjugation of 3-CN-NHS to aaU-RNA had occurred. The Raman spectrum of CN-aaU-RNA clearly showed the presence of a CN resonance (2238 cm^{-1}) in the Raman transparent window of the cell (Figure 2.13A). When combined with the fact that no peak for 3-CN-NHS was detected by HPLC following reaction purification, this result showed that the CN labeling reaction was successful. As stated previously, the Raman data gathered for this thesis cannot be examined quantitatively so the absolute scattering cross-section per CN mode could not be determined.

As with D-RNA, Raman microscopy analysis of CN-aaU-RNA was conducted to demonstrate that contrast specific to the CN mode could be generated (Figure 2.13B). The results of this experiment clearly showed that the CN and O-P-O nucleotide backbone vibrational modes co-localized, which gave definitive confirmation that the CN mode was conjugated to aaU-RNA. They also showed that image contrast specific to the CN mode could be generated.

The characterization of aaU-RNA and CN-aaU-RNA has demonstrated that effective incorporation of aaU and efficient modification of aaU with 3-CN-NHS enabled the introduction of approximately one CN mode for every 10 nt into HCV RNA. Attaining such a high density of CN modes per HCV RNA molecule facilitated the generation of excellent image contrast specific to the CN mode using confocal Raman microscopy. These results suggested that CN-aaU-RNA will be an excellent candidate for *in vivo* analysis using CARS microscopy. However, before proceeding to live-cell imaging experiments it was important to characterize these RNAs for any functional or structural changes resulting from modification.

Functional Validation of Modified RNAs

The structural complexity of the HCV genome underscores the importance of characterizing the functional and structural consequences of biomolecular modification. Research shows that subtle changes to the primary sequence of HCV RNA can result in drastic functional consequences[40-43]. It is logical to conclude, therefore, that incorporating a heavily modified nucleotide analogue throughout the length of the genome was likely to have significant deleterious effects. Owing to this, functional validation of the modified HCV

RNAs was carried out using the luciferase reporter assay described in the results section of this chapter.

Following transfection of the modified RNAs into Huh-7 cells, a luciferase assay was performed at 24 and 48 hour endpoints to examine the functional consequences of different RNA modifications. The success of the transfection was apparent from the 2 – 3 fold increase in luciferase activity when cells transfected with HCV RNA were contrasted to the cells only and mock transfection controls at 24 and 48 hour endpoints (Figure 2.14). When comparing the luciferase activity of HCV RNA with cells exposed to the modified RNAs, clear differences in luciferase activity were observed. For aaU-RNA and CN-aaU-RNA the luciferase activity had effectively been eliminated. 5'-F had limited activity when contrasted against the control reactions and 5'-CN showed no activity that was statistically different from control reactions. Finally, D-RNA maintained a substantial percentage of activity relative to unmodified HCV RNA.

The luciferase activity of D-RNA was expected to be very close to that of the unmodified HCV RNA because the substitution of deuterium for hydrogen was a minimal structural change. A precise explanation for the observed decrease in luciferase activity is unknown. However, a comparison of the luciferase activities of HCV RNA that was synthesized with only one of the deuterated nucleotides incorporated revealed an interesting comparison between the activities of RNA synthesized with deuterated ATP/UTP versus GTP/CTP (Figure 2.15A). These results suggested that the decrease in activity was related to the number of hydrogen bonds donated by the base. Definitive reasons for the observed decrease in luciferase activity are still under investigation.

Initially, the luciferase activity of these modified HCV RNAs was very surprising – especially considering the extent of activity lost for 5'-labeled samples that possess minimal

modifications to the RNA. Upon closer inspection of the genomic structure of HCV RNA, a potential explanation for these results became apparent. The 5'- and 3'-UTRs of the HCV genome are highly structured and play important roles in the translation of viral proteins and viral replication (for reviews see [1, 44]). As such, it was not surprising that modest perturbations could severely affect the function of these structured domains.

Nucleotides 5 – 24 form domain I of the HCV 5'-UTR and are known to be important in viral replication[43]. The proximity of domain I to the 5'-terminus of the HCV genome suggested that perturbations introduced by 5'-modifications may be partly responsible for the loss of luciferase activity displayed by 5'-F and 5'-CN. While this explanation fit well with the 5'-F luciferase activity, it seemed unlikely that a decrease in replicative capacity was the sole determinant of the abolished activity displayed by 5'-CN. It was also possible that the 5'-modifications were disrupting a long-range interaction within the 5'-UTR that was important to the translation of the luciferase gene.

Currently, no evidence exists for long-range interactions localized to domain I, but the HCV IRES is known to adopt a complex three-dimensional architecture that could bring the modified 5'-terminus in proximity of the HCV IRES[42]. In doing so, the 5'-modification could directly interfere with other 5'-UTR structural elements or prevent key RNA-protein interactions. While speculative, this theory effectively accounts for the decrease in luciferase activity of the 5'-modified HCV RNA in the absence of evidence supporting alternative theories.

The elimination of luciferase activity for aaU-RNA and CN-aaU-RNA required a more complex analysis than the 5'-modified RNA because aaU was incorporated randomly throughout the entire length of the replicon RNA. The simplest explanation was that aaU was integrated into the AUG start codon and was interfering directly with the recruitment of

translational machinery. The random nature of aaU incorporation meant that aaU would be incorporated into the AUG start codon in 50% of transcripts. At best, such a situation could only account for 50% of the observed decrease in luciferase signal. A second option was that aaU was preventing secondary structures from melting to facilitate viral replication. This was postulated because aaU maintains Watson-Crick base-pairing and stabilizes RNA-RNA duplexes[20]. Similar to the explanation for 5'-CN, a replicative deficiency alone is not likely to account for the observed decrease in luciferase activity. A third explanation was that RNA-RNA and protein-RNA interactions within the 3'-UTR poly(U/UC) domain were disrupted due to the abundance of aaU residues in this region[45]. Finally, a more holistic theory pointed to the replicon-wide distribution of aaU directly affecting translation of luciferase and viral proteins and inhibiting viral replication. This theory takes structural detriments and decreases in the efficacy of RNA-protein interactions resulting from aaU incorporation into account. It was likely an amalgamation of all or some of these possible reasons that combined to give the observed decreases in luciferase activity.

For the purposes of investigating processes directly related to HCV RNA, modified RNAs needed to maintain as much wild-type function as possible. This was especially important for live-cell tracking of HCV RNA, as an accurate picture of RNA dynamics and processing would be impossible to obtain if the majority of the function of the RNA were abolished due to the modifications introduced to enable tracking. However, the extent of modification must also be balanced with the detection limits of CARS microscopy. Therefore, it would be advantageous to be able to control the extent of aaU incorporation and 3-CN-NHS modification of aaU-RNA such that the detection limits of CARS microscopy and the activity of the modified HCV RNA were mutually accommodated.

The extent of 3-CN-NHS modification of RNA containing aaU was investigated by performing a titration of 3-CN-NHS concentration in the labeling reaction. Again, to avoid the complexities of optimizing this approach in a system as elaborate as HCV RNA, the 163mer model system was used to establish the validity of the experiment. HPLC analysis demonstrated a correlation between the concentration of 3-CN-NHS in the labeling reaction and the extent of aaU modification (Figure 2.11A). This was also evident when the electrophoretic migrations of the labeling reactions were examined. There was a large shift in mobility upon 10-fold dilution of 3-CN-NHS, which was indicative of the extent of modification decreasing significantly. Interestingly, even with a 100-fold dilution in 3CN-NHS concentration, 25% of aaU residues were still modified. Application of this approach to aaU-RNA gave similar results, with a 10-fold dilution of 3-CN-NHS resulting in a 10% decrease in the extent of aaU modification (Figure 2.11B).

Demonstrating that the extent of aaU modification could be regulated was important, but it was equally vital to show that the amount of aaU incorporated during the IVT reaction could be controlled. This reaction was performed directly on the HCV RNA template as the products would be used for subsequent functional characterization (see below). The results of this experiment clearly showed the correlation between aaU concentration and the amount of aaU used in the IVT reaction (Figure 2.7A). Furthermore, as the amount of aaU in the IVT reaction decreased the electrophoretic migration of the transcript approached that of HCV RNA. This offered clear evidence that the increased migration velocity of aaU-RNA was causally linked to the presence of aaU. When the transcripts produced from these IVT reactions were analyzed for functional activity, there was a two-fold increase in the luciferase activity upon 4-fold dilution of the aaUTP concentration in the IVT reaction (Figure 15B).

These results demonstrated that the functional consequences of modifying HCV RNA could be modulated by decreasing the extent of aaU incorporation. Furthermore, despite the modest increase in luciferase activity (still only 10% of HCV RNA activity), the fact that the activity could be rescued supported the use of CN-aaU-RNA as a tool for investigating dynamical processes *in vivo* using CARS microscopy. In addition to modulating the extent of aaU incorporation during the IVT reaction, control over the degree of 3-CN-NHS modification will also be an important avenue when fine-tuning CN-aaU-RNA for both *in vivo* function and detection via CARS microscopy.

Structural Validation of Modified RNAs

Many of the plausible theories for the decreased luciferase activity of the modified RNAs were centered on perturbations to secondary and tertiary structural elements. Working with such a large RNA transcript limited the techniques available to investigate the validity of these assumptions by examining the entire system.

Dynamic light scattering (DLS) is a spectroscopic technique used primarily to size particle suspensions. In particular, due to the intense scattering of light from the metallic surface, DLS has been widely used to characterize colloidal nanoparticle solutions to obtain a measure of the degree of polydispersion[46]. DLS has also been used to characterize the hydrodynamic radius of biomolecules, including proteins, lipids and oligonucleotides[47-52].

As a first-line means of investigating the structural effects of modifying HCV RNA, the hydrodynamic radii of modified HCV RNAs was measured. The results obtained were unable to distinguish a significant difference between the different RNA samples (Figure 2.16). This was not interpreted to mean there were no structural differences between these samples. On the contrary, the functional data clearly suggests that there was a difference.

The nature of DLS analysis necessitated that the buffer contain a physiological concentration of Mg^{2+} to obtain reproducible results[53, 54]. The reason for the sporadic data obtained in the absence of Mg^{2+} was a result of electrostatic repulsion of the negatively charged phosphates. Addition of Mg^{2+} resulted in screening of the negative charges and lead to the RNA adopting a compacted conformation often referred to as a collapsed state[53]. The size of the collapsed state (~30 nm) fit well with the expected size necessary to fit into the intact HCV virion[13]. However, while collapsed states are well established intermediates in many RNA folding pathways, there was no evidence supporting a role in the folding and packing of HCV RNA.

AFM has been used extensively in the study of DNA and, more recently, was extended to include the investigation of RNA secondary structure and viral RNAs[55-63]. The current study employed AFM to investigate the bulk structural effects of modification to aaU-RNA and CN-aaU-RNA relative to HCV RNA. These samples are the most amenable to study with AFM because the nature of their modifications imply that they would experience the largest structural perturbations and were therefore likely to be within the resolution limits of AFM.

To facilitate the adhesion of polyanionic RNA to the anionic mica surface a sufficient concentration of Mg^{2+} (millimolar) must be present in the AFM analysis buffer to overcome the coulobmic repulsion between the like charges[53, 64]. Having established that millimolar concentrations of Mg^{2+} induced the electrostatic condensation of the modified RNAs to the collapsed state, it seemed as though AFM may yield results similar to those obtained by DLS. Indeed, the apparent radii of the modified RNAs following surface deposition appeared similar, with the dispersion consistently ranging from 80 – 120 nm. It is well established that during deposition long polymers often undergo a three-to-two dimensional transition[65]. This is caused by partial dissolution of the condensed state due to interactions

with surface Mg^{2+} that become energetically favourable as the deposition buffer is removed. The discrepancy between the AFM and DLS radii was likely the result of these transitions.

The morphology of the RNA following deposition provided valuable information regarding the structural changes introduced in the presence of aaU and aaU-CN. While the condensed state was not representative of native tertiary structure, it contained non-specific structural elements that could be used as a model for the effects of labeling on native HCV RNA structure[53]. Comparison of the AFM images acquired for aaU-RNA, CN-aaU-RNA and HCV RNA revealed distinct differences in morphology that implied the modified RNAs adopted a more open conformation on the mica surface (Figure 2.17). Also, single-stranded RNA fragments were observed with a much higher frequency for the modified RNAs.

These results were best explained by considering the energetics of the condensed state tertiary (and possible secondary) structural elements in the modified versus unmodified RNAs. The morphology of HCV RNA suggested a tightly packed condensed state that had spread slightly during the deposition process. The tight globules present on the molecule suggested that non-specific tertiary interactions were largely maintained during the deposition process. Energetically this meant that the Mg^{2+}-induced non-specific tertiary interactions were more favourable than RNA interactions with the Mg^{2+}-coated mica surface. Application of identical reasoning to aaU-RNA and CN-aaU-RNA lead to the conclusion that the non-specific tertiary interactions in the condensed states were weakened as result of the modifications introduced to enable live-cell RNA tracking using CARS microscopy. Thus, the more relaxed conformation of the modified RNAs showed that Mg^{2+}-induced intramolecular interactions were energetically higher than interactions with mica-bound Mg^{2+}. This evidence supported the theory that the decrease in luciferase activities observed

for the modified RNAs was largely a result of structural perturbations introduced through RNA modification.

Summary

The incorporation of deuterium and CN Raman modes into HCV RNA was carried out to establish a means of tracking dynamical processes related to RNA processing, motility and localization in real-time *in vivo* using CARS microscopy. Characterizations of these materials by HPLC/LC-MS demonstrated the validity of the methodologies used to incorporate these endogenous Raman modes into HCV RNA. Raman microscopy and spectroscopy provided preliminary evidence that contrast specific to the C-D and CN modes could be generated, but sensitivity limits prevented the use of these techniques to analyze the modified RNAs *in vivo* using Raman-based techniques. CARS microscopy analyses of these materials have yet to be attempted.

Functional and structural characterization showed that, with the exception of D-RNA, most of the modifications introduced had a severe effect on the activity of the luciferase reporter assay. HCV genomic structure and subsequent characterizations by AFM revealed that the decrease in luciferase activity was likely the result of perturbations to integral tertiary (and possible secondary) structural elements. Modulation of the extent of aaU incorporation and CN-modification of aaU-RNA has the potential to alleviate some of these deleterious functional deficits, but the detection limits of CARS microscopy must be taken into consideration when determining how many CN modes per RNA molecule are required.

The results presented here provide a solid framework for understanding the response of HCV RNA to modifications and demonstrated that HCV RNA functionalized with C-D

and CN modes can be specifically visualized by tuning to these modes using confocal Raman microscopy.

References

1. Lindenbach, B.D. and Rice, C.M., Unravelling hepatitis C virus replication from genome to function. 2005. **436**(7053): p. 933-938.
2. Levsky, J.M. and Singer, R.H., Fluorescence in situ hybridization: past, present and future. *J Cell Sci*, 2003. **116**(14): p. 2833-2838.
3. Femino, A.M., Fay, F.S., Fogarty, K., and Singer, R.H., Visualization of Single RNA Transcripts in Situ. *Science*, 1998. **280**(5363): p. 585-590.
4. Dirks, R.W., Molenaar, C., and Tanke, H.J., Visualizing RNA molecules inside the nucleus of living cells. *Methods*, 2003. **29**(1): p. 51-57.
5. Gosert, R., Egger, D., Lohmann, V., Bartenschlager, R., Blum, H.E., Bienz, K., and Moradpour, D., Identification of the Hepatitis C Virus RNA Replication Complex in Huh-7 Cells Harboring Subgenomic Replicons. *J. Virol.*, 2003. **77**(9): p. 5487-5492.
6. Mhlanga, M.M., Vargas, D.Y., Fung, C.W., Kramer, F.R., and Tyagi, S., tRNA-linked molecular beacons for imaging mRNAs in the cytoplasm of living cells. *Nucl. Acids Res.*, 2005. **33**(6): p. 1902-1912.
7. Li, Q., Kim, Y., Namm, J., Kulkarni, A., Rosania, G.R., Ahn, Y.-H., and Chang, Y.-T., RNA-Selective, Live Cell Imaging Probes for Studying Nuclear Structure and Function. *Chemistry & Biology*, 2006. **13**(6): p. 615-623.
8. Nan, X., Tonary, A., M., Stolow, A., Xie, X.S., and Pezacki, J.P., Intracellular imaging of HCV RNA and lipids: simultaneous fluorescence and coherent anti-stokes Raman scattering microscopy. *ChemBioChem*, 2006.
9. Andersen, J.S., Lam, Y.W., Leung, A.K.L., Ong, S.-E., Lyon, C.E., Lamond, A.I., and Mann, M., Nucleolar proteome dynamics. 2005. **433**(7021): p. 77-83.
10. Bertrand, E., Chartrand, P., Schaefer, M., Shenoy, S.M., Singer, R.H., and Long, R.M., Localization of ASH1 mRNA Particles in Living Yeast. *Molecular Cell*, 1998. **2**(4): p. 437-445.
11. Dyer, B.W., Ferrer, F.A., Klinedinst, D.K., and Rodriguez, R., A Noncommercial Dual Luciferase Enzyme Assay System for Reporter Gene Analysis. *Analytical Biochemistry*, 2000. **282**(1): p. 158-161.
12. Krieger, N., Lohmann, V., and Bartenschlager, R., Enhancement of Hepatitis C Virus RNA Replication by Cell Culture-Adaptive Mutations. *J. Virol.*, 2001. **75**(10): p. 4614-4624.
13. Ishida, S., Kaito, M., Kohara, M., Tsukiyama-Kohora, K., Fujita, N., Ikoma, J., Adachi, Y., and Watanabe, S., Hepatitis C virus core particle detected by immunoelectron microscopy and optical rotation technique. *Hepatology Research*, 2001. **20**(3): p. 335-347.
14. Nils Johnsson, N.G., Kai Johnsson,, Protein Chemistry on the Surface of Living Cells. *ChemBioChem*, 2005. **6**(1): p. 47-52.
15. van Swieten, P.F., Leeuwenburgh, M.A., M.K., B., and Overkleeft, H.S., Bioorthogonal organic chemistry in living cells: novel strategies for labeling biomolecules. *Org. Biomol. Chem.*, 2005. **3**: p. 20-27.
16. Meier, J.L., Mercer, A.C., Rivera, H., and Burkart, M.D., Synthesis and Evaluation of Bioorthogonal Pantetheine Analogues for in Vivo Protein Modification. *J. Am. Chem. Soc.*, 2006.

17. Gamper, H.B., Gewirtz, A., Edwards, J., and Hou, Y.-M., Modified Bases in RNA Reduce Secondary Structure and Enhance Hybridization. *Biochemistry*, 2004. **43**(31): p. 10224-10236.
18. Kawai, R., Kimoto, M., Ikeda, S., Mitsui, T., Endo, M., Yokoyama, S., and Hirao, I., Site-Specific Fluorescent Labeling of RNA Molecules by Specific Transcription Using Unnatural Base Pairs. *J. Am. Chem. Soc.*, 2005. **127**(49): p. 17286-17295.
19. Vaught, J.D., Dewey, T., and Eaton, B.E., T7 RNA Polymerase Transcription with 5-Position Modified UTP Derivatives. *J. Am. Chem. Soc.*, 2004. **126**(36): p. 11231-11237.
20. Schoetzau, T., Langner, J., Moyroud, E., Roehl, I., Vonhoff, S., and Klussmann, S., Aminomodified Nucleobases: Functionalized Nucleoside Triphosphates Applicable for SELEX. *Bioconjugate Chem.*, 2003. **14**(5): p. 919-926.
21. Evans, C.E., Personal communication with C.E. Evans. 2006.
22. Bergstrom, D.E. and Ruth, J.L., Synthesis of C-5 Substituted Pyrimidine Nulceosides via Organopalladium Intermediates. *J. Am. Chem. Soc.*, 1976. **98**(6): p. 1587-1589.
23. Ruth, J.L. and Bergstrom, D.E., C-5 substituted pyrimidine nucleosides. 1. Synthesis of C-5 allyl, propyl, and propenyl uracil and cytosine nucleosides via organopalladium intermediates. *J. Org. Chem.*, 1978. **43**(14): p. 2870-2876.
24. Bergstrom, D.E. and Ogawa, M.L., C-5 substituted pyrimidine nucleosides. 2. Synthesis via olefin coupling to organopalladium intermediates derived from uridine and 2'-deoxyuridine. *J. Am. Chem. Soc.*, 1978. **100**(26): p. 8106-8112.
25. Inoue, J. and Ueda, T., Synthesis of 6-Cyano- and 5-Cyano-uridines and Their Derivatives (Nucleosides and Nucleotides. XXI). *Chem. Pharm. Bull.*, 1978. **26**(9): p. 2657-2663.
26. Chen, C., Gorin, M., and Sigman, D., Sequence-Specific Scission of DNA by the Chemical Nuclease Activity of 1, 10-Phenanthroline-Copper (I) Targeted by RNA. *PNAS*, 1993. **90**(9): p. 4206-4210.
27. 't Hoen, P.A.C., de Kort, F., van Ommen, G.J.B., and den Dunnen, J.T., Fluorescent labelling of cRNA for microarray applications. *Nucl. Acids Res.*, 2003. **31**(5): p. e20-.
28. Xiang, C.C., Kozhich, O.A., Chen, M., Inman, J.M., Phan, Q.N., Chen, Y., and Brownstein, M.J., Amine-modified random primers to label probes for DNA microarrays. 2002. **20**(7): p. 738-742.
29. Kirpekar, F., Douthwaite, S., and Roepstorff, P., Mapping posttranscriptional modifications in 5S ribosomal RNA by MALDI mass spectrometry. *RNA*, 2000. **6**(2): p. 296-306.
30. Kellersberger, K.A., Yu, E.T., Merenbloom, S.I., and Fabris, D., Atmospheric pressure MALDI-FTMS of normal and chemically modified RNA. *Journal of the American Society for Mass Spectrometry*, 2005. **16**(2): p. 199-207.
31. Berkenkamp, S., Kirpekar, F., and Hillenkamp, F., Infrared MALDI Mass Spectrometry of Large Nucleic Acids. *Science*, 1998. **281**(5374): p. 260-262.
32. Ke, A. and Doudna, J.A., Crystallization of RNA and RNA-protein complexes. *Methods Macromolecular Crystallization*, 2004. **34**(3): p. 408-414.
33. Finn Kirpekar, T.N.K., RNA fragmentation studied in a matrix-assisted laser desorption/ionisation tandem quadrupole/orthogonal time-of-flight mass spectrometer. *Rapid Communications in Mass Spectrometry*, 2001. **15**(1): p. 8-14.
34. Buck, M., Connick, M., and Ames, B.N., Complete analysis of tRNA-modified nucleosides by high-performance liquid chromatography: The 29 modified

nucleosides of Salmonella typhimurium and Escherichia coli tRNA. *Analytical Biochemistry*, 1983. **129**(1): p. 1-13.
35. Crain, P.F., *Preparation and enzymatic hydrolysis of DNA and RNA for mass spectrometry.*, in *Mass Spectrometry*, J.A. McCloskey, Editor. 1990, Academic Press. p. 782-790.
36. Pomerantz, S.C. and McCloskey, J.A., *Analysis of RNA hydrolyzates by liquid chromatography-mass spectrometry.*, in *Mass Spectrometry*, J.A. McCloskey, Editor. 1990, Academic Press. p. 796-824.
37. Gelhaus, S.L. and LaCourse, W.R., Separation of modified 2'-deoxyoligonucleotides using ion-pairing reversed-phase HPLC. *Journal of Chromatography B*, 2005. **820**(2): p. 157-163.
38. Buncek, M., Backovska, V., Holasova, S., Radilova, H., Safarova, M., Kunc, F., and Haluza, R., Unusual chromatographic behavior of oligonucleotide sequence isomers on two different anion exchange HPLC columns. *Analytical Biochemistry*, 2006. **348**(2): p. 300-306.
39. Desai, N.A. and Shankar, V., Single-strand-specific nucleases. *FEMS Microbiology Reviews*, 2003. **26**(5): p. 457-491.
40. Lee, H., Shin, H., Wimmer, E., and Paul, A.V., cis-Acting RNA Signals in the NS5B C-Terminal Coding Sequence of the Hepatitis C Virus Genome. *J. Virol.*, 2004. **78**(20): p. 10865-10877.
41. Friebe, P., Boudet, J., Simorre, J.-P., and Bartenschlager, R., Kissing-Loop Interaction in the 3' End of the Hepatitis C Virus Genome Essential for RNA Replication. *J. Virol.*, 2005. **79**(1): p. 380-392.
42. Odreman-Macchioli, F., Baralle, F.E., and Buratti, E., Mutational Analysis of the Different Bulge Regions of Hepatitis C Virus Domain II and Their Influence on Internal Ribosome Entry Site Translational Ability. *J. Biol. Chem.*, 2001. **276**(45): p. 41648-41655.
43. Friebe, P., Lohmann, V., Krieger, N., and Bartenschlager, R., Sequences in the 5' Nontranslated Region of Hepatitis C Virus Required for RNA Replication. *J. Virol.*, 2001. **75**(24): p. 12047-12057.
44. François Penin, J.D., Felix A. Rey, Darius Moradpour, Jean-Michel Pawlotsky,, Structural biology of hepatitis C virus. *Hepatology*, 2004. **39**(1): p. 5-19.
45. Bradrick, S.S., Walters, R.W., and Gromeier, M., The hepatitis C virus 3'-untranslated region or a poly(A) tract promote efficient translation subsequent to the initiation phase. *Nucl. Acids Res.*, 2006. **34**(4): p. 1293-1303.
46. Panacek, A., Kvitek, L., Prucek, R., Kolar, M., Vecerova, R., Pizurova, N., Sharma, V.K., Nevecna, T., and Zboril, R., Silver Colloid Nanoparticles: Synthesis, Characterization, and Their Antibacterial Activity. *J. Phys. Chem. B*, 2006. **110**(33): p. 16248-16253.
47. Langowski, J. and Giesen, U., Configurational and dynamic properties of different length superhelical DNAs measured by dynamic light scattering. *Biophysical Chemistry*, 1989. **34**(1): p. 9-18.
48. Reddie, K.G., Roberts, D.R., and Dore, T.M., Inhibition of Kinesin Motor Proteins by Adociasulfate-2. *J. Med. Chem.*, 2006. **49**(16): p. 4857-4860.
49. Guo, J., Harn, N., Robbins, A., Dougherty, R., and Middaugh, C.R., Stability of Helix-Rich Proteins at High Concentrations. *Biochemistry*, 2006. **45**(28): p. 8686-8696.

50. Marika Ruponen, C.S.B., C. Russell Middaugh,, Biophysical characterization of polymeric and liposomal gene delivery systems using empirical phase diagrams. *Journal of Pharmaceutical Sciences*, 2006. **95**(10): p. 2101-2114.
51. Zhu, D.-M. and Evans, R.K., Molecular Mechanism and Thermodynamics Study of Plasmid DNA and Cationic Surfactants Interactions. *Langmuir*, 2006. **22**(8): p. 3735-3743.
52. A. A. Timchenko, J.L., I. N. Serdyuk,, Structural changes in 16S RNA from Escherichia coli upon unfolding by urea. *Biopolymers*, 1993. **33**(11): p. 1747-1755.
53. Draper, D.E., Grilley, D., and Soto, A.M., Ions and RNA Folding. *Annual Review of Biophysics and Biomolecular Structure*, 2005. **34**(1): p. 221-243.
54. Draper, D.E., A guide to ions and RNA structure. *RNA*, 2004. **10**(3): p. 335-343.
55. Umemura, K., Nagami, F., Okada, T., and Kuroda, R., AFM characterization of single strand-specific endonuclease activity on linear DNA. *Nucl. Acids Res.*, 2000. **28**(9): p. e39.
56. Zhiguo Liu, Z.L., Hualan Zhou, Gang Wei, Yonghai Song, Li Wang,, Imaging DNA molecules on mica surface by atomic force microscopy in air and in liquid. *Microscopy Research and Technique*, 2005. **66**(4): p. 179-185.
57. Hansma, H.G., Kasuya, K., and Oroudjev, E., Atomic force microscopy imaging and pulling of nucleic acids. *Current Opinion in Structural Biology*, 2004. **14**(3): p. 380-385.
58. Hansma, H.G., Oroudjev, E., Baudrey, S., and Jaeger, L., TectoRNA and 'kissing-loop' RNA: atomic force microscopy of self-assembling RNA structures. *Journal of Microscopy*, 2003. **212**(3): p. 273-279.
59. Medalia, O., Heim, M., Guckenberger, R., Sperling, R., and Sperling, J., Gold-Tagged RNA--A Probe for Macromolecular Assemblies. *Journal of Structural Biology*, 1999. **127**(2): p. 113-119.
60. Hansma, H.G., Golan, R., Hsieh, W., Daubendiek, S.L., and Kool, E.T., Polymerase Activities and RNA Structures in the Atomic Force Microscope. *Journal of Structural Biology*, 1999. **127**(3): p. 240-247.
61. Kuznetsov, Y.G., Daijogo, S., Zhou, J., Semler, B.L., and McPherson, A., Atomic Force Microscopy Analysis of Icosahedral Virus RNA. *Journal of Molecular Biology*, 2005. **347**(1): p. 41-52.
62. Andrea Giro, A.B., Giampaolo Zuccheri, Hugo H.J. Bink, Cornelis W.A. Pleij, Bruno Samorì,, Single molecule studies of RNA secondary structure: AFM of TYMV viral RNA. *Microscopy Research and Technique*, 2004. **65**(4-5): p. 235-245.
63. Drygin, Y.F., Bordunova, O.A., Gallyamov, M.O., and Yaminsky, I.V., Atomic force microscopy examination of tobacco mosaic virus and virion RNA. *FEBS Letters*, 1998. **425**(2): p. 217-221.
64. Sushko, M.L., Shluger, A.L., and Rivetti, C., Simple Model for DNA Adsorption onto a Mica Surface in 1:1 and 2:1 Electrolyte Solutions. *Langmuir*, 2006. **22**(18): p. 7678-7688.
65. Rivetti, C., Guthold, M., and Bustamante, C., Scanning Force Microscopy of DNA Deposited onto Mica: EquilibrationversusKinetic Trapping Studied by Statistical Polymer Chain Analysis. *Journal of Molecular Biology*, 1996. **264**(5): p. 919-932.

Chapter 3 – Chemical Modification of Model Protein Systems

Introduction

Driven it part by the development of a cell-based replicon model of HCV replication the localization, cellular interactions and mechanism of action of the HCV proteins have been extensively characterized (for reviews see [1-4]). However, similar to the analysis of processes related to HCV RNA, studies investigating HCV proteins are almost exclusively static analyses – snapshots of intracellular interactions and protein localization, i.e.: immunofluorescence or fluorescent fusion proteins. This creates an information gap surrounding dynamic processes involving HCV proteins. For example, the migration of mature HCV core protein from the ER to lipid droplets and the subsequent development of steatosis has yet to be investigated dynamically[5, 6]. In general, the delineation of this and other dynamical processes involving HCV proteins would enhance our understanding of HCV molecular virology, which could lead to new treatment options and expose previously unknown therapeutic targets.

Recognizing the aforementioned information gap as a problem, two groups have recently reported on the live-cell analysis of HCV proteins. Using a green fluorescent protein (GFP) fused to the C-terminus of NS5A, McCormick and coworkers examined the localization of the GFP-NS5A fusion to try and establish kinetic aspects of HCV replication complex formation in cell culture[7]. Similarly, Kien and coworkers used an enhanced GFP-E2 fusion to localize E2 in living cells. In addition, Kien and coworkers performed a functional validation of the enhanced GFP-E2 fusion protein, which was an important consideration when fusing a 27 kDa protein like GFP to another biomolecule[8]. Their results showed that E2 retained wild-type function, which suggested that other HCV proteins could be tracked *in vivo* via the rational design and engineering of GFP-fusions.

While successful in the context of the study done by Kien and coworkers, the application of GFP fusion proteins to the live-cell imaging of dynamical processes still suffers from the limitations associated with all *in vivo* fluorescence-based techniques. Expanding the utility of CARS microscopy to include the analysis of specific molecular targets will surmount these problems and enable the dynamic visualization of HCV proteins in real-time *in vivo* over time periods not accessible using fluorescence-based techniques. Achieving these goals required the development of a method to introduce the bioorthogonal C-D and CN Raman modes from Chapter 2, which were shown to generate Raman image contrast when integrated into HCV RNA.

The nominal functional consequences of incorporating deuterated nucleotides into HCV RNA suggested that using deuterated amino acids would be an excellent method of tracking HCV proteins *in vivo* using CARS microscopy. However, due to the low Raman scattering cross-section of the C-D mode, a very high mode density would be required to generate CARS image contrast specific to the C-D resonance. Introduction of the C-D mode in a method analogous to that used for RNA (all non-exchangeable protons substituted for deuterium) could produce the required C-D mode density, but would necessitate the growth of bacteria over-expressing the protein of interest in isotopically-enriched growth medium, which is a time consuming and expensive method of incorporating additional functionality[9, 10].

Therefore, rather than attempt to biosynthesize isotopically labelled proteins, we considered a variety of co- and post-translational methods that are currently used to incorporate additional functionality into proteins. In Chapter 1, click reactions and the Staudinger ligation were mentioned as examples of chemical approaches to site-specifically incorporate exogenous functionality to biomolecules (Figure 3.1A and 3.1B)[11, 12].

Additionally, the *in vivo* compatible condensation of hydrazides with aldehydes and ketones has been used to chemically modify proteins (Figure 3.1C)[13, 14]. The common theme amongst these chemical transformations is the need to synthesize and incorporate modified amino acids into the protein before the reactions can be performed. To accomplish this, genetically encoded (co-translational) protein modification and protein semi-synthetic strategies are utilized.

The most frequently used genetically encoded strategy is the amber suppressor methodology, which uses an evolved tRNA-tRNA synthetase pair that recognizes the amber codon (CUA) and a modified amino acid, respectively (Figure 3.2A)[15]. In contrast to the genetically encoded amber suppressor approach, native chemical ligation involves the semi-synthesis of proteins using two smaller peptides that contain a terminal amine and thiol. The peptide fragments are usually made by solid-phase synthesis and either fragment can contain modified amino acids provided that the terminal residues facilitate the ligation reaction (for a review see [16]; Figure 3.2B). While both of these techniques facilitate the incorporation of modified amino acids, they would not generate the mode density necessary to facilitate C-D image contrast using CARS microscopy. Thus, the cost of synthesizing metabolically labelled proteins and the inability of chemical, genetic and semi-synthetic modifications to meet the C-D focal volume density requirements, precluded using deuterium substitution for the dynamical *in vivo* analysis of HCV proteins using CARS microscopy.

In addition to not facilitating a high mode density (C-D or CN), genetic and semi-synthetic approaches require the optimization of several variables to obtain the modified protein. As such, the potential for high-throughput production of several modified proteins (i.e.: HCV proteins) was limited. Ideally, the amount of optimization required by the

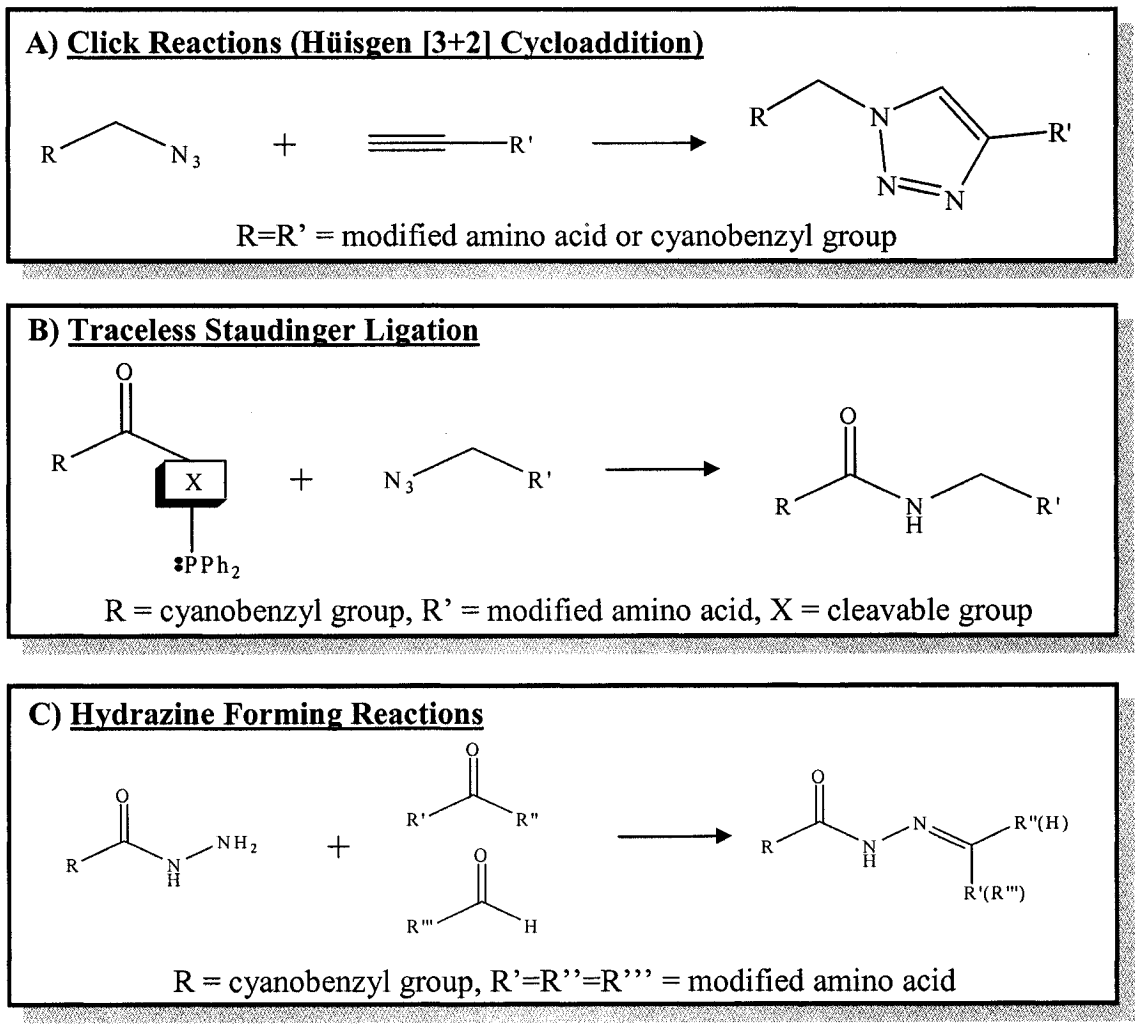

Figure 3.1: Chemical methods of modifying proteins. A) Click reactions require a suitable alkyne-azide pair, which means that a modified amino acid must be used. B) The traceless Staudinger ligation requires the phosphine containing the cyanobenzyl group for CARS contrast and 'X' to remove the phosphine oxide formed during the reaction. The easiest approach has the azide on a modified amino acid. C) Hydrazine formation is mediated by the condensation of a hydrazide with an aldehyde or ketone. Ease of synthesis would likely place the aldehyde or ketone functional groups onto the modified amino acid.

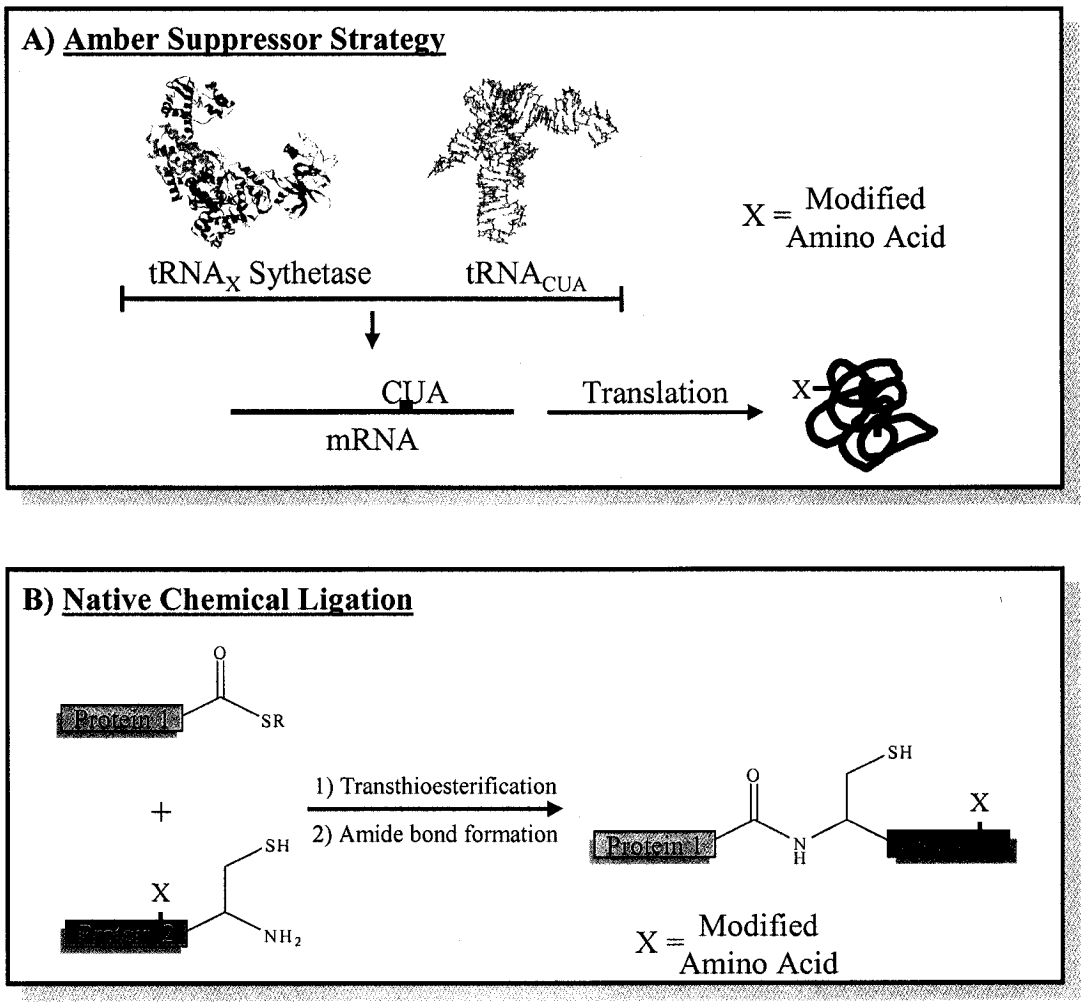

Figure 3.2: Genetically encoded and semi-synthetic methods of protein modification. A) The amber supporesor approach requires the generation of a tRNA-tRNA synthetase pair that only recognize the modified amino acid for incorporation at the amber codon (CUA). B) Native chemical ligation utilizes a transthioesterification reaction followed by formation of the more stable amide bond to semi-synthesize proteins. Either Protein 1 or Protein 2 can contain modified amino acids.

modification protocol should be minimized to allow for rapid application to an entire family of HCV proteins. Therefore, the NHS bioconjugation reaction was employed to incorporate CN modes onto extant proteins for the purpose of *in vivo* tracking using CARS microscopy. The widespread and well optimized use of NHS-activated small molecules for protein modification made this approach well suited to modifying proteins with different physicochemical properties (i.e.: membrane-bound or soluble, with minimal trouble-shooting).

Applying NHS bioconjugation strategies to RNA required that additional functionality in the form of aaU be introduced. Contrary to this, the chemically diverse nature of the wild-type amino acid sidechains affords residue-specific labeling without prior manipulation of the protein – the ϵ-amino group of lysine and the free N-terminus react with NHS-functionalized probes (Figure 3.3A). Reaction with hydroxylated amino acids has also been reported, but this occurs infrequently due to strict sequence requirements (His-Xaa-Ser)[17].

Using 4-CN-NHS, this chapter will describe the incorporation of CN modes into proteins for the purpose of expanding the utility of CARS microscopy to include the *in vivo* analysis of specific proteins in real-time. Optimization of the protocol was demonstrated using bovine serum albumin (BSA; Figure 3.3B) and functional validation of a 4-CN-NHS modified single-domain antibody (sdAb) was carried out to determine the functional effects of introducing the CN modes to a model system. Single-domain anti-bodies were chosen because they are small, structurally simple proteins with a well defined function (antigen recognition) that was easily assayed.

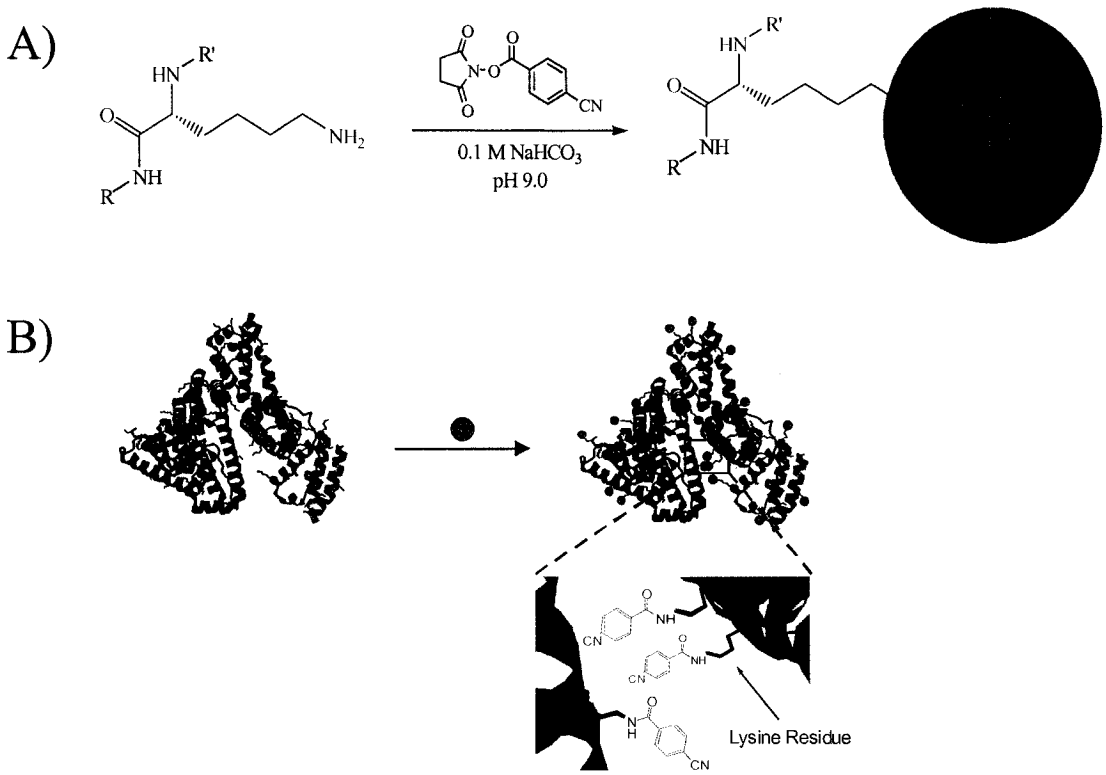

Figure 3.3: Protein modification using NHS-activated acids. A) 4-CN-NHS will selectively react with the ϵ-amino group of lysine sidechains to yield CN-modified proteins. B) Schematic representation of the approach used to modify the model protein BSA. Lysine residues are highlighted in red. R=R' = peptide backbone.

Results

BSA Modification

Modification of BSA was performed as described in the materials and methods. MALDI analysis of normal and 4-CN-NHS modified BSA (BSA-CN) revealed a mass difference of 901 Da, which corresponded to the addition of seven 4-CN-NHS (130 Da/label) groups onto the protein (Figure 3.4). SDS-PAGE analysis of modified and unmodified BSA was also conducted, but no difference in migration was observed (data not shown).

Raman microscopy analysis of BSA-CN was carried out as described in the materials and methods. Integrating the Raman images between 2220 – 2250 cm^{-1} revealed the presence of a distinct CN resonance in the BSA-CN spectrum that was absent in unmodified samples (Figure 3.5). In addition, the CN resonance colocalized with the amide I band at approximately 1650 cm^{-1}. This gave strong evidence that the labeling reaction was successful.

Single-Domain Antibody Modification

Modification of sdAb directed against bacterial protein A (HVHP428) was performed as described in the materials and methods. MALDI analysis of 4-CN-NHS modified (HVHP428-CN) and unmodified HVHP428 revealed a mass difference of 248 Da (Figure 3.6). Given an error of ± 10 Da on the experimentally determined molecular weight, the MALDI data indicated that approximately two 4-CN-NHS groups were conjugated to the antibody. Further confirmation of labeling success was obtained using Raman spectroscopy (Figure 3.7). The limited number of CN modes per HVHP428 yielded an ambiguous signal-to-noise ratio that was not suitable for generating image contrast using Raman microscopy (data not shown).

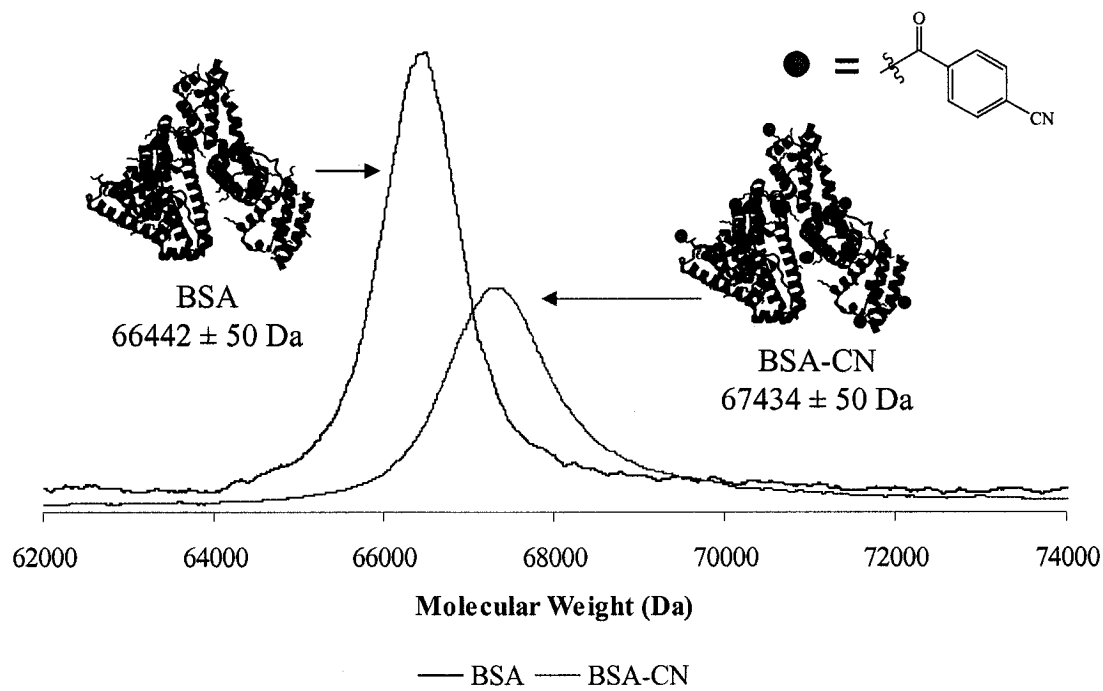

Figure 3.4: MALDI analysis of BSA modification. The mass difference of approximately 900 Da corresponded to the incorporation of approximately 7 4-CN-NHS CARS contrast agents per protein. The positions of the CN labels on BSA-CN are not indicative of the actual residues modified, but were shown for illustrative purposes.

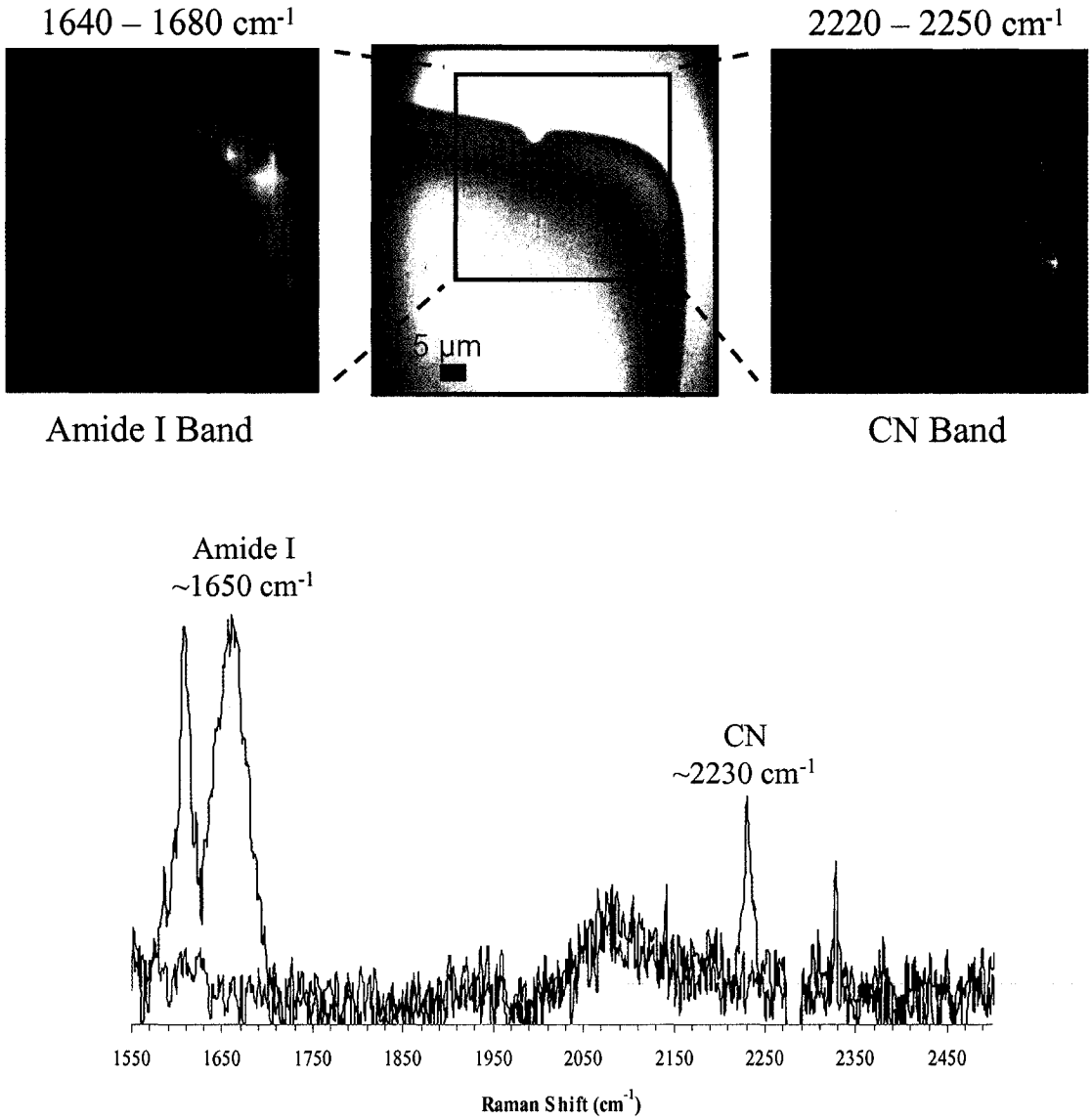

Figure 3.5: Raman microscopy analysis of BSA-CN. The intensity map of the CN Raman band (top right) depicts the intense regions specific to the presence of CN mode at approximately 2230 cm-1. Integration of the amide I band (top left; approximately 1650 cm-1) yielded an intensity image that was spatially co-localized with the CN intensity map. This strong spatial correlation between the CN and amide I modes suggested that modification was successful and specific to the protein rather than to residual 4-CN-NHS. The blue spectrum taken from an intense region (blue circle) of the imaged area showed both amide I and CN vibrational modes. The red spectrum taken from a dark region of the map (red circle) was devoid of any analyte-specific vibrational bands. The blue rectangle in the optical image (top center) shows the region that was imaged.

To establish the functional effects of modifying HVHP428 with 4-CN-NHS, surface plasmon resonance (SPR) analysis of the interaction between HVHP428-CN and its' antigen (protein A) was measured using Biacore analysis as described in the materials and methods. Comparison of the dissociation constants (K_d) for the unmodified (1.5 ± 0.1 μM) and modified (1.7 ± 0.2 μM) HVHP428 revealed that 4-CN-NHS modification had no statistically significant effect on the ability of the HVHP428 to recognize its antigenic target (Figure 3.8).

Discussion

The labour-intensive production of large quantities of recombinant proteins from bacterial and mammalian over-expression systems makes these materials a precious commodity. Therefore, rather than use recombinant HCV proteins to optimize the incorporation of CN modes, it would advantageous to use a cheap, soluble protein that is available in gram quantities; BSA fit this profile. BSA is an approximately 64 kDa soluble protein that has been used extensively as a model system in the development of protein labeling strategies. In particular, due to the presence of 60 lysine residues (~10% of primary sequence), BSA has been successfully applied to the development of amine-directed labeling using NHS- and isothiocyanate-functionalized small molecules[18-25]. BSA has also been used to characterize a variety of M-based approaches to protein labeling[26-29]. However, the M group reacts with cysteine residues, which are in low abundance (2.3% of mammalian codons code for cysteine) and when present are frequently oxidized to form disulfide bonds that are integral to protein structure and function. Owing to this a high CN mode density, which is vital for detection via CARS microscopy, would be difficult to obtain using M-

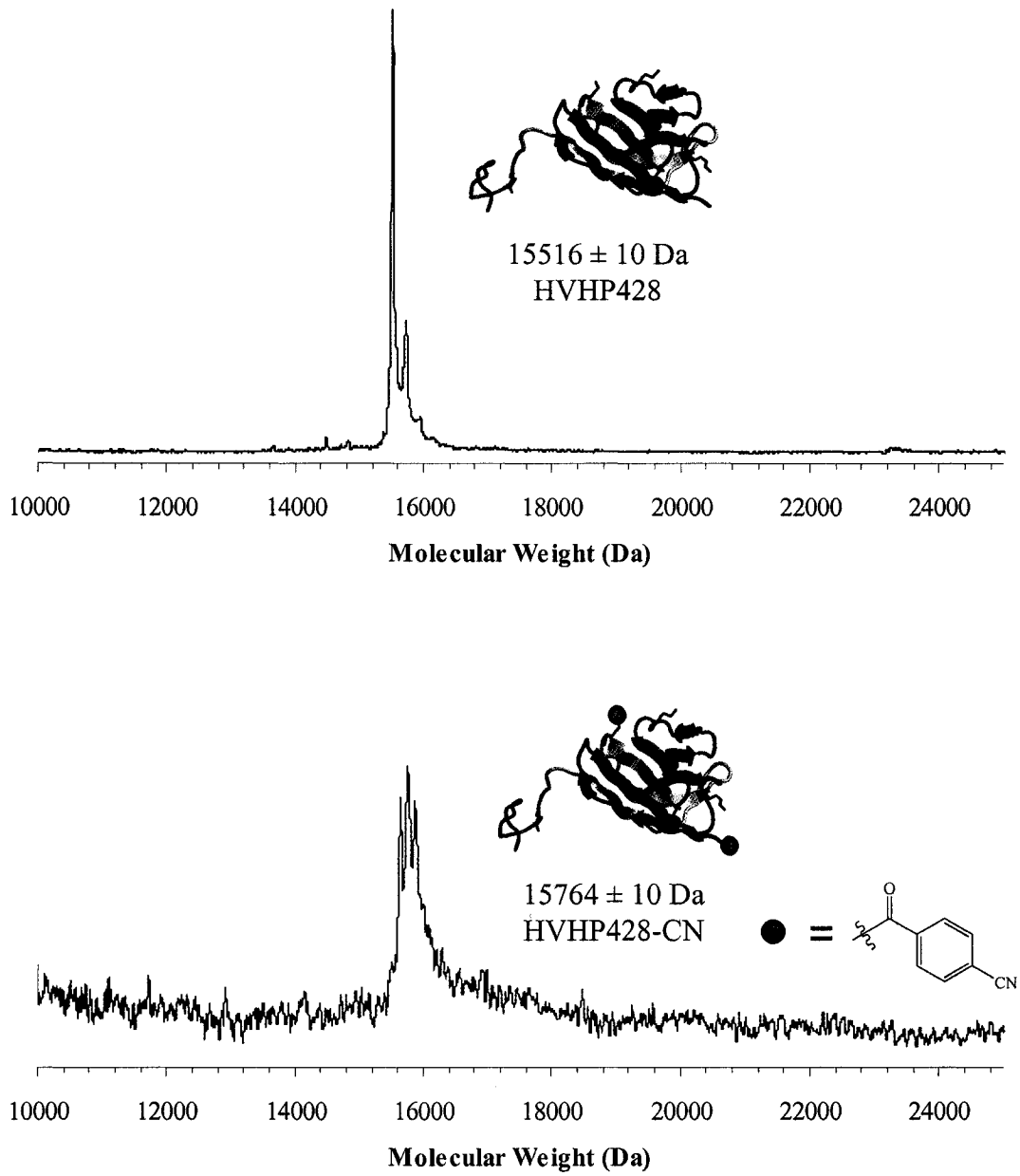

Figure 3.6: MALDI analysis of HVHP428-CN. The mass difference between unmodified (top) and modified (bottom) HVHP428 correlated to approximately two 4-CN-modified lysine residues per protein. Crystals structures and sites of modification are shown for illustrative purposes and do not represent HVHP428.

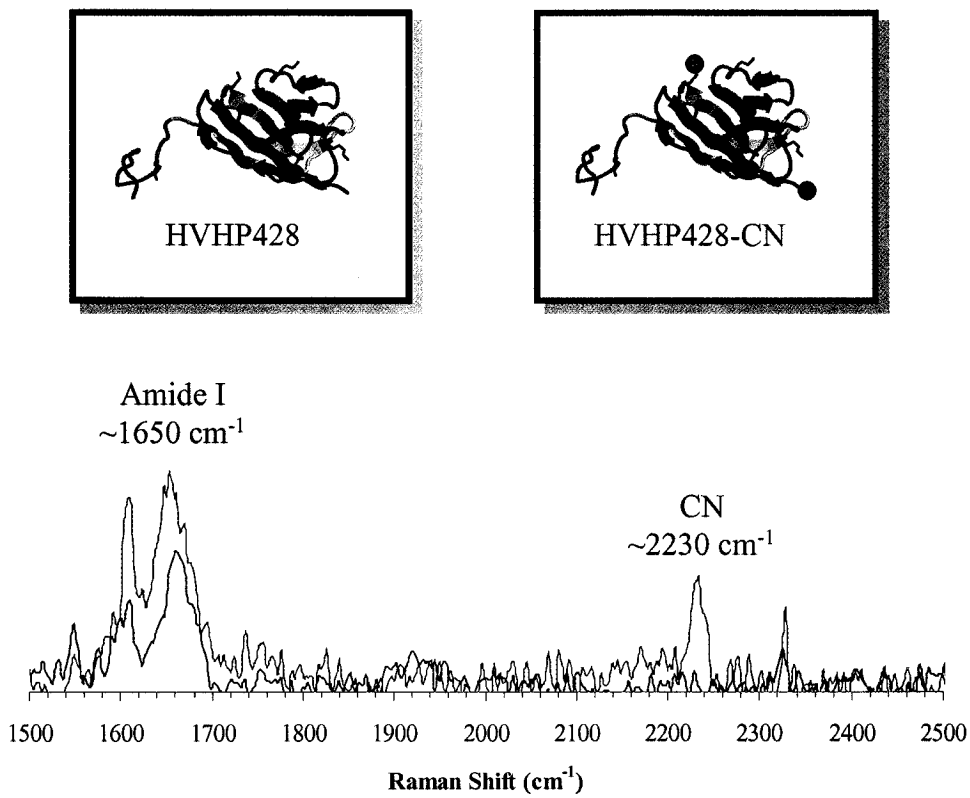

Figure 3.7: Raman spectroscopy of HVHP428-CN. Spectroscopic analysis revealed the presence of the amide I resonance (~1650 cm^{-1}) in both spectra, which confirmed that is was protein being examined. Further analysis showed that HVHP428-CN (pink) clearly displayed a CN resonance (~2230 cm^{-1}) that was absent for HVHP428 (blue).

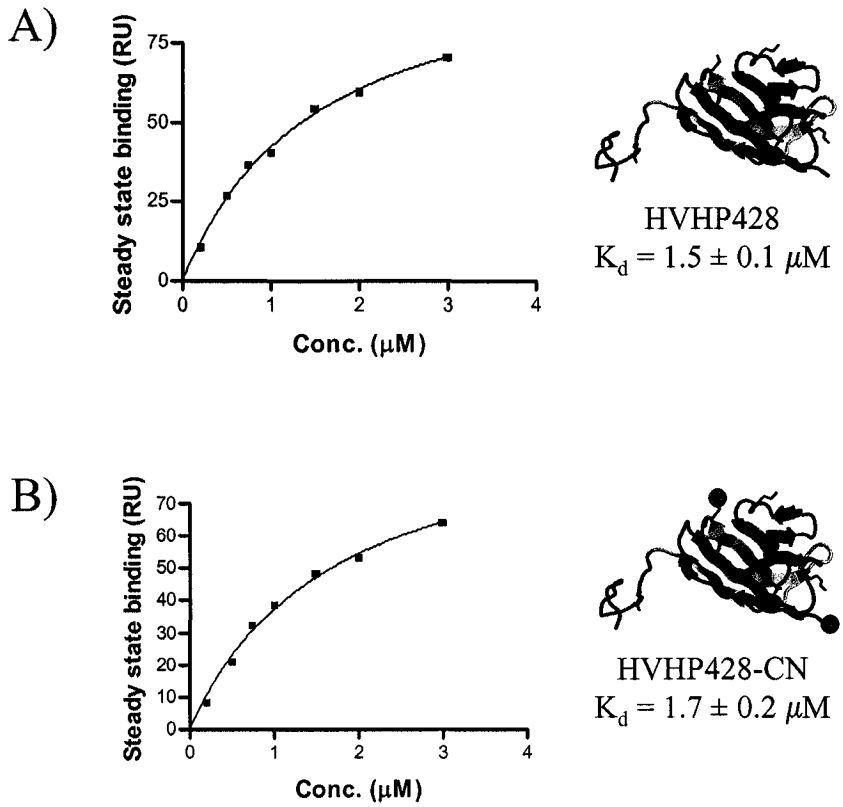

Figure 3.8: Functional validation of HVHP428-CN. A) Analysis of HVHP428 showed that it bound protein A with a K_d = 1.5 ± 0.2 μM μM. B) Similar analysis of HVHP428-CN revealed little statistically significant difference in protein A binding, with K_d = 1.7 ± 0.2 μM. Crystals structures and sites of modification are shown for illustrative purposes and do not represent HVHP428.

based labeling. Therefore, the use of 4-CN-M to modify proteins for *in vivo* analysis was not pursued. MALDI analysis of BSA-CN showed an increased mass for the labelled protein that corresponded to the modification of 7 residues with 4-CN-NHS (Figure 3.4). Assuming that productive labeling occurred only on lysine residues, this correlated to a labeling efficiency of approximately 10% as determined by primary sequence analysis. While seemingly low, this value was likely skewed because all lysine residues were considered. In reality, many lysine residues are buried in the protein's tertiary structure or involved in salt-bridge formation, both of which makes them less likely to react with 4-CN-NHS. Since the modification of BSA was undertaken to show that proteins could be functionalized with CN modes and subsequently imaged using Raman and CARS microscopy, the low labeling efficiency was not investigated further. Supporting this decision was the data obtained from the Raman analysis of BSA-CN that showed a clear CN resonance in the Raman transparent region of the cell that localized with the protein amide I resonance at approximately 1650 cm^{-1} (Figure 3.5).

As with the analysis of modified RNAs, the study of HCV proteins *in vivo* in real-time requires that the function(s) of modified proteins are near wild-type levels. Doing so minimizes the chance of identifying phenotypic changes resulting from protein modification and ensures that dynamical aspects of protein function are unperturbed. The prevalence of chemically modified antibodies that have been successfully utilized for indirect immunofluorescence demonstrates that modified proteins can maintain there efficacy following functionalization. Conversely, the chemical modification of proteins has been shown to affect the physicochemical properties of the modified proteins and alter their *in vivo* function[30-32]. These dichotomous findings were resolved when the functional and

structural diversity of proteins (including co- and post-translation modifications) was considered.

Given the above considerations it may seem that a labeling methodology that was successful for BSA would not be predictive of successfully modifying other proteins. However, the successful application of protocols established on BSA and subsequently used on other proteins show that this approach has merit[18-25]. Therefore, a model system with a well-defined and easily assayed function was needed to determine the functional consequences of 4-CN-modification using the protocol established for BSA.

An obvious choice to fulfill these requirements would be to exploit antibody-antigen recognition to assay for the effects of 4-CN-NHS modification because the primary function of an antibody is closely linked to antibody structure. However, using normal mono- and poly-clonal antibodies could complicate the analysis of the functional effects of labeling. In particular, the size of these proteins (approximately 160 kDa) decreases the mass resolution of MALDI, which can limit the quantification of the number of CN modes incorporated. Additionally, the complex secondary and tertiary structural interactions that define antibody function greatly increase the number of modifications that may contribute to changes in the function of the modified protein. Using a smaller, simpler protein would give a much clearer picture as to what effects the CN-modifications have on protein function. Single-domain antibodies, which are structurally simplistic and smaller (~16 kDa) than mono- and poly-clonal antibodies, fit these requirements precisely. Furthermore, despite being a much simpler protein, the function of sdAbs is still the same – antigen recognition. Therefore, the functional consequences of 4-CN-NHS modification of sdAbs could still be easily assayed. For the current study, the sdAb used (HVHP428) was directed against bacterial protein A.

MALDI analysis of HVHP428 following reaction with 4-CN-NHS revealed that two 4-CN-NHS groups were incorporated per protein (Figure 3.6). Raman spectral analysis of revealed the clear presence of the CN mode (Figure 3.7). Subsequent attempts to confirm this result using Raman microscopy were hindered due to the low number of modifications per HVHP428 (data not shown). As such, it would be advantageous to investigate methods of increasing the labeling efficiency of the 4-CN-NHS reaction. This is currently under investigation. Despite the poor signal-to-noise for the CN mode by Raman microscopy, the combination of MALDI and Raman spectral data gave definitive evidence that the modification of HVHP428 with 4-CN-NHS was successful. Therefore, further characterization of HVHP428-CN was carried out.

SPR analysis was performed to determine the functional effects of HVHP428 modification with 4-CN-NHS. Analysis revealed that the K_d of HVHP428 for protein A was 1.5 ± 0.1 μM and 1.7 ± 0.2 μM for HVHP428-CN, indicating that there was little statistically significant functional consequence of incorporating 4-CN-NHS (Figure 3.8). The structural and functional variability inherent to proteins means that the effects of small molecule modifications can vary depending on the system under investigation. This fact precluded the direct application of the HVHP428 results to the study of HCV proteins. However, studies that used BSA as a model labeling system were able to extend the same methodology to unrelated proteins. Therefore, the HVHP428 results were interpreted to provide preliminary information indicating that the incorporation of 4-CN-NHS did not cause significant functional perturbations to a system with a known correlation between structure and function. Moreover, that lack of functional effects showed that the modified lysine residues are not likely to fill an integral role in the structure and/or function of HVHP428. The

proven ability of mono- and poly-clonal antibodies to maintain their antigen recognition capacity following various modifications further supported this conclusion[33-35].

Summary

The results outlined in this Chapter showed that larger proteins capable of accommodating more modifications (BSA) are able to generate Raman image contrast that is specific to the CN mode contained on labelled proteins. In addition, the modification of HVHP428 with 4-CN-NHS appeared to have no effect on the wild-type function of the antibody. Factoring in previous studies, these results demonstrated that the application of the labeling methodology outlined in this Chapter should enable the analysis of specific proteins *in vivo* using CARS microscopy. In particular, the study of HCV proteins in real-time *in vivo* by tuning the CARS microscope to the CN resonance carried by the modified proteins will enable the delineation of dynamical components surrounding the function of HCV proteins.

References

1. Lohmann, V., Körner, F., Koch, J.-O., Herian, U., Theilmann, L., and Bartenschlager, R., Replication of Subgenomic Hepatitis C Virus RNAs in a Hepatoma Cell Line. *Science*, 1999. **285**(5424): p. 110-113.
2. Moradpour, D. and Blum, H.E., A primer on the molecular virology of hepatitis C virus. *Liver International*, 2004. **24**(6): p. 519-525.
3. François Penin, J.D., Felix A. Rey, Darius Moradpour, Jean-Michel Pawlotsky,, Structural biology of hepatitis C virus. *Hepatology*, 2004. **39**(1): p. 5-19.
4. Brass, V., Moradpour, D., and Blum, H.E., Molecular Virology of Hepatitis C Virus (HCV): 2006 Update. *Int. J. Med. Sci.*, 2006. **3**(2): p. 29-34.
5. Moriya, K., Yotsuyanagi, H., Shintani, Y., Fujie, H., Ishibashi, K., Matsuura, Y., Miyamura, T., and Koike, K., Hepatitis C virus core protein induces hepatic steatosis in transgenic mice. *J Gen Virol*, 1997. **78**(7): p. 1527-1531.
6. McLauchlan, J., Lemberg, M.K., Hope, G., and Martoglio, B., Intramembrane proteolysis promotes trafficking of hepatitis C virus core protein to lipid droplets. *EMBO J.*, 2002. **21**(15): p. 3980-8.
7. McCormick, C.J., Maucourant, S., Griffin, S., Rowlands, D.J., and Harris, M., Tagging of NS5A expressed from a functional hepatitis C virus replicon. *J Gen Virol*, 2006. **87**(3): p. 635-640.
8. Kien, F., Abraham, J.-D., Schuster, C., and Kieny, M.P., Analysis of the subcellular localization of hepatitis C virus E2 glycoprotein in live cells using EGFP fusion proteins. *J Gen Virol*, 2003. **84**(3): p. 561-566.
9. Sattler, M. and Fesik, S.W., Use of deuterium labeling in NMR: overcoming a sizeable problem. *Structure*, 1996. **4**(11): p. 1245-1249.
10. Venters, R.A., Huang, C.C., Farmer, B.T.n., Trolard, R., Spicer, L.D., and Dierke, C.A., High Level 2H/13C/15N labeling of proteins for NMR studies. *J. Biomol. NMR*, 1995. **5**(4): p. 339-344.
11. Kiick, K.L., Saxon, E., Tirrell, D.A., and Bertozzi, C.R., Incorporation of azides into recombinant proteins for chemoselective modification by the Staudinger ligation. *PNAS*, 2002. **99**(1): p. 19-24.
12. Oh, K. and Guan, Z., A convergent synthesis of new beta-turn mimics by click chemistry. *Chem Commun (Camb)*, 2006. **29**: p. 3069-71.
13. Zhang, Z., Smith, B.A.C., Wang, L., Brock, A., Cho, C., and Schultz, P.G., A New Strategy for the Site-Specific Modification of Proteins in Vivo. *Biochemistry*, 2003. **42**(22): p. 6735-6746.
14. Mahal, L.K., Yarema, K.J., and Bertozzi, C.R., Engineering Chemical Reactivity on Cell Surfaces Through Oligosaccharide Biosynthesis. *Science*, 1997. **276**(5315): p. 1125-1128.
15. Ryu, Y. and Schultz, P.G., Efficient incorporation of unnatural amino acids into proteins in Escherichia coli. 2006. **3**(4): p. 263-265.
16. Dawn S. Y. Yeo, R.S., Grace Y. J. Chen, Shao Q. Yao,, Expanded Utility of the Native Chemical Ligation Reaction. *Chemistry - A European Journal*, 2004. **10**(19): p. 4664-4672.
17. Miller, B.T., Collins, T.J., Rogers, M.E., and Kurosky, A., Peptide Biotinylation with Amine-Reactive Esters: Differential Side Chain Reactivity. *Peptides*, 1997. **18**(10): p. 1585-1595.

18. Schafer-Hales, K.J., Belfield, K.D., Yao, S., Frederiksen, P.K., Hales, J.M., and Kolattukudy, P.E., Fluorene-based fluorescent probes with high two-photon action cross-sections for biological multiphoton imaging applications. *Journal of Biomedical Optics*, 2005. **10**(5): p. 051402.
19. de Jong, E.P. and Lucy, C.A., Low-picomolar limits of detection using high-power light-emitting diodes for fluorescence. *The Analyst*, 2006. **131**: p. 664-669.
20. Salmain, M., Gorfti, A., and Jaouen, G., Side-chain selective and covalent labeling of proteins by organometallic complexes of heavy transition metals. Possible application in radio-crystallography of proteins. *European Journal of Biochemistry*, 1998. **258**(1): p. 192-199.
21. Akhavan-Tafti, H., DeSilva, R., Sugioka, K., Handley, R.S., and Schaap, A.P., Chemiluminescent acridan phosphate labeling compounds for detection in gels. 2001. **16**(2): p. 187-191.
22. Hoefelschweiger, B.K., Duerkop, A., and Wolfbeis, O.S., Novel type of general protein assay using a chromogenic and fluorogenic amine-reactive probe. *Analytical Biochemistry*, 2005. **344**(1): p. 122-129.
23. Osella, D., Pollone, P., Ravera, M., Salmain, M., and Jaouen, G., Use of Heavy-Metal Clusters in the Design of N-Succinimidyl Ester Acylation Reagents for Side-Chain-Specific Labeling of Proteins. *Bioconjugate Chem.*, 1999. **10**(4): p. 607-612.
24. Bautista, J. and Mateos-Nevado, M.D., Immunological detection and quantification of oxidized proteins by labeling with digoxigenin. *Bioscience Biotechnology and Biochemistry*, 1998. **62**(3): p. 419-423.
25. Weibel, N., Charbonniere, L.J., Guardigli, M., Roda, A., and Ziessel, R., Engineering of Highly Luminescent Lanthanide Tags Suitable for Protein Labeling and Time-Resolved Luminescence Imaging. *J. Am. Chem. Soc.*, 2004. **126**(15): p. 4888-4896.
26. Rudolf, B., Palusiak, M., Zakrzewski, J., Salmain, M., and Jaouen, G., Sulfhydryl-Selective, Covalent Labeling of Biomolecules with Transition Metallocarbonyl Complexes. Synthesis of (eta5-C5H5)M(CO)3(eta1-N-maleimidato) (M = Mo, W), X-ray structure, and reactivity studies. *Bioconjugate Chem.*, 2005. **16**(5): p. 1218-1224.
27. Yu, L.-R., Conrads, T.P., Uo, T., Issaq, H.J., Morrison, R.S., and Veenstra, T.D., Evaluation of the Acid-Cleavable Isotope-Coded Affinity Tag Reagents: Application to Camptothecin-Treated Cortical Neurons. *J. Proteome Res.*, 2004. **3**(3): p. 469-477.
28. Prezelj, A., Strancar, J., Gubensek, F., Pecar, S., and Degand, G., Quantification of binding of some thiol-reactive clenbuterol analogues to bovine serum albumin by electron paramagnetic resonance spectroscopy. *Analytical Biochemistry*, 2003. **315**(2): p. 202-207.
29. Heredia, K.L., Bontempo, D., Ly, T., Byers, J.T., Halstenberg, S., and Maynard, H.D., In Situ Preparation of Protein-"Smart" Polymer Conjugates with Retention of Bioactivity. *J. Am. Chem. Soc.*, 2005. **127**(48): p. 16955-16960.
30. Bingaman, S., Huxley, V.H., and Rumbaut, R.E., Fluorescent Dyes Modify Properties of Proteins Used in Microvascular Research. *Microcirculation*, 2003. **10**(2): p. 221-231.
31. Rumbaut, R.E., Harris, N.R., Sial, A.J., Huxley, V.H., and Granger, D.N., Leakage responses to L-NAME differ with the fluorescent dye used to label albumin. *Am J Physiol Heart Circ Physiol*, 1999. **276**(1): p. H333-339.

32. Soares, A.M. and Giglio, J.R., Chemical modifications of phospholipases A2 from snake venoms: effects on catalytic and pharmacological properties. *Toxicon*, 2003. **42**(8): p. 855-868.
33. Simons, B., Kaplan, H., and Hefford, M.A., Novel cross-linked enzyme-antibody conjugates for Western blot and ELISA. *Journal of Immunological Methods*. **In Press, Corrected Proof**.
34. Zhu, H. and Snyder, M., Protein chip technology. *Current Opinion in Chemical Biology*, 2003. **7**(1): p. 55-63.
35. Shaunak, S., Godwin, A., Choi, J.-W., Balan, S., Pedone, E., Vijayarangam, D., Heidelberger, S., Teo, I., Zloh, M., and Brocchini, S., Site-specific PEGylation of native disulfide bonds in therapeutic proteins. 2006. **2**(6): p. 312-313.

Chapter 4 – Summary and Future Work

Summary

This thesis focused on the structural and functional changes that accompany the chemical modification of biomolecules, with the underlying goal of developing a solid framework from which the utility of CARS microscopy can expand and fundamental aspects of HCV molecular virology can be investigated. A discussion on the rational design of CARS contrast agents identified the C-D and CN vibrational modes as ideal candidates to meet these goals. These modes were chosen due to their biostability, ease of biomolecular incorporation and the fact that there respective vibrational modes reside in a spectral region that is devoid of endogenous Raman resonances.

Incorporation of C-D modes into HCV RNA yielded D-RNA that contained approximately 75,000 C-D modes per RNA. Raman microscopy showed that image contrast specific to the C-D mode contained on the D-RNA could be generated and subsequent functional analysis revealed minimal deleterious effects of deuterium substitution. These results indicated that D-RNA was an excellent candidate for studying dynamical aspects of HCV RNA in real-time *in vivo* using CARS microscopy.

Generating CN-aaU-RNA first required the incorporation of aaU, to which 3-CN-NHS could be chemically coupled. Characterization of the aaU-RNA transcript before and after reaction with 3-CN-NHS was done using a combination of HPLC and LC-MS. In addition to facilitating the characterization of these materials for the degree of aaU incorporation and CN-modification, the development and validation of this quantitative methodology makes it possible to modulate the deleterious consequences of modifying HCV RNA. Thus, while CN-aaU-RNA had severe functional and structural deficits, optimization of the labeling reactions using the quantitative methods developed herein will enable the

minimization of these problems, while accommodating the detection limit of CARS microscopy for the CN mode.

Further to the incorporation of CN modes, 5'-CN was successfully synthesized with the hope that it could be used as an alternative to CN-aaU-RNA. This avenue was pursued because it was postulated that a 5'-modification would have less of a functional effect on HCV RNA than poly-labeling, i.e.: aaU incorporation followed by reaction with 3-CN-NHS. Surprisingly, the activity of 5'-CN was severely inhibited, which limited the potential application of this material to studying HCV with CARS microscopy. Precise reasons for this result remain unclear.

The application of CN labeling to protein modification was also investigated, with the end goal of modifying HCV proteins for *in vivo* tracking using CARS microscopy. Raman image contrast specific to BSA-CN was shown, as was spectral data indicating the clear presence of CN modes on HVHP428-CN. Additionally, functional analysis revealed little difference between normal and CN-modified HVHP428. When taken together these results gave conclusive evidence that reaction with 4-CN-NHS yielded CN-modified proteins. Furthermore, they gave preliminary evidence that CN-modification may not result in functional deficits to modified HCV RNA proteins.

Overall the work presented in this thesis has unambiguously demonstrated that C-D and CN vibrational modes can provide excellent Raman image contrast when chemically integrated into biomolecules. Moreover, they confirm that care must be taken when introducing exogenous functionality to biomolecules, as minor perturbations can elicit severe structural and/or functional consequences. Careful application of the labeling strategies outlined herein to the *in vivo* real-time study of RNA and proteins using CARS microscopy

has the potential to provide a plethora of information on previously unstudied dynamical processes.

Future Work

Further characterization of the monosubstituted D-RNA transcripts to determine the source of the functional difference between G/C and A/U substitutions would be beneficial, as it may enable the activity of D-RNA to be increased. Provided that the CARS detection limits for the C-D mode could still be met, the increased activity of mono- and/or disubstituted D-RNA transcripts would enable the analysis of a system that was functionally closer to HCV RNA, which is the desired situation when performing real-time *in vivo* analyses.

The luciferase assay is a direct measure of the translational competency of the HCV IRES and the luciferase gene and an indirect examination of replication competency. However, no information on the translational competency of the EMCV IRES and HCV coding region of HCV RNA is available from this assay. This was particularly relevant to 5'-modified HCV RNAs, as they were the most likely to show different expression levels of luciferase and HCV proteins. Therefore, the expression of the HCV coding region should be investigated. It was also difficult to quantify the extent of activity loss that was directly related to replicative deficiencies, as opposed to a combination of replicative and translational deficits. Thus, further characterization of modified HCV RNAs to determine their relative replicative deficiencies is required.

Having shown that 4-CN-NHS modification of BSA enabled image contrast specific to the CN mode of BSA-CN to be generated and that the activity of HVHP428-CN was on par with that of unmodified HVHP428, the next step to take for the elaboration of proteins

for *in vivo* tracking using CARS microscopy should be the application of these methods to HCV proteins. Also, it would be beneficial to try and increase the number of CN modes that are incorporated per protein. Provided that the functional effects were nominal, this would improve the detection limits for the CN-modified proteins.

Finally, all of these samples require thorough investigation under CARS microscopy conditions that have been optimized for detection of the C-D and CN vibrational modes. Once positive identification of CN-aaU-RNA and D-RNA has been achieved, the optimization of the modification conditions can be investigated such that the activity of the modified RNAs are maximized, while still maintaining sufficient modifications to facilitate detection using CARS microscopy. Fulfilling these experiments will facilitate the end-goal of using CARS microscopy to investigate dynamical processes of HCV molecular virology *in vivo* in real-time.

Chapter 5 – Materials and Methods

All chemicals were purchased from Aldrich (Oakville, ON, Canada) and used as received. Eighteen mΩ H_2O was obtained from a NANOpure® DIamond™ Life Science Series 1370 water filtration system (Barnstead International, Dubuque, IO, USA) and was used for all applications not requiring RNase-free conditions. The $pFK_{I389}luc/NS3\text{-}3'/5.1$ plasmid, which codes for the HCV subgenomic replicon, was obtained from Ralph Bartenschlager (Institute of Hygiene, University of Heidelberg, Heidelberg, Germany). Huh-7 cells were generously provided by Lubica Supekova (Scripps Research Institute, La Jolla, CA, USA). RNA quantification was performed on a ND-1000 spectrophotometer (NanoDrop Technologies, Rockland, DE, USA) and RNA integrity was verified by electrophoresis using the Agilent 2100 bioanalyzer with the RNA LabChip® Nano and Pico kits according to the manufacturer's protocol (Agilent Technologies, Palo Alto, CA, USA). RNA migration behavior and the heterogeneity of transcript populations were determined using the gel and electropherogram functions of the 2100 Expert software, respectively (v.B.01.02.SI136; Agilent Technologies). All cyanobenzyl compounds were kindly prepared by Dr. Qingyan Hu (National Research Council of Canada, Steacie Institute for Molecular Sciences, Ottawa, ON, Canada). The sdAb HVHP428 PSJF2 was provided by Dr. Roger Mackenzie (National Research Council of Canada, Institute for Biological Sciences, Ottawa, ON, Canada).

Cell Culture

Huh-7 cells were cultured at 37 °C and 5% CO_2 in complete cell culture medium that consisted of Dulbecco's modified Eagle medium (DMEM; Invitrogen, Burlington, Ontario, Canada) supplemented with 10% (v/v) fetal bovine serum (FBS; Cansera International,

Rexdale, Ontario, Canada), 100 nM minimal essential medium nonessential amino acids (NEaa; Invitrogen), 50 U/mL penicillin and 50 μg/mL streptomycin (Invitrogen).

In Vitro Transcription

HCV RNA was generated using the MEGAscript™ IVT kit (Ambion Incorporated, Austin, TX, USA). In brief, $pFK_{I389}luc/NS3\text{-}3'/5.1$ template DNA was linearized with the Sca I restriction enzyme (New England BioLabs, Pickering, ON, Canada). Following an ethanol precipitation, the linearized vector was resuspended in RNase-free H_2O (Ambion) to a final concentration of 0.5 $\mu g/\mu L$. The transcription reaction was set up according to the manufacturer's protocol and incubated at 37 °C for 2 hours Additionally, the pTriEx-4 Neo vector (EMD Biosciences Incorporated, San Diego, CA, USA) was digested with Nco I and Sma I restriction enzymes to yield template DNA that produced 163mer and 270mer RNA transcripts, respectively, following IVT as described above.

To generate transcripts incorporating aaU a 1:1 (v:v) mixture of 75 mM UTP and 75 mM aaUTP (Aldrich) was prepared and used in place of UTP in the IVT reaction – all other steps were performed as above. To generate D-RNA, perdeuterated rNTPs (50 mM; Silantes GmbH, München, Germany) were substituted for normal rNTPs in the transcription reaction – all other steps were performed as above. For transcripts containing only one of the deuterated rNTPs, the appropriate nucleotide was substituted with the deuterated analogue and the IVT reaction was performed as above. All transcripts were cleaned using a MEGAclear™ RNA purification kit (Ambion Incorporated) according to the manufacturer's protocol.

RNA Labeling

HCV RNA transcripts were conjugated to either fluorescein (32 mM; Vector Laboratories, Burlingame, CA, USA) or 4-CN-M (32 mM), which were dissolved in RNase-free DMSO (Aldrich), with the 5′ EndTag™ Nucleic Acid Labeling System (Vector Laboratories) according to the manufacturer's protocol. Following purification by phenol extraction, the labeled RNA was analyzed for quantity and integrity as outlined above.

To label the reactive amine presented by aaU, 3-CN-NHS, 4-CN-NHS and Bz-NHS were utilized. In a typical reaction 10 μg of RNA containing aaU (or approximately 100 nmol of aaU mononucleoside) was dissolved in labeling reaction buffer (30 mM $NaHCO_3$, pH 9). Following this, an equal volume of 25 mM NHS-activated label (dissolved in RNase-free DMSO) was added. After 1 hour at 37 °C the reaction was diluted 1:10 with RNase-free H_2O and purified by passage through a YM10 MWCO filter (Millipore, Billerica, MA, USA). Following two RNase-free H_2O washes the collected retentate was analyzed for quantity and integrity as outlined above.

RNA Digestion and Dephosphorylation

RNA (modified and unmodified) was digested with S1 (Invitrogen, Burlington, ON, Canada) to afford the constituent mononucleotides. In a typical reaction 5 μg of RNA was incubated with 50 U of S1 in 30 mM sodium acetate, 1 mM zinc acetate and 5% (v/v) glycerol, pH 4.6 at 37 °C. Digestions were stopped at 1, 2, 4, 8 and 24 hours by passage through a YM10 MWCO filter to examine the time-dependence of the digestion reaction. All other digestion reactions were incubated for 24 hours and subsequently used without purification. Additionally, the concentration-dependence of RNA digestion was investigated by conducting the digestion reaction with 2, 10 and 25 U of S1.

The mononucleotide solution was dephosphorylated by adjusting the buffer conditions to 100 mM NaCl, 50 mM Tris-HCl, 10 mM $MgCl_2$ and 1 mM dithiothreitol, after which 50 U of CIP (New England Biolabs) was added. Following incubation at 37 °C for 24 hours, the constituent mononucleosides were analyzed by HPLC and LC-MS without purification.

HPLC and LC-MS Analysis

HPLC was performed on an Agilent 1100 Series LC system (Agilent Technologies), equipped with a Waters SunFire™ C18 reverse-phase column (3.5 μm, 2.1x100 mm; Waters Corporation, Milford, MA, USA). The elution gradient used was adapted from previous studies investigating RNA by HPLC[1-3]. Resolution was achieved by using a MeOH/0.1 M NH_4OAc, pH 6.5 mixed mobile phase running at 0.2 mL/min. as follows (the first number is the percent MeOH and the second is the elapsed time in min.): 1, 0; 10, 15; 50, 16; 50, 20; 95, 30; 95, 35. The elution gradient was linear over all intervals (Figure 4.1). Typically, 15% (by volume) of a 5 μg HCV-RNA digestion/dephosphorylation reaction was analyzed per HPLC run.

LC-MS was carried out on a Waters 2795 Separations Module (Waters Corporation) equipped with the above outlined Waters SunFire™ C18 reverse-phase column. In-line monitoring of column eluate was achieved via detection with a Waters 996 Photodiode Array Detector (Waters Corporation) set to 254 nm and a Waters Micromass ZQ 2000 MS (Waters Corporation). The MS was set to positive ion electrospray detection, with the following defined parameters: Capillary Voltage – 3.50 kV; Cone Voltage – 10 V; Source Temperature - 80 °C; Desolvation Temperature – 200 °C; Desolvation Gas Flow – 347 L/hr.; Cone Gas

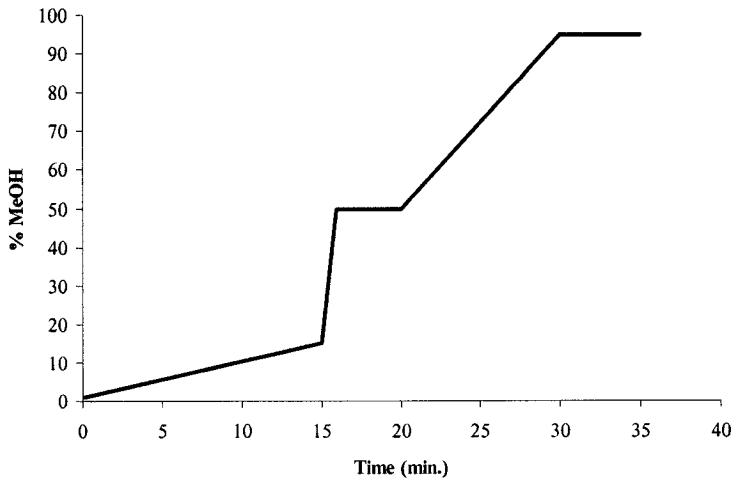

Figure 4.1: HPLC elution gradient as a function of MeOH.

Flow – 49 L/hr.; Scan Time – 0.5 sec.; Mass Range – 100 to 1000. Elution conditions were the same as for HPLC.

Standard curves of absorbance as a function of concentration were constructed for C, U, aaU, G and A (Aldrich) from 0.01 – 1 mM. The extent of aaU incorporation and 3-CN-NHS modification of RNA containing aaU was quantified using the U and aaU standard curves. Concentrations of the constituent nucleotides following RNA digestion and dephosphorylation were also determined using the standard curves. This data was then used to establish the percentage of RNA that was digested.

Transfection of RNA

For transient expression of $pFK_{I389}luc/NS3\text{-}3'/5.1$ derived HCV-RNA, Huh-7 cells were seeded at $5.0x10^4$ cells per well in a 24-well plate in 500 µL of complete Huh-7 medium. Cells were transfected once they reached 90% confluency (usually around 24 hours post-seeding). Prior to transfection cells were washed once with phosphate-buffered saline (PBS; 137 mM NaCl, 2.7 mM KCl, 10.1 mM Na_2HPO_4, 1.8 mM KH_2PO_4, pH 7.4) and placed in FBS- and antibiotic-free DMEM at 37 °C while preparing transfection complexes.

Transfection complexes were prepared by mixing 500 ng of RNA with 3.0 µL of DMRIE-C transfection reagent (Invitrogen) in 500 µL per well of FBS- and antibiotic-free DMEM in a 24-well plate as per the manufacturer's protocol. After 4 hours of exposure to the transfection complexes one equivalent (by volume) of antibiotic-free DMEM containing 20% (v/v) FBS and 100 nM NEaa was added. Transfected cells were then incubated at 37 °C and 5% CO_2 until desired endpoint(s). All transfection conditions were performed in triplicate.

Cell Lysis, Luciferase Assay and Protein Quantification

All luciferase assays were performed on lysates from 24-well cell cultures. At the desired time post-transfection cells were washed once with PBS and subsequently lysed via the addition of 100 μL of 1x cell culture lysis buffer (Promega Corporation, Madison, WI, USA) per well. After 20 min. at room temperature the cells were put at -20 °C for 24 hours to aid lysis.

Luciferase assay substrate (25 mM glycylglycine, 15 mM KH_2PO_4, 4 mM EGTA, 2 mM ATP, 1 mM dithiothreitol, 15 mM $MgSO_4$, 0.1 mM acetyl CoA, and 75 μM beetle luciferin, pH adjusted to 8.0) was prepared fresh prior to use [4]. Forty microliters of each cellular lysate was transferred to a Microlite white 96-well plate (VWR International, Mississauga, ON, Canada) and the luciferase activity was measured on an Lmax luminometer (Molecular Devices, Sunnyvale, CA, USA) equipped with SOFTmax Pro for Lmax 1.1L software (Molecular Devices). The following parameters were used for data acquisition: 50 μL of luciferase substrate was injected into each well, followed by a 2 sec delay and finally a 10 sec. integration to quantify the relative light units (RLU) produced.

Total protein content of cellular lysates was quantified using the Bio-Rad DC Protein Assay (Bio-Rad Laboratories, Mississauga, ON, Canada) as per the manufacturer's instructions, with BSA (Aldrich) as the protein standard. The absorbance was read using a BioPhotometer (Eppendorf, Mississauga, ON, Canada) at 595 nm after 15 min. of incubation at room temperature. All luciferase and protein data was collected in triplicate. The luciferase signal was normalized against protein content and is presented as mean values ± one standard deviation.

Raman Spectroscopy and Microscopy

All samples for Raman analysis were analyzed on a phosphorous-doped N-type silicon substrate (single-side polished, 250 ± 25 μm thickness; Virginia Semiconductor Incorporated, Fredericksburg, VA, USA). Raman spectroscopy and microscopy were carried out using a confocal Raman microscope (Horiba Jobin Yvon, Edison, NJ, USA) aligned in a back scattering configuration, which was coupled to an Olympus BX51 microscope (Olympus America Incorporated, Center Valley, PA, USA). Scattered light was collected through a high numerical aperture (N_a = 0.95) 100x objective (Olympus America Incorporated) and was detected on a 1024×256 element thermo-electrical cooled CCD detector (Andor Technology, South Windsor, CT, USA). Sample excitation was achieved via a HeNe laser (λ = 632.8 nm) sharply focused to a diffraction-limited spot, with a focal power density of approximately 10^5 W/cm^2 (10 mW focused to 1 um^2). Typically, spectra were acquired with three accumulations of 20 sec., with multiple accumulations serving to improve the overall spectral signal to noise ratio, as well as allowing the spectral processing software to efficiently remove cosmic spikes. All spectral processing was performed within the manufacturer's instrumental control software, LabSpec 5.04 (Horiba Jobin Yvon). Spectral smoothing was achieved using the Savitsky-Golay smoothing routine. Baseline removal was accomplished by subtracting the raw data to a polynomial fitted baseline function – this correction is performed automatically by the LabSpec software.

Atomic Force Microscopy

For imaging, RNA was diluted in AFM imaging buffer (40 mM HEPES, 10 mM $MgCl_2$, pH 7) to 2 – 5 ng/μL. Five microliters of the diluted RNA solution was dropped onto freshly cleaved mica (grade V2; Ted Pella Incorporated, Redding, CA, USA) and allowed to

adsorb for five min. at room temperature. Non-absorbed RNA was removed by washing three times with RNase-free H_2O (500 μL per wash), after which the sample was dried under a stream of nitrogen. Imaging was performed under ambient conditions in tapping mode on a NanoScope IIIa atomic force microscope (Digital Instruments, Woodbury, NY, USA) equipped with an E-piezoscanner (Digital Instruments). Pointprobe® plus non-contact, high-resonance frequency tips (Nanosensors, Neuchatel, Switzerland), with a force constant of 21 - 78 N/m and a resonance frequency of 260 – 410 KHz, were used for all measurements. Fields of 0.5 – 3.0 μm were scanned at 1 – 1.5 Hz. Images were flattened and approximate cluster diameters were determined using NanoScope v5.12r4 software (Digital Instruments) to account for Z offsets and sample tilt and exported as .TIF files. The same software was used to manually determine cluster diameters. Following imaging all diluted RNA was analyzed to verify integrity.

Dynamic Light Scattering

DLS measurements were recorded on a Zetasizer 3000 HSA (Malvern Instruments Limited, Worcestershire, United Kingdom). Scattered light was produced by a 633 nm incident beam and was detected at an angle of 90° and a temperature of 25 °C. All measurements were taken in a Quartz SUPRASIL cuvette (Hellma GmbH & Co KG, Müllheim, Germany) with a 3 mm path length and 45 μL sample volume. Samples were prepared in AFM imaging buffer and allowed to incubate for 10 min. at room temperature prior to measurement. The integrity of all RNA was verified following analysis. Data is reported as the mean hydrodynamic radius (nm) ± the polydispersion factor calculated by the Zetasizer software.

Expression and Purification of sdAbs

For a complete review the generation of sdAbs see [5, 6]. Expression and purification of the recombinant sdAb was carried out as outlined in [7], except periplasmic extraction was performed instead of cell lysis. Briefly, harvested *E. coli* containing the expressed sdAbs were washed once with 10 mM Tris, pH 8.0 after which a 10 min. incubation at room temperature in sucrose solution (25% sucrose, 1 mM EDTA, 10 mM Tris, pH 8.0) was performed. Following centrifugation the resulting pellet was resuspended in ice cold shock solution (10 mM Tris, pH 8.0, 0.5 mM $MgCl_2$) for 5 – 10 min. at on ice. After centrifugation the retentates were further purified as outlined in [7].

Protein Labeling

Labeling of BSA and HVHP428 was accomplished by mixing ≥1 mg/mL protein (100 mM $NaHCO_3$, pH 8.3) with an equal volume of 25 mM 4-cyanobenzyl-NHS, which was dissolved in DMSO. The labeling reaction was allowed to proceed for 1 hour at 37 °C. After a 1:10 dilution with H_2O the labelled protein was purified by passage through a YM10 MWCO filter and further cleaned via two H_2O washes. The retentate was collected and characterized MALDI and SDS-PAGE (4% stacking, 12% resolving gel), as well as Raman spectroscopy and microscopy.

MALDI

For MALDI analysis protein samples were desalted on a C4 ZipTip (Millipore) and eluted with 70% (v/v) aqueous acetonitrile containing 0.1% (v/v) TFA. The desalted sample (1 μL) was spotted on a target plate with an equal volume of sinapinic acid solution (12 mg/mL in aqueous solution with 0.1% (v/v) TFA and 33% (v/v) acetonitrile) and dried. The

plate was analyzed on a Voyager DE-Pro MALDI-ToF (Applied Biosystem: Foster City, CA, USA) mass spectrometer operated in the linear/positive-ion mode. Instrument configuration was as follows: Accelerating voltage - 25000; Grid Voltage - 92%; Guide Wire Voltage - 0.010%; Delay Time - 380 nsec.; Low Mass Gate - 2000 Da; LaserPower - 2174; Shots/spectrum - 200.

SPR Analysis of Modified sdAb

Dissociation constants for modified and unmodified sdAb were determined by SPR using BIACORE 3000 biosensor system (Biacore, Incorporated, Piscataway, NJ, USA). Four hundred RUs of Protein A (Amersham, Buckinghamshire, UK) and 780 RUs of unrelated F_{ab} as a reference protein were immobilized on research grade CM5 sensorchip (BIACORE). Immobilizations were carried out at protein concentrations of 25 – 50 μg/ml in 10 mM acetate buffer, pH 4.5 using the amine coupling kit supplied by the manufacturer. All measurements were carried out at 25°C in 10 mM HEPES, pH7.4, containing 150 mM NaCl, 3 mM EDTA and 0.005% P20 at a flow rate of 40 μl/min. No surface regeneration was required. Data was evaluated using BIAevaluation 4.1 (Biacore, Incorporated) and GraphPad Prism (v 4.01; GraphPad Software, San Diego, CA, USA) software.

References

1. Crain, P.F., *Preparation and enzymatic hydrolysis of DNA and RNA for mass spectrometry.*, in *Mass Spectrometry*, J.A. McCloskey, Editor. 1990, Academic Press. p. 782-790.
2. Pomerantz, S.C. and McCloskey, J.A., *Analysis of RNA hydrolyzates by liquid chromatography-mass spectrometry.*, in *Mass Spectrometry*, J.A. McCloskey, Editor. 1990, Academic Press. p. 796-824.
3. Buck, M., Connick, M., and Ames, B.N., Complete analysis of tRNA-modified nucleosides by high-performance liquid chromatography: The 29 modified nucleosides of Salmonella typhimurium and Escherichia coli tRNA. *Analytical Biochemistry*, 1983. **129**(1): p. 1-13.
4. Dyer, B.W., Ferrer, F.A., Klinedinst, D.K., and Rodriguez, R., A Noncommercial Dual Luciferase Enzyme Assay System for Reporter Gene Analysis. *Analytical Biochemistry*, 2000. **282**(1): p. 158-161.
5. Arbabi-Ghahroudi, M., Tanha, J., and MacKenzie, R., Isolation of monoclonal antibody fragments from phage display libraries. *Methods Mol. Biol.*, 2006. **In Press**.
6. To, R., Hirama, T., Arbabi-Ghahroudi, M., MacKenzie, R., Wang, P., Xu, P., Ni, F., and Tanha, J., Isolation of Monomeric Human VHS by a Phage Selection. *J. Biol. Chem.*, 2005. **280**(50): p. 41395-41403.
7. Zhang, J., Li, Q., Nguyen, T.-D., Tremblay, T.-L., Stone, E., To, R., Kelly, J., and Roger MacKenzie, C., A Pentavalent Single-domain Antibody Approach to Tumor Antigen Discovery and the Development of Novel Proteomics Reagents. *Journal of Molecular Biology*, 2004. 341(1): p. 161-169.

Related to Thesis Work

Noestheden, M., Hu, Q., Tay, L., Tonary, A.M., Pezacki, J.P. Labeling Strategies for Live Cell Tracking of HCV RNA Using Raman and Coherent Anti-Stokes Raman Scattering Microscopies. *In preparation.*

Noestheden, M., Hu, Q., Tay, L, Tonary, A.M., Mackenzie, R., Tanha, J., Pezacki, J.P. A single-domain antibody recognizing Staphylococcal protein A modified for use as a vibrational contrast agent. *Submitted to Bioorg. Chem. 11/01/06.*

Unrelated to Thesis Work

Hu, Q.,Tay, L., **Noestheden, M.**, Pezacki, J.P. Mammalian Cell Surface Imaging with Nitrile-Functionalized Nanoprobes: Biophysical Characterization of Aggregation and Polarization Anisotropy in SERS Imaging. *Accepted to J. Am. Chem. Soc. 12/01/06.*

Rakic, B., Sagan, M S., **Noestheden, M.**, Belanger, S., Nan, X., Evans, L. C., Xie, X. S., Pezacki, J. P. Peroxisome Proliferator-Activated Receptor α Antagonism Inhibits Hepatitis C Virus Replication. *Chem. Bio.*, (2006) **13**, 23-30.